Location-Based Activity Recognition

Lin Liao

A dissertation submitted in partial fulfillment of
the requirements for the degree of

Doctor of Philosophy

University of Washington

2006

Program Authorized to Offer Degree: Computer Science and Engineering

University of Washington
Graduate School

This is to certify that I have examined this copy of a doctoral dissertation by

Lin Liao

and have found that it is complete and satisfactory in all respects,
and that any and all revisions required by the final
examining committee have been made.

Co-Chairs of the Supervisory Committee:

Dieter Fox

Henry Kautz

Reading Committee:

Dieter Fox

Henry Kautz

Martha E. Pollack

Date:

Signature______________________________

Date__________________________________

University of Washington

Abstract

Location-Based Activity Recognition

Lin Liao

Co-Chairs of the Supervisory Committee:
Associate Professor Dieter Fox
Computer Science and Engineering

Professor Henry Kautz
Computer Science and Engineering

Automatic recognition of human activities can support many applications, from context aware computing to just-in-time information systems to assistive technology for the disabled. Knowledge of a person's location provides important context information for inferring a person's high-level activities. This dissertation describes the application of machine learning and probabilistic reasoning techniques to recognizing daily activities from location data collected by GPS sensors.

In the first part of the dissertation, we present a new framework of activity recognition that builds upon and extends existing research on conditional random fields and relational Markov networks. This framework is able to take into account complex relations between locations, activities, and significant places, as well as high level knowledges such as number of homes and workplaces. By extracting and labeling activities and significant places simultaneously, our approach achieves high accuracy on both extraction and labeling. We present efficient inference algorithms for aggregate features using Fast Fourier Transform or local Markov Chain Monte Carlo within the belief propagation framework, and a novel approach for feature selection and parameter estimation using boosting with virtual evidences.

In the second part, we build a hierarchical dynamic Bayesian network model for transportation routines. It can predict a user's destination in real time, infer the user's mode of

transportation, and determine when a user has deviated from his ordinary routines. The model encodes general knowledge such as street maps, bus routes, and bus stops, in order to discriminate different transportation modes. Moreover, our system could automatically learn navigation patterns at all levels from raw GPS data, without any manual labeling! We develop an online inference algorithm for the hierarchical transportation model based on the framework of Rao-Blackwellised particle filters, which performs analytical inference both at the low level and at the higher levels of the hierarchy while sampling other variables.

TABLE OF CONTENTS

LIST OF FIGURES

Figure Number Page

LIST OF TABLES

ACKNOWLEDGMENTS

During my Ph.D. study, I am extremely fortunate to have two great advisors, Dieter Fox and Henry Kautz. I am deeply indebted to Dieter for teaching me how to do research, write papers, and give presentations. His tireless pursuit of excellence and extreme sharpness on discovering new problems strongly influence me. I would like to thank Henry for guiding me to the world of artificial intelligence and to the fruitful project of Assisted Cognition. His insights and broad knowledge always help me stay on the right track.

I would like to thank other members in my thesis committee, Gaetano Borriello, Martha E. Pollack, and R. Jeffrey Wilkes, for their inspiring questions and suggestions. Their supports are important for me to complete the dissertation smoothly. I am also grateful to Jeff Bilmes, Pedro Domingos, Carl Ebeling, Alon Halevy, Steve Seitz, and Dan Weld, for their valuable comments and warm encouragements during my study.

I am very lucky to have the chance to collaborate with many great researchers at the University of Washington and the Intel Research Lab at Seattle. I have learned a lot from Don J. Patterson during the countless hours we spent together to discuss the algorithms and to make them work with real data. I thank Tanzeem Choudhury for her help when I was an intern at the Intel Research Lab; the project I worked on there and the thorough discussions with her were truly enlightening. I would like to express my appreciation and gratitude to other collaborators, Gaetano Borriello, Krzysztof Gajos, Jeff Hightower, Jonathan Lester, Benson Limketkai and Dirk Schulz for teaching me so many things. Enormous thanks to many other friends in my department for helping me in various ways and bringing so much fun to my life.

I would give my special thank to my wife, Xiaolin. It is such a wonderful thing that we can meet in Seattle and get married. Finally I thank my parents and sister. Although they live in China and I cannot see them often, their care and support is invaluable.

Chapter 1
INTRODUCTION

In our daily lives, we always try to understand the activities of people around us and adjust our behavior accordingly. At home, we are curious about whether other family members are cooking, reading or watching TV; during work, we may need to know if a coworker is in a meeting or on the phone; when driving, we must be aware of the behavior of surrounded cars. This ability of activity recognition seems so natural and simple for ordinary people, but it actually requires complicated functions of *sensing*, *learning*, and *inference*. Think, for example, how we recognize a cooking activity. Maybe we happen to see some person is in the kitchen at the dinner time, or we smell something is cooked, or we just find the stove is on. From such evidences, we could infer the activity based on our past experiences. All these functions of sensing the environments, learning from past experience, and applying knowledge for inference are still great challenges for modern computers. The goal of our research is to enable computers to have similar capabilities as humans for recognizing people's activities. If eventually we develop computers that can reliably recognize people's various activities, we can dramatically improve the way people interact with computers, we will have huge impact on behavior, social and cognitive sciences, and we are much closer to our dreams of developing robots that can offer help in our daily lives. To achieve this goal, we must provide computers with the two types of functions that ordinary people possess.

The first is the function of *sensing*. That is, we need to equip the computers with eyes, ears, noses, or other sensors. Different sensors have their own strengths and weaknesses. For example, cameras are very useful for low-level activities, but they are often limited to small environments and hard to be used at large scales. Our work focuses on location sensors, which can record people's physical locations at a large scale over long periods of time. As we

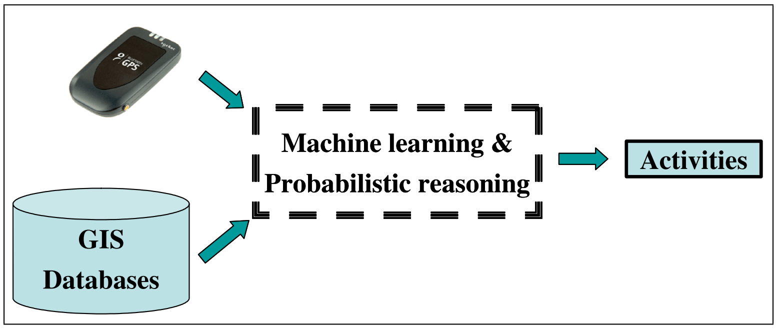

Figure 1.1: The architecture of our system for location-based activity recognition. On the left, the inputs are GPS measurements and geographic information systems (GIS). On the right, the outputs are the inferred user activities.

will show in the thesis, we can extract very rich context information by combining location information with relevant geographic knowledge. Note that the goal of this thesis in not to introduce a better location technique, but to develop fundamental techniques for activity recognition using the state-of-the-art location systems.

Second, the machines must have the mechanism of *learning* and *inference*. Developing the mechanism in the context of activity recognition is the theme of this thesis. We believe probabilistic reasoning and machine learning techniques are powerful tools for this task. However, even with the state-of-the-art tools, it is extremely challenging to build a comprehensive system that works in real-world settings. In the thesis, we will develop novel techniques of learning and inference that enable machines to recognize a variety of human activities from real sensor data.

The basic architecture of the system for location-based activity recognition is shown in Fig. 1.1. The inputs include GPS measurements collected by a wearable device and relevant geographic information, such as street maps, bus maps, and points of interests. The outputs of the system are the inferred activities, such as working, shopping, visiting, and transportation routines between places. Our technique can be applied to many practical applications:

- **Context-aware information services:** for example, providing "just-in-time" traffic and accident information by predicting users' destinations and paths, or adapting the interface of mobile devices based on current activities.

- **Technologies for long term healthcare:** for example, in Chapter 6 we will discuss a system called *Opportunity Knocks* that is able to help cognitively-impaired people use public transit independently and safely.

- **"Life log":** automatically recording people's daily activities, which will be very useful for the healthcare for senior or mentally retarded people and for the research of behavior science and social science.

In this chapter, we first explain the main challenges for automatic activity recognition. Then we provide an overview of the techniques. Finally we discuss related work, followed by the outline of the thesis.

1.1 Challenges of Activity Recognition

The significant potentials of automatic activity recognition have been realized for decades in computer science communities. Since 1980's, researchers have been pushing the envelope of activity recognition techniques. However, most early systems only work in toy examples and not until recent years had researchers begun to build systems using real data. Even today, activity recognition systems still have very limited capabilities. For instance, they focus on only a small set of activities and work only in specific environments. It is extremely challenging to build practical systems that are able to recognize a variety of daily activities at a large scale. One type of challenge is related to the function of sensing: it is difficult to develop a sensing platform that can collect information over long periods of time and is unintrusive to users. This thesis addresses the second type of challenge, which is related to the capabilities of learning and inference.

- First, there exists a big gap between low level sensor measurements and high level activities. To bridge the gap, inference has to go through a number of intermediate layers. For example, when predicting a person's destinations from raw GPS measurements, the system may have to infer street, mode of transportation, and travel route in order to make reliable predictions of destinations.

- Second, many factors affect human behaviors and some of them are hard to determine precisely. For instance, preferences and capabilities of people strongly affect their activity patterns but are difficult to characterize. Therefore for learning and inference, the system has to take into account many sources of vague evidence.

- Third, activities are strongly correlated. As a consequence, the system should consider their relationships during inference rather than recognizing each activity separately.

- Finally, the system requires a large amount of domain knowledge. For example, what are the features that distinguish the variety of activities (working, shopping, visiting, driving, *etc.*)? And how to combine them for making inference? Manually feeding the knowledge is apparently infeasible in practice and we must develop appropriate learning mechanisms.

1.2 Overview

Because of the uncertainty and variability of human activities, it is impractical to model activities in a deterministic manner. Probabilistic reasoning thus becomes the dominant approach for activity recognition. Our system is built upon the recent advances on probabilistic reasoning for large and complex systems.

1.2.1 Discriminative Approach vs. Generative Approach

Although a lot of models have been proposed for probabilistic reasoning, no single model has been found to outperform others in all the situations. In general, there are two main types of models: *discriminative* models and *generative* models [111, 79]. Discriminative models, such as logistic regression and conditional random fields, directly represent the conditional distributions of the hidden labels given all the observations. During training, the parameters could be adjusted to maximize the conditional likelihood of the data. In contrast, generative models, such as naive Bayesian models, hidden Markov models, and dynamic Bayesian networks, represent the joint distributions and use the Bayes rule to obtain the conditional distribution. Generative models are usually trained by maximizing the joint likelihood. Because of the differences on representation and training methods, the two approaches often behave differently:

- Generative models often assume the independence of observations given the hidden labels. When this assumption does not hold, generative models could have significant *bias* and thereby perform worse than their discriminative counterparts [58, 104].

- On the other hand, generative models can converge relatively faster during training and have less *variance*. Therefore, when the independence assumption holds, or when only small amount of training data are available, generative approach could outperform discriminative approach [79].

- Training generative models is usually easier than training discriminative models, especially when there are missing labels.

In this thesis, we apply both discriminative and generative approaches. Specifically, we apply discriminative models (conditional random fields and relational Markov networks) to *activity classification*, and apply generative models (dynamic Bayesian networks) to *inferring transportation routines*. This is due to the different characteristics of the two tasks: The goal of classifying activities is to learn the *discriminative features* of various activities, while the goal of inferring transportation routines is to estimate the *transition patterns* so as to predict distant destinations and paths. Furthermore, in order to classify various activities, we must take many sources of evidence into account. Discriminative models are well-suited for such tasks that involve complex and overlapped evidences. And for learning transportation routines generative approach may be more suitable because we can use standard algorithms for unsupervised learning.

1.2.2 Contributions of the Thesis

The goal of this thesis is to develop probabilistic reasoning techniques for activity recognition. From the perspective of activity recognition, the main contributions are:

1. We present a new framework of activity recognition that builds upon and extends existing research on conditional random fields and relational Markov networks. We demonstrate using the framework for location-based activity recognition as well as preliminary results on classifying finer-grained activities from other sensors. This framework is able to take into account complex relations between locations, activities, and significant places, as well as high level knowledges such as number of homes and workplaces. By extracting and labeling activities and significant places simultaneously, our approach achieves high accuracy on both extraction and labeling. Using GPS data collected by different people, we have demonstrated the feasibility of transferring knowledge from people who have labeled data to those who have no or very little labeled data.

2. We present an effective approach for learning motion models based on the graphical structure of environments, such as outdoor street maps and indoor Voronoi graphs (*i.e.*, skeletons of free space). The graphs provide a compact and natural way of delineating human movements, so that motion patterns can be readily learned in an unsupervised manner using the Expectation Maximization (EM) algorithm.

3. We build a hierarchical dynamic Bayesian model for transportation routines. The model can predict a user's destination in real time, even hundreds of city blocks away; it can infer the user's mode of transportation, such as foot, bus or car; and it can determine when a user has deviated from his ordinary routines. The model encodes general knowledge such as street maps, bus routes, and bus stops, in order to discriminate different transportation modes. Moreover, our system could automatically learn navigation patterns at all levels from raw GPS data, without any manual labeling! Based on this work we have developed a personal guidance system called Opportunity Knocks, to help people with cognitive disabilities use public transit. The system warns the user if it infers a high likelihood of user error (*e.g.*, taking the wrong bus), and provides real-time instructions on how to recover from the error.

From the machine learning and probabilistic reasoning perspective, the main contributions of the thesis are:

1. We extend the relational Markov networks to handle aggregate features. Especially, we develop efficient inference algorithms by combining belief propagation and Fast Fourier Transform (FFT) or Markov Chain Monte Carlo. This technique can be valuable in other probabilistic inference scenarios involving aggregate features.

2. We introduce a novel training method for CRFs, called virtual evidence boosting, which simultaneously performs feature selection and parameter estimation. To achieve this, we extend standard boosting algorithm to handle virtual evidence, *i.e.*, an observation is specified as a distribution rather than a single number. This extension allows us to develop a unified framework for learning both local and compatibility features in CRFs. In experiments on synthetic data as well as real classification problems, the new training algorithm significantly outperforms other training approaches.

3. We develop an online inference algorithm for the hierarchical transportation model based on the framework of Rao-Blackwellised particle filters. We perform analytical inference both at the low level and at the higher levels of the hierarchy while sampling other variables. This technique allows us to infer goals, transportation modes, and user errors simultaneously in an efficient way.

1.3 Related Work

In this section we discuss two types of work related to this thesis: activity recognition and location techniques.

1.3.1 Probabilistic Models for Activity Recognition

Activity recognition, also known as plan recognition, goal recognition, or behavior recognition [1], has been a long-term endeavor in the communities of artificial intelligence, ubiquitous

[1] Although different terms may emphasize different aspects of human activities, their essential goals are the same. Thus we do not distinguish the minor differences and use the term activity recognition throughout the thesis.

computing, and human computer interaction. Early efforts tackled the problem using deterministic models (*e.g.*, [49]), but they could hardly be used for practical applications because of the uncertainty inherent in human activities. In this section, we give a brief survey of a variety of probabilistic models used for activity recognition. Specifically, we will discuss four representative models: Bayesian networks, probabilistic grammars, probabilistic logic models and dynamic Bayesian models. We focus on two aspects of these models: the *expressiveness* and the *efficiency*.

Bayesian networks

A Bayesian network [86] is a directed, acyclic graph whose nodes represent random variables and whose edges indicate direct influence between variables. Bayesian networks provide a compact way to represent the joint distributions of the variables by capturing the conditional independence among variables. Since Bayesian networks have been successfully applied in many areas for inference under uncertainty, it is natural to choose Bayesian networks for human behavior modeling. Bayesian networks have many strengths: they are expressive, flexible, and many off-the-shelf learning and inference algorithms have been developed.

The model proposed by Charniak and Goldman is one of the earliest [15]. Their approach manually translates activity knowledge into an associative network (Fig. 1.2). Then it uses a number of rules to automatically convert an associative network to the corresponding Bayesian network. Charniak and Goldman's approach is *bottom-up*: it only considers the activity hypothesis compatible with the observations and tries to keep the network as small as possible. As shown in Fig. 1.3, their approach constructs Bayesian networks in a dynamic way to incorporate the latest evidence. This model has a number of weaknesses. It relies on general Bayesian network inference engines to solve the problem and thereby it cannot utilize the special relations among the variables. This approach seems only suitable for abstraction and decomposition relations (*i.e.*, part-subpart relations); for example, it is unclear how to express the temporal constraints in this model.

Huber *et al.* presented a *top-down* approach [47]. That is, the Bayesian networks are constructed from the plan library before receiving any observations. The plan language

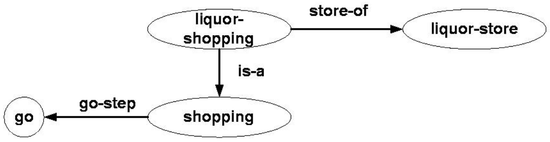

Figure 1.2: An associative network of liquor shopping (courtesy to [15]). The meanings of the edges are: each shopping activity includes a "go" step, liquor-shopping is an instance of shopping, and the store of liquor-shopping is a liquor store.

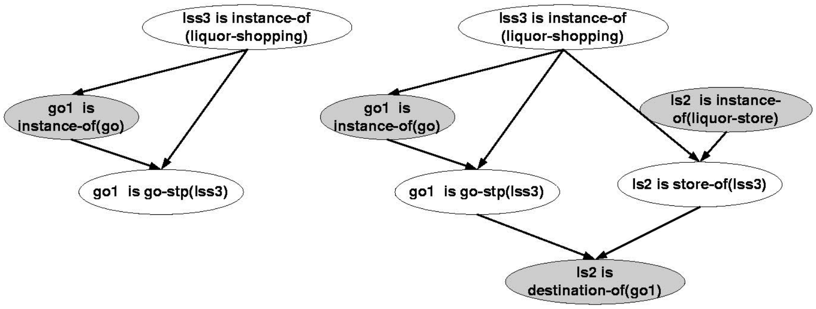
lss3 is instance-of (liquor-shopping)
go1 is instance-of(go)
go1 is go-stp(lss3)
lss3 is instance-of (liquor-shopping)
go1 is instance-of(go)
ls2 is instance-of(liquor-store)
go1 is go-stp(lss3)
ls2 is store-of(lss3)
ls2 is destination-of(go1)

Figure 1.3: Bayesian networks constructed for the activity of liquor shopping (courtesy to [15]). The nodes with grey background are observations and those without grey background are hidden variables for explanation. On the left is the network after observing a "go" action (named go1); on the right is the network after observing another evidence: the destination of the "go" action is a liquor store (named ls2). Given the observations, the explanation is lss3, which is an instance of liquor-shopping.

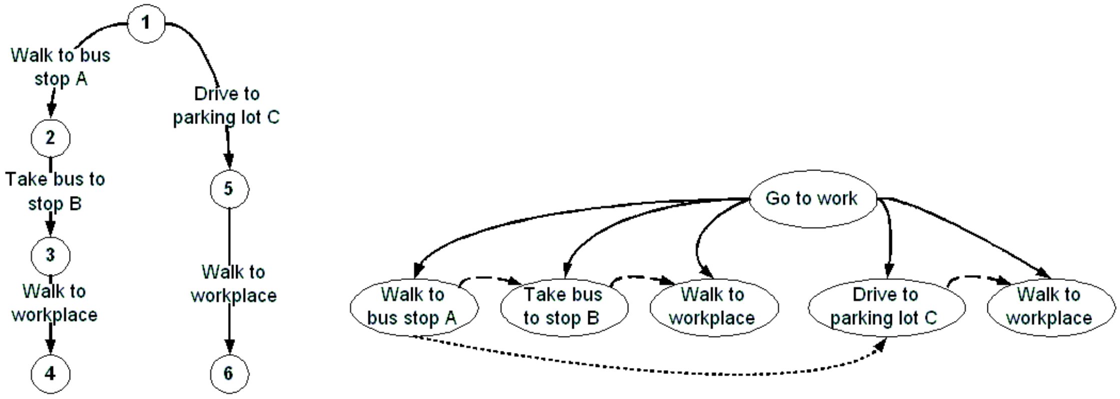

Figure 1.4: On the left is the PRS for the activity of going to work, which has two optional but exclusive branches, a bus route and a car route. On the right is the Bayesian network translated automatically from the PRS. Solid lines indicate decomposition relation, dashed lines indicate the temporal constraints, and dot lines indicate the exclusive relations between the two routes.

they employed is called Procedural Reasoning System (PRS). PRS is expressive enough to handle many types of relations, such as explicit sequencing, exclusive branches, iteration, and context influence. Similar to Charniak and Goldman's approach, they designed rules that convert PRS into Bayesian networks automatically. In Fig. 1.4, we show an example of PRS and the corresponding Bayesian network. The Bayesian network in this example encodes decomposition relation, temporal relation, and exclusive relation. However, it is unclear how to perform efficient inference in the networks by taking advantages of the special structures. In this case, using generic inference algorithms is unable to scale well to large domains.

Probabilistic grammars

In the formalism of probabilistic grammars [91, 10], a given plan-generation process is described using a set of grammatical rules. The simplest model in this formalism is Probabilistic Context-Free Grammars (PCFG), which starts with a Context-Free Grammar and assigns a probability to each production rule. For example, the rule

[go-to-work] → [walk-to-bus-stop-A] [take-bus-to-stop-B] [walk-to-workplace] (0.6) means that an agent has a 0.6 probability to take the bus route when he goes to work. Standard parsing algorithms can be used to infer the most probable plan that explains the observed sequence. However, parsing algorithms are hard to use in practice, because they require complete sequence for inference and cannot handle partial strings, but a plan recognizer rarely has complete observations. In [91], the problem is solved by converting a PCFG to a Bayesian network and then performing inference in the Bayesian network. Another problem for PCFG is that it is overly restrictive, since it does not keep track of the current state of the agent. One way to overcome this difficulty is to use Context-Sensitive Grammars, but that quickly leads to intractable complexity. Another alternative is the so-call Probabilistic State-Dependent Grammars (PSDG) [92]. PSDG introduces explicit variables to represent the states of the world and the agent, while still imposing enough structures to simplify inference. In PSDG, the probability assigned to each production rule is a function of the states. For example, the rule of going to work becomes

$$\begin{aligned}\text{[go-to-work]} \rightarrow \quad & \text{[walk-to-bus-stop-A] [take-bus-to-stop-B] [walk-to-workplace]} \\ & \qquad\qquad \text{(0.5 if rain and 0.8 if no rain)}\end{aligned}$$

where “rain” is a *state* variable. When doing inference, the approach translates PSDG into dynamic Bayesian networks (DBN) [77] and uses a specialized inference algorithm that exploits the independence properties and the restricted set of queries. However, this inference algorithm has been found inadequate for complex domains [14].

Logic models

Activity models based on logic formalism have a long history. Kautz’s *event hierarchy* is one of the earliest models for activity recognition [49]. His model uses first-order logic to represent the abstraction and decomposition relations. However, the model does not take uncertainty into account.

Goldman *et al.* [40] formalized activity recognition as a problem of Probabilistic Horn Abduction (PHA) [90]. PHA uses Prolog-like Horn rules to distinguish various *hypotheses.* In the scenario of activity recognition, the hypotheses are the possible activities that explain the observations. Goldman *et al.* [40] showed that such a formalism is able to handle a number of situations that will cause troubles in other formalisms, such as partial ordering, plan interleaving, context influence, and the interactions between the recognizer and the agent. For inference, an abductive theorem prover [89] is used. Although such a model is quite expressive, the efficiency of inference was ignored in the paper. Using a general-purpose theorem prover seems hard to scale to large domains.

Dynamic Bayesian models

It is natural to think activity recognition as a state estimation problem in a *dynamic* system, in which the hidden states represent the sequence of activities. However, standard dynamic models, such as hidden Markov models, are inadequate to handle the variety of relations and features for activities, such as decomposition, abstraction, duration, long-range dependencies, and so on. Thus many extensions have been proposed, including layered hidden Markov models [80], quantitative temporal Bayesian networks [18], propagation networks [100], aggregate dynamic Bayesian models [83].

The most relevant example of these extensions is the abstract hidden Markov model (AHMM) presented by Bui *et al.*, which is closely related to our dynamic Bayesian network of transportation routines (Chapter 6). AHMM bridges the gap between activities and low level states using a hierarchical structure, which can be converted to DBN for efficient inference. A key to AHMM is that a strong conditional independence exists: given the current level k activity as well as its starting time and starting state, the activities above level k and below level k are independent. By exploiting such a conditional independence, Bui *et al.* developed an approximate inference scheme using Rao-Blackwellised particle filters [25]. It has been shown that this algorithm scales well as the number of levels in the hierarchy increases. However, AHMM is limited in its expressiveness; in particular, it can only represent *memoryless* policies. The abstract hidden Markov memory model (AHMEM) [12] extends the AHMM by adding a memory node at each level. The expressiveness of AHMEM encompasses that of PSDG [91]. More importantly, the Rao-Blackwellised particle filters for AHMM can be easily extended to AHMEM, which ensures AHMEM be computationally attractive.

1.3.2 Location Techniques

A vast variety of techniques have been developed to obtain people's locations. In this section we briefly discuss location techniques based on satellites, WiFi beacons, and mobile phone networks, all of which have been widely used for location estimation at a large scale. See [46] for an excellent survey and comparison of various location systems.

Satellite-based location systems

The most widely used location system is the global positioning system (GPS), which relies on the 24 satellites operated by the United States. The other two satellite-based systems are the GLONASS by Russia and the Galileo system by the Europe Union. In order to determine the locations of an object, satellite-based systems require the object be equipped with a specially-designed receiver that can receive satellite signals using pre-defined channels. A receiver measures the travel time from satellites and computes the distances. If an receiver could receive signals from at least three satellites, it can determine its 3D position using *triangulation*. In practice, because the internal clock in a receiver is usually imperfect, a fourth satellite is needed to resolve the clock error.

The satellite-based systems can provide location information at almost any place on the earth. For state-of-the-art GPS receivers, the location errors could be as small as a few meters, given enough visible satellites. However, when a receivers are indoor or close to tall buildings, the location errors could be much bigger, or even worse, receivers may fail to localize. This is the severe limitation of satellite-based systems.

WiFi-based location systems

In contrast with satellite-based systems, WiFi-based systems can potentially work both outdoors and indoors. For example, RADAR is an indoor location system based on WiFi signals [4]. It uses two methods to calculate locations from signal information. The first is to use a *signal propagation model*, which quantifies how wireless signal attenuates with distance. Then it estimates the distances from multiple access points from signal strengths. Triangulation can then be used to determine the location. However, signal strength is influenced by a number of factors other than distance, including obstacles, reflection, and refraction, so in practice it is virtually impossible to obtain an accurate propagation model. As a consequence, this method can only provide coarse location information. The second method is based on *fingerprinting.* This method works by building a database that maps each location cell to the signal statistics measured at that cell. After the database is built, location can be determined by mapping the signal information back. Fingerprinting can give good location accuracy, however, it requires intense manual work to build the mapping database. Therefore, it can hardly be applied at a large scale.

One large scale location system based on WiFi signals is the place lab, which works both indoors and outdoors [59, 61]. The place lab emphasizes the coverage of the system rather than the accuracy. The critical part of the place lab system is to build *beacon databases* that record the locations of the WiFi access points. These location data may come from the WiFi deployment specifications, or from the *war-drivers* who drive around recording both WiFi signals and GPS measurements. The place lab system can cover indoor places and many "urban canyons" where GPS does not work. It does not require any specific location hardware and thus have a cost advantage. However, the location information is less accurate and less reliable, and maintaining the up-to-date beacon databases is a very challenging task.

Mobile-phone-based location systems

Similar to WiFi-based systems, location systems based on mobile phone networks can also work both indoors and outdoors. There are two different architectures for mobile phone location systems: *station-based* and *client-based.* For station-based system, cell-phone companies track a phone user by measuring the wireless signal strength or time-of-flight at a number of base stations. The location information is used for emergency reasons or sold to the user for a fee. For client-based systems [112], a handset measures the signal strengths from a number of base stations and determines its locations, in a similar way as WiFi-based systems. Although the mobile phone systems have high coverage, they suffer from the problem of low accuracy — the average error at this time is about 100 meters. Station-based systems are relatively more accurate, but end users may have the concerns of privacy and cost. Client-based systems are cheaper and give end users more controls, but the handsets have to maintain the location databases and support complex programming interface.

1.4 Outline

The technical contents of the thesis are divided into two parts.

The first part is from Chapter 2 to Chapter 5. In this part, we develop a probabilistic framework for extracting and classifying activities from sequences of sensor readings. Our framework is based on discriminative models such as conditional random fields and relational Markov networks. In Chapter 2, we provide the background of these models and explain our extensions. We discuss the inference and learning techniques in Chapter 3 and Chapter 4, respectively. Then in Chapter 5, we demonstrate how this general framework can be applied to activity recognition. We focus on location-based recognition systems, but also present initial results of activity recognition using other sensors.

The second part consists of Chapter 6 and Chapter 7. The goal of this part is to develop generative models for learning and inferring people's transportation routines as well as indoor movement patterns. In Chapter 6, we build a hierarchical dynamic Bayesian network for estimating travel destinations, modes of transportation, and user errors from raw GPS measurements. We explain how to perform efficient inference and unsupervised learning in such a complicated model. Then in Chapter 7, we show how to apply similar techniques indoors with sparse and noise location sensors.

We conclude and discuss future work in Chapter 8. In Appendix A, we provide derivation details of some equations in the thesis.

Chapter 2

RELATIONAL MARKOV NETWORKS AND EXTENSIONS

In the first part of this thesis (Chapter 2 to Chapter 5), our goal is to develop a probabilistic framework that can extract and label high-level activities from sequences of sensor readings. This task can be described as a supervised learning problem: different activity patterns are learned automatically from the manually labeled data, and are then applied to data without labels. Because of the strong correlation between activities, traditional techniques that assume the independence between labels become inadequate. We build the framework upon the more recent development of the conditional random field (CRF) [58] and its relational counterpart, the relational Markov network (RMN) [104]. Compared with traditional classification models that label each sample independently (*e.g.*, logistic regression), CRF and RMN allow us to specify the relations between labels and to label all the data in a *collective* manner. However, existing CRF and RMN models do not meet all our needs. We make two extensions to RMN. First, we allow the specification of aggregate features, such as summations. Second, we extend the language to handle the case where the model structure depends on hidden labels. This chapter is focused on the syntax and semantics of the model, and the discussions of inference and learning are left to the next two chapters.

Note that CRF and RMN are examples of statistical models for *relational* data. In recent years, a number of other models have been proposed, including knowledge-based model construction [53, 50], stochastic logic programming [75], probabilistic relational models [35], Markov logic [95], probabilistic entity-relationship models [45], dynamic probabilistic relational models [96], and so on (see [36] for more discussions in this area). In this thesis, we only focus on CRF and RMN, although many techniques can be easily adapted to other models.

Throughout this chapter, we use a simple example of activity recognition to ground our

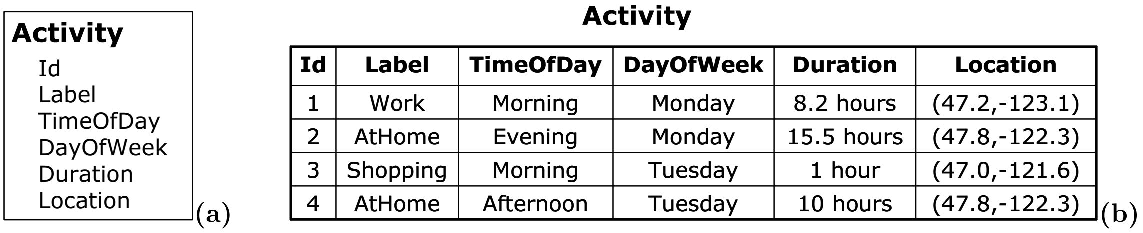

Activity

Id
Label
TimeOfDay
DayOfWeek
Duration
Location

(a)

Activity

Id	Label	TimeOfDay	DayOfWeek	Duration	Location
1	Work	Morning	Monday	8.2 hours	(47.2,-123.1)
2	AtHome	Evening	Monday	15.5 hours	(47.8,-122.3)
3	Shopping	Morning	Tuesday	1 hour	(47.0,-121.6)
4	AtHome	Afternoon	Tuesday	10 hours	(47.8,-122.3)

(b)

Figure 2.1: (a) Relational schema in the example of activity recognition. (b) An example of data instance.

discussions. In this example, there are a sequence of activities in the database. The schema of the database is shown in Fig. 2.1(a), which consists of only one table "Activity." Each activity instance includes its label, time of day, day of week, duration, and location. The attribute "Id" is the primary key and is sequentially incremented, so that we can get the neighbor relations between activities. Fig. 2.1(b) gives a sample instance of the database. During training, all the attributes are given and the data are used to learn a discriminative activity model. Then during test, the labels are unspecified and can be determined using the learned model.

This chapter is organized as follows. we first provide the background of CRF and RMN, then we discuss our extensions. The novel contributions of this chapter are the extensions of RMN to handle aggregate features and structural uncertainties.

2.1 Background

2.1.1 Conditional Random Field (CRF)

CRFs are undirected graphical models that were developed for labeling structured data [58]. Similar to hidden Markov models (HMMs), nodes in CRFs represent hidden states, denoted as $\mathbf{y}$, and observations, denoted as $\mathbf{x}$. These nodes, along with the connectivity structure imposed by undirected edges between them, define the conditional distribution $p(\mathbf{y}|\mathbf{x})$. Fig. 2.2 shows an example of CRF that corresponds to the data instance in Fig. 2.1(b). To infer the labels of activities, the CRF takes into account the evidence such as time of day, day of week, duration, and the pairwise relation between the labels. Note that in

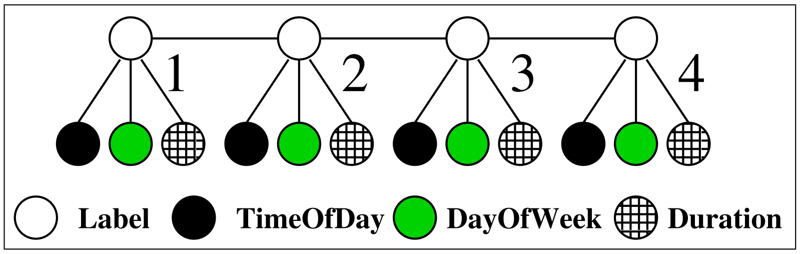

Figure 2.2: An example of CRF for activity recognition, where each Label represents a hidden state and TimeOfDay, DayOfWeek, and Duration are observations.

general CRFs can have arbitrary graph structures even though this example has a chain structure. Instead of relying on the Bayes rule, CRFs *directly* represent the conditional distribution over hidden states given the observations. Unlike HMMs, which assume that observations are independent given the hidden states, CRFs make no assumptions on the dependency structure between observations. CRFs are thus especially suitable for classification tasks with *complex* and *overlapped* features. CRFs have been successfully applied in areas such as natural language processing [58, 99], information extraction [87, 54], web page classification [104], and computer vision [56, 93].

The fully connected sub-graphs of a CRF are called *cliques*. For example, in Fig. 2.2, label 1 and its time of day is a clique, and label 1 and label 2 is another clique. Cliques play a key role in the definition of the conditional distribution represented by a CRF. Let $\mathbf{C}$ be the set of all cliques in a given CRF. Then, a CRF factorizes the conditional distribution into a product of *clique potentials* $\phi_c(\mathbf{x}_c, \mathbf{y}_c)$, where every $c \in \mathbf{C}$ is a clique of the graph and $\mathbf{x}_c$ and $\mathbf{y}_c$ are the observed and hidden nodes in such a clique. Clique potentials are functions that map variable configurations to non-negative numbers. Intuitively, a potential captures the "compatibility" among the variables in the clique: the larger the potential value, the more likely the configuration. For example, in the clique potential $\phi_c(\text{label } 1, \text{label } 2)$, the pair (AtHome,Work) should have a relatively high value, because it is common to go to work from home. Using clique potentials, the conditional distribution over the hidden states is written as

$$p(\mathbf{y} \mid \mathbf{x}) \quad = \quad \frac{1}{Z(\mathbf{x})} \prod_{c \in \mathbf{C}} \phi_c(\mathbf{x}_c, \mathbf{y}_c), \tag{2.1}$$

where $Z(\mathbf{x}) = \sum_{\mathbf{y}'} \prod_{c \in \mathbf{C}} \phi_c(\mathbf{x}_c, \mathbf{y}'_c)$ is the normalizing partition function. The computation of this partition function is exponential in the size of hidden states since it requires summation over all possible configurations. Hence, exact inference is possible for a limited class of CRF models only.

Without loss of generality, potentials $\phi_c(\mathbf{x}_c, \mathbf{y}_c)$ are described by log-linear combinations of *feature functions* $\mathbf{f}_c()$, *i.e.*,

$$\phi_c(\mathbf{x}_c, \mathbf{y}_c) \quad = \quad \exp\left\{\mathbf{w}_c^T \cdot \mathbf{f}_c(\mathbf{x}_c, \mathbf{y}_c)\right\}, \tag{2.2}$$

where $\mathbf{w}_c^T$ is the transpose of a weight vector $\mathbf{w}_c$, and $\mathbf{f}_c(\mathbf{x}_c, \mathbf{y}_c)$ is the feature vector. Each feature is a binary or real valued function and is typically designed by the user. As we will show in Chapter 4, the weights are learned from labeled training data. Intuitively, the weights represent the importance of different features for correctly identifying the hidden states. The log-linear feature representation (2.2) is very compact and guarantees the non-negativeness of potential values. We can now rewrite the conditional distribution (2.1) as

$$\begin{aligned} p(\mathbf{y} \mid \mathbf{x}) &= \frac{1}{Z(\mathbf{x})} \prod_{c \in \mathbf{C}} \exp\left\{\mathbf{w}_c^T \cdot \mathbf{f}_c(\mathbf{x}_c, \mathbf{y}_c)\right\} \\ &= \frac{1}{Z(\mathbf{x})} \exp\left\{\sum_{c \in \mathbf{C}} \mathbf{w}_c^T \cdot \mathbf{f}_c(\mathbf{x}_c, \mathbf{y}_c)\right\}. \end{aligned} \tag{2.3}$$

where (2.3) follows by moving the products into the exponent.

2.1.2 Relational Markov Networks (RMN)

In the CRF shown in Fig. 2.2, there are three pairwise cliques: (label 1, label 2), (label 2, label 3), and (label 3, label 4). Intuitively, because these cliques represent the same *type* of

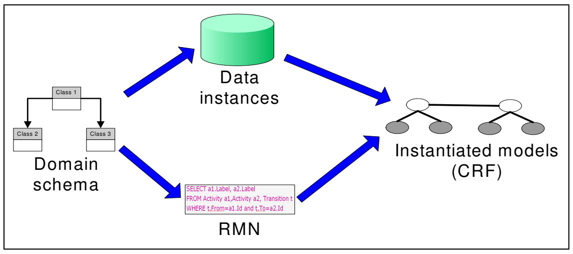

```
SELECT a1.Label, a2.Label
FROM Activity a1,Activity a2, Transition t
WHERE t.From=a1.Id and t.To=a2.Id
```

Figure 2.3: The relationship between RMN and CRF.

relation (*i.e.*, compatibility between adjacent activities), their features and weights should be tied. This idea is called *parameter sharing*. Relational Markov networks (RMNs) [104, 106] extend CRFs by providing a relational language for describing clique structures and enforcing parameter sharing at the template level. Fig. 2.3 explains the relationship between RMN and CRF. The *schema* (see Fig. 2.1(a) for an example) specifies the set of *classes* (*i.e.*, entity types) and *attributes* in each class. An attribute could be an observation, a hidden label, or a reference that specifies a relation between classes. A *data instance* $\mathcal{I}$ of a schema specifies the set of entities for each class and their attribute values (see Fig. 2.1(b)). RMN is defined over the domain schema. In a nutshell, an RMN consists of a set of *relational clique templates* $\mathcal{C}$, and each template $C \in \mathcal{C}$ is associated with a *potential function* Φ_C (represented as a log-linear combination of features). Given a data instance, the clique templates are used to instantiate the structure of CRF and the potential function of a template is shared by all the cliques from the template. Below we explain how the templates are defined and how the instantiation works.

A relational clique template $C \in \mathcal{C}$ is defined as a relational database query (*e.g.*, SQL), which selects tuples from the data instance $\mathcal{I}$. Formally, a basic template consists of three parts:

- **FROM** clause: indicating the classes that are involved in the template.

- **WHERE** clause: a boolean formula that defines the filtering criterion: only the data satisfying the criterion are relevant to the template.

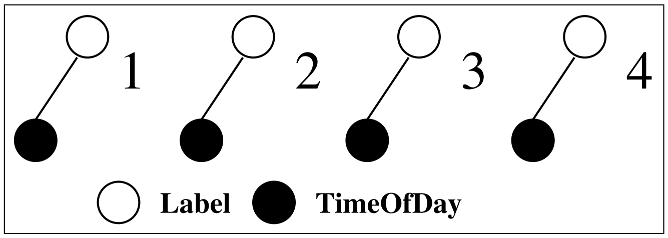

Figure 2.4: The instantiated CRF after using only the template of time of day.

- **SELECT** clause: the particular variables that are directly connected by the template.

By applying the query to a data instance $\mathcal{I}$, we get the query result $\mathcal{I}(C)$. Each tuple $\mathbf{v}_C \in \mathcal{I}(C)$ generates a clique in the instantiated CRF. For example, the following template captures the relation between an activity label and its time of day:

SELECT Label, TimeOfDay

FROM Activity .

Given the data instance in Fig. 2.1(b), this query selects four tuples and each tuple consists of an activity label and corresponding time of day, which are then connected in the instantiated CRF, as shown in Fig. 2.4. As another example, the template capturing this relation between adjacent activities is defined as

SELECT a1.Label, a2.Label

FROM Activity a1, Activity a2

WHERE a1.Id + 1 = a2.Id ,

where the adjacency is encoded in the values of the primary key "Id." If we apply this pairwise template as well as all the local templates including time of day, day of week, and duration, we get the CRF in Fig. 2.2.

After the structure of an instantiated CRF is generated, the clique potential of a template is shared by all the cliques built by that template. Thus we get a complete specification of the CRF.

In summary, given a specific data instance $\mathcal{I}$, an RMN defines a conditional distribution $p(\mathbf{y}|\mathbf{x})$ by instantiating the CRF. The cliques of the unrolled network are built by applying each clique template $C \in \mathcal{C}$ to the instance, which can result in several cliques per template. All cliques that originate from the same template must share the same feature function $\mathbf{f}_C(\mathbf{x}_C, \mathbf{y}_C)$ and weights $\mathbf{w}_C$. From (2.1), we can write the conditional distribution as

$$\begin{aligned} p(\mathbf{y} \mid \mathbf{x}) &= \frac{1}{Z(\mathbf{x})} \prod_{C \in \mathcal{C}} \prod_{(\mathbf{x}_C, \mathbf{y}_C) \in \mathcal{I}(C)} \phi_C(\mathbf{x}_C, \mathbf{y}_C) \\ &= \frac{1}{Z(\mathbf{x})} \prod_{C \in \mathcal{C}} \prod_{(\mathbf{x}_C, \mathbf{y}_C) \in \mathcal{I}(C)} \exp\{\mathbf{w}_C^T \cdot \mathbf{f}_C(\mathbf{x}_C, \mathbf{y}_C)\} \\ &= \frac{1}{Z(\mathbf{x})} \exp\{\mathbf{w}^T \cdot \mathbf{f}(\mathbf{x}, \mathbf{y})\}. \qquad (2.4) \end{aligned}$$

Eq. (2.4) follows by moving the products into the exponent and combining all summations into $\mathbf{w}$ and $\mathbf{f}$, where $\mathbf{w}$ and $\mathbf{f}$ are concatenations from the $K = |\mathcal{C}|$ templates:

$$\mathbf{w} = \left(\mathbf{w}_{C_1}, \cdots, \mathbf{w}_{|C_K|}\right)^T, \qquad (2.5)$$

and

$$\mathbf{f}(\mathbf{x}, \mathbf{y}) = \left(\sum_{(\mathbf{x}_{C_1}, \mathbf{y}_{C_1}) \in \mathcal{I}(C_1)} \mathbf{f}_{C_1}(\mathbf{x}_{C_1}, \mathbf{y}_{C_1}), \cdots, \sum_{(\mathbf{x}_{C_K}, \mathbf{y}_{C_K}) \in \mathcal{I}(C_K)} \mathbf{f}_{C_K}(\mathbf{x}_{C_K}, \mathbf{y}_{C_K}) \right)^T \qquad (2.6)$$

Intuitively, $\mathbf{f}(\mathbf{x}, \mathbf{y})$ are the counts (sums) of all the feature values in the instantiated CRF, which play an important role for parameter learning (see Chapter 4).

2.2 Extensions of Relational Markov Networks

In this section, we make two extensions to the original RMNs: one extension is aggregate features, and the other is structural uncertainty. The extensions are motivated by our work on activity recognition, which will be illustrated in Chapter 5.

2.2.1 Aggregate Features

In most machine learning tasks, we must encode human knowledge into the models. Many sources of knowledge can be described using aggregate functions, such as count (*i.e.*, cardinality of a set), sum, mean, variance, median, maximum, and minimum. For instance, in an image the color variance of the same type of objects is usually small; in a sentence the numbers of noun phrases and verb phrases could be related; and in human activity recognition, we know that most people only have one lunch and one dinner everyday. How can this type of knowledge help the labeling of an individual object, phrase, or activity? In this section, we extend RMN to encode such aggregate features that can be used for the inference of individual labels. To achieve this, we extend the syntax of relational clique templates as follows:

- First, we allow *aggregates* of tuples, such as COUNT(), SUM(), MEAN(), and MEDIAN() in the **SELECT** clause. Therefore, we can group tuples using **GROUP BY** clause and define potentials over aggregates of the groups.

- Second, the **WHERE** clause can include label attributes. Because labels are hidden during inference, such templates can generate cliques that potentially involve all the tuples.

We use a concrete example to illustrate how such aggregate templates can be used to instantiate CRFs. For instance, to have a *soft* constraint that limits the number of “DiningOut” activity per day of week, we can define the following clique template:

SELECT COUNT(*)
FROM Activity
WHERE Label = DiningOut
GROUP BY DayOfWeek ,

where the **GROUP BY** clause groups tuples with the same DayOfWeek. The potential function of this template indicates the likelihood of each possible count. For example, we can define the potential function as a geometric distribution (a discrete counterpart of the exponential distribution) to penalize big counts.

To illustrate how to unroll the aggregate template, we apply the above SQL query to the data in Fig. 2.1(b). The instantiated CRF is shown in Fig. 2.5. This query results in two groups and an aggregate (count) node is created for each group (node “count 1” and “count 2”). We define local potentials for aggregate nodes using the template potential.

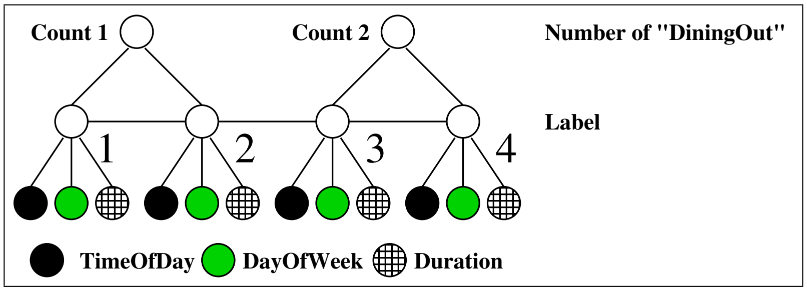

Figure 2.5: The instantiated CRF after using the aggregate features.

For instance, the local potential of count 1 could be a geometric distribution, which implies dining out multiple times a day is less likely. Then we build a clique that consists of each aggregate node and all the variables used for computing the aggregate, and the clique potential encodes the aggregation. For example, we build a clique over count 1 (c1), label 1 (l1), and label 2 (l2), and the potential function encodes the counting relation as:

$$\phi_c(l1, l2, c1) \quad = \quad \begin{cases} 1 & \text{if } c1 = \delta(l1 = DiningOut) + \delta(l2 = DiningOut); \\ 0 & \text{otherwise,} \end{cases} \tag{2.7}$$

To summarize, to instantiate an aggregate template, we create an aggregate node for each aggregate in the query result, and then we generates two types of cliques. The first type of clique is the standard: it connects the variables in the SELECT clause. This type of clique includes aggregate nodes and perhaps other regular nodes as well, and shares the clique potential defined in the template. The second type of clique connects each aggregate node with all the variables used for computing the aggregate. The potentials of such cliques encode the relation of aggregation, such as count or sum, so that they are often deterministic functions. Note that in practical applications, the second type of clique could be very large and make the inference very challenging. We will discuss efficient inference over aggregations in Section 3.3.

2.2.2 Structural Uncertainty

So far we have assumed we know the exact structures of the instantiated CRFs and thus the only uncertainties in our models are the hidden labels. However, in many domains there may be *structural uncertainty* [81, 34]. One example is the *reference uncertainty* [34], *i.e.*, the reference relations between the entities could be unknown. In this section we discuss another type of structural uncertainty, called *instance uncertainty.* Such uncertainties could appear when the existence of objects depends on hidden variables. For instance, suppose in the running example we have a new class “Restaurant” that stores the list of restaurants the person has been to. If all the activity labels are given, we can simply generate the list of restaurants based on the locations of “DiningOut” activities. However, since the activity labels are unknown, the instances in “Restaurant” and thereby the structure of the unrolled model are not fixed. In general, enumerating all the possible structures is intractable, so we only consider a small set of structures based on certain heuristics. For example, we could use the most likely configuration of the labels or the top n configurations to generate the model structures. To encode such heuristics in our model , we add a new keyword BEST(n) in the RMN syntax to specify the best n configurations in a query; thus BEST(1) is the most likely configuration.

As an example, the following template generates the instances in “Restaurant” from the most likely configuration of activity labels:

INSERT INTO Restaurants (Location)
SELECT Location
FROM BEST(1) Activity
WHERE Label = DiningOut.

When this template is used, the most likely sequence of labels is first inferred. Based on the most likely sequence, we can find the “DiningOut” activities and insert those locations to the set of “Restaurant.” Then we can instantiate the complete CRF involving both activities and restaurants. We may repeat this procedure until the structure converges, as will be discussed in Chapter 5. We can also use BEST(n) ($n > 1$) to generate n sets of “Restaurant” and thereby n different model structures. In that case, we could perform inference in the n models separately and select the "best" model based on certain criterion. However, the discussion of model selection in RMNs is beyond the scope of this thesis.

The extension of instance uncertainty greatly enhances the applicability of RMN. As another example, we can express the *segmentation* of temporal sequences using clique templates. Suppose we have a sequence of temporal objects stored in table "TemporalSequence." Each temporal object consists of a hidden label, a timestamp, *etc.* The goal of segmentation is to chop the sequence into a list of segments so that the temporal objects within each segment are consecutive and have identical label. This procedure can be represented using the following template:

```
INSERT INTO Segment (Label, StartTime, EndTime)
SELECT Label, MIN(Timestamp), MAX(Timestamp)
FROM BEST(1) TemporalSequence
GROUP CONSECUTIVELY BY Label.
```

The input to this template is the tuples in TemporalSequence, and the output is the tuples in table Segment. Each segment consists of a start time, an end time, and a label of that segment. Because the hidden variable "Label" appear in the "GROUP BY" clause, we again have the problem of instance uncertainty. To deal with it, we indicate BEST(1) so that the segmentation is based on the most likely labels. Note in the "GROUP BY" clause we add a new keyword "CONSECUTIVELY." This extension makes sure the temporal objects in a group are alway consecutive.

2.3 Summary

In this chapter, we began with the discussion of the conditional random field (CRF) model, a probabilistic model developed for structured data. Then we explained the relational Markov network (RMN) model that defines CRF at the template level. However, we found the original RMN is inadequate to define all the features in activity recognition. So we have made two extensions in this chapter: aggregate features and instance uncertainty.

Chapter 3

INFERENCE IN RELATIONAL MARKOV NETWORKS

In last chapter, we have demonstrated that the relational Markov network (RMN) is a very flexible and concise framework for defining features that can be used in the activity recognition context. After we have specified an RMN, there are still two essential tasks to do: inference and learning. In this chapter we discuss the inference, and the learning is left to the next chapter. The novel contributions in this chapter are the efficient inference algorithms for aggregate features, such as the application of Fast Fourier Transform (FFT) for summation features and the local MCMC algorithm that can be applied to generic aggregates.

The task of inference in the context of RMN is to infer the hidden values (*e.g.*, activity labels) from the observations (*e.g.*, time of day, duration, *etc.*). Because the correlations between the hidden labels, we would like to perform *collective classification* to infer their values simultaneously. Given a model of RMN including the set of features and their weights (we will discuss how to estimate the weights in next chapter), we first instantiate the CRF from the data instance, as discussed in Chapter 2, then we do inference over the instantiated CRF. Exact inference in a general Markov network (including CRF) is NP-hard [19], so it often becomes intractable in practice. In this chapter, we first discuss two widely used approximated algorithms – Markov Chain Monte Carlo (MCMC) and belief propagation (BP), and then we present optimized inference algorithms for aggregate features.

Note that the inference in a CRF could have two meanings: to estimate the posterior distribution of each hidden variable, and to estimate the most likely configuration of the hidden variables (*i.e.*, the maximum aposteriori, or MAP, estimation). Here we focus on posterior distribution estimation; we briefly discuss the MAP inference in the section of belief propagation.

3.1 Markov Chain Monte Carlo (MCMC)

When the exact form of the posterior distribution $p(\mathbf{y} \mid \mathbf{x})$ is difficult to estimate, we could approximate it by drawing enough samples from $p(\mathbf{y} \mid \mathbf{x})$ and simply counting the frequencies. This is the basic idea of *Monte Carlo* approaches. However, because the state space of $p(\mathbf{y} \mid \mathbf{x})$ is exponential to the number of hidden variables, it often becomes prohibitive to draw samples independently. One strategy is to generate samples using a Markov chain mechanism, which is called *Markov Chain Monte Carlo* (MCMC). The basic idea of MCMC is to start with some point in the state space, sample the next point based on the current point and a given transition matrix (or transition kernel for continuous state space), and repeat sampling until it has enough samples. The transition matrix must be carefully designed so that the process can efficiently obtain enough samples from the *target distribution* $p(\mathbf{y} \mid \mathbf{x})$. There exist a large variety of MCMC algorithms, which have been widely used in statistics, economics, physics and computer science [38, 1, 82]. In this section we give a brief introduction to applying MCMC for CRF inference. Specifically, we discuss how to initialize MCMC samples, how to generate new samples, when to stop the process, and how to approximate posterior distributions from samples.

- **Initialization:** The exact initial point is usually not important. A simple way to get started is to randomly sample each hidden label.

- **State transition:** Given the current configuration $\mathbf{y}^{(i)}$, we sample the next configuration $\mathbf{y}^{(i+1)}$ using a specific transition matrix. The design of the transition matrix is key to the correctness and efficiency of the algorithm. The following three strategies are often used:

  Gibbs sampling: The Gibbs sampler [33] flips one label at a time, by conditioning on all other labels. That is, the labels of $\mathbf{y}^{(i+1)}$ are identical to those of $\mathbf{y}^{(i)}$ except for one component j. Specifically, we obtain $\mathbf{y}^{(i+1)}$ as

$$\begin{cases} y_{j'}^{(i+1)} = y_{j'}^{(i)} \quad \text{if } j' \neq j; \\ y_j^{(i+1)} \sim p(y_j \mid \mathbf{y}_{-j}^{(i)}, \mathbf{x}) = p\left(y_j \mid \mathrm{MB}^{(i)}(y_j)\right), \end{cases} \tag{3.1}$$

where $\mathbf{y}_{-j}$ stand for all the labels except label y_j and $\mathrm{MB}(y_j)$ is the *Markov blanket* of label y_j, which contains the immediate neighbors of y_j in the CRF graph. The conditional distribution $p\left(y_j \mid \mathrm{MB}^{(i)}(y_j)\right)$ is usually easy to compute and to sample from. Sometimes it is more efficient to flip a block of variables at a time, and thus we get *block* Gibbs sampler.

Metropolis-Hastings sampling: A Metropolis-Hastings (MH) sampler [43, 72] uses a *proposal distribution* $q(\mathbf{y}' \mid \mathbf{y}^{(i)}, \mathbf{x})$ to sample a candidate configuration $\mathbf{y}'$. To guarantee the desired target distribution, the next configuration $\mathbf{y}^{(i+1)}$ is set to the candidate $\mathbf{y}'$ with an acceptance probability, defined as:

$$\begin{aligned} a(\mathbf{y}', \mathbf{y}^{(i)}) &= \min\left\{1, \frac{p(\mathbf{y}' \mid \mathbf{x}) q(\mathbf{y}^{(i)} \mid \mathbf{y}', \mathbf{x})}{p(\mathbf{y}^{(i)} \mid \mathbf{x}) q(\mathbf{y}' \mid \mathbf{y}^{(i)}, \mathbf{x})}\right\} && (3.2) \\ &= \min\left\{1, \frac{\exp\{\mathbf{w}^T \cdot \mathbf{f}(\mathbf{x}, \mathbf{y}')\}}{\exp\{\mathbf{w}^T \cdot \mathbf{f}(\mathbf{x}, \mathbf{y}^{(i)})\}}\right\}, && (3.3) \end{aligned}$$

and otherwise $\mathbf{y}^{(i+1)} = \mathbf{y}^{(i)}$. To get (3.3) from (3.2), we assume the proposal distribution is *symmetric*, *i.e.*, $q(\mathbf{y}^{(i)} \mid \mathbf{y}', \mathbf{x}) = q(\mathbf{y}' \mid \mathbf{y}^{(i)}, \mathbf{x})$, and we apply (2.4) in which the partition functions for $p(\mathbf{y}' \mid \mathbf{x})$ and $p(\mathbf{y}^{(i)} \mid \mathbf{x})$ are canceled out. The performance of MH sampling strongly depends on the choice of the proposal distribution, which could be some generic heuristics (*e.g.*, switching two labels) or could encode domain knowledge.

Mixtures of transition matrices: It is also possible to mix several transition matrices into an MCMC sampler. For example, at each time step, we can choose a Gibbs sampler with probability $\gamma (0 < \gamma < 1)$, and choose an MH sampler with probability $1 - \gamma$. If each individual sampler converges to the desired target distribution, so does the mixed one [109]. In some cases using mixtures of transition matrices could be much more efficient than using any individual sampler.

- **Stop criterion:** It is difficult to estimate how many samples are needed for a given problem, and there has no satisfactory theoretical answer yet. In practice people often make decisions by observing the MCMC outputs and performing some statistical tests, although none of these tests can give complete guarantee. One popular test is the G-R statistics [38]. Roughly speaking, the test runs parallel chains with different initial points, then it measures the sample variances within chains and across chains. If the two kinds of variances become very close, *i.e.*, G-R statistics approaches 1, then the test claims the chains have "forgotten" their initial points and converged to the target distribution.

- **Approximation of the distribution:** After the MCMC is stopped, we often discard an initial set of samples (*e.g.*, 20% of all samples) to reduce the starting biases. Then we can simply count the frequencies of labels for each hidden variable y_j, and the posterior distribution $p(y_j \mid \mathbf{x})$ is the normalized frequencies.

3.2 Belief Propagation (BP)

Another widely-used inference framework is *belief propagation* (BP) [115, 86], which works by sending local messages through the graph structure defined by a CRF. BP generates provably correct results if the CRF graph has a tree structure. If the graph contains loops, in which case BP is called *loopy* BP, then the algorithm is only approximate and might not even converge [86, 78]. Fortunately, in practice loopy BP often converges to good approximates and has been successfully applied in many applications [30, 28]. In this section, we discuss the (loopy) BP algorithm in the context of *pairwise* CRFs, which are CRFs that only contain cliques of size two. This is not a restriction, since non-pairwise CRFs can be easily converted to pairwise ones [115]. Note that before running the inference algorithm, it is possible to remove all observed nodes $\mathbf{x}$ by merging their values into the corresponding potentials; that is, a potential $\phi(\mathbf{x}, \mathbf{y})$ can be written as $\phi(\mathbf{y})$ because $\mathbf{x}$ is fixed. Therefore, the only potentials in a pairwise CRF are local potentials, $\phi(y_i)$, and pairwise potentials, $\phi(y_i, y_j)$.

Corresponding to the two types of inference problems, there are two types of BP algorithms: *sum-product* for posterior estimation and *max-product* for MAP estimation.

3.2.1 Sum-product for Posterior Estimation

In the BP algorithm, we introduce a "message" $m_{ij}(y_j)$ for each pair of neighbors y_i and y_j, which is a distribution (not necessarily normalized) sent from node i to its neighbor j about which state variable y_j should be in. The messages propagate through the CRF graph until they (possibly) converge, and the marginal distributions can be estimated from the stable messages. A complete BP algorithm defines how to initialize messages, how to update messages, how to schedule the order of updating messages, and when to stop passing messages.

- **Message initialization:** Usually all messages $m_{ij}(y_j)$ are initialized as uniform distributions over y_j.

- **Message update rule:** The message $m_{ij}(y_j)$ sent from node i to its neighbor j is updated based on local potentials $\phi(y_i)$, the pairwise potential $\phi(y_i, y_j)$, and all the messages to i received from i's neighbors other than j (denoted as $n(i) \setminus j$). More specifically, for sum-product, we have

$$m_{ij}(y_j) \quad = \quad \sum_{y_i} \phi(y_i)\phi(y_i, y_j) \prod_{k \in n(i) \setminus j} m_{ki}(y_i) \tag{3.4}$$

- **Message update order:** The algorithm iterates the message update rule until it (possibly) converges. Usually at each iteration, it updates each message once, and the specific order is not important (although it might affect the convergence speed).

- **Convergence conditions:** To test whether the algorithm converges at an iteration, for each message, BP measures the difference between the old message and the updated one, and the convergence condition is met when all the differences are below a given threshold ϵ. More formally, the condition is

$$||m_{ij}(y_j)^{(k)} - m_{ij}(y_j)^{(k-1)}|| < \epsilon, \forall i, \text{ and } \forall j \in n(i) \tag{3.5}$$

where $m_{ij}(y_j)^{(k)}$ and $m_{ij}(y_j)^{(k-1)}$ are the messages after and before iteration k, respectively.

In the sum-product algorithm, after all messages converge, it is easy to calculate the marginals of each node and each pair of neighboring nodes as

$$p(y_i \mid \mathbf{x}) \propto \phi(y_i) \prod_{j \in n(i)} m_{ji}(y_i) \tag{3.6}$$

$$p(y_i, y_j \mid \mathbf{x}) \propto \phi(y_i)\phi(y_j)\phi(y_i, y_j) \prod_{k \in n(i)\setminus j} m_{ki}(y_i) \prod_{l \in n(j)\setminus i} m_{lj}(y_j) \tag{3.7}$$

The above algorithm can be applied to any topology of pairwise CRFs. When the network structure does not have a loop (such as a tree), the obtained marginals are guaranteed to be exact. When the structure has loops, empirical experiments show that loopy BP often converges to a good approximation of the correct posterior.

When the network structure does not have any loops, we do not have to initialize all the messages as uniforms. Instead, we start the BP with the nodes at the edge of the graph (*i.e.*, nodes with only one neighbor), and compute a message $m_{ij}(y_j)$ only when all the messages on the right side of (3.4) are available. By doing this, the algorithm converges by only computing each message once, and the results are guaranteed to be exact.

3.2.2 Max-product for MAP Estimation

We denote the messages sent in the max-product algorithm as $m_{ij}^{max}(y_j)$. The whole algorithm of max-product is very similar to the sum-product, except that in the message update rule the summation is replaced by maximization. The new rule becomes

$$m_{ij}^{max}(y_j) = \max_{y_i} \phi(y_i)\phi(y_i, y_j) \prod_{k \in n(i)\setminus j} m_{ki}^{max}(y_i) \tag{3.8}$$

We can run the max-product algorithm the same as sum-product. After the algorithm converges, we calculate the MAP belief at each node y_i as

$$b(y_i) \quad \propto \quad \phi(y_i) \prod_{j \in n(i)} m_{ji}^{max}(y_i) \tag{3.9}$$

Suppose there is a unique MAP configuration $\mathbf{y}^*$. Then each component of $\mathbf{y}^*$ is simply the most likely value in MAP belief:

$$y_i^* \quad = \quad \underset{y_i}{\operatorname{argmax}}\, b(y_i) \tag{3.10}$$

3.3 Efficient Inference with Aggregate Features

In Section 2.2, we extend the original RMN to model aggregate features, such as summation. Although the syntax is fairly simple, those aggregate features could generate cliques that contain all nodes over which the aggregation is performed. Because the size of the potential is exponential to the number of variables in the aggregation, those large cliques can easily make standard (loopy) BP intractable. In these cases, we could use MCMC for inference. However, standard MCMC algorithms, such as Gibbs sampling, often converge very slow in complex models, and developing customized and efficient transition matrices is extremely challenging. For example, we initially applied an MCMC algorithm for location-based activity recognition that uses a mixture of Gibbs sampler and MH sampler [66]. However, we found such Monte Carlo algorithms usually scale up to only a few hundred variables in an aggregation. Here we present two more efficient inference algorithms for aggregate features. The first is specifically developed for *summation* features, by combining BP and the Fast Fourier Transform (FFT). Summation features are very common and some other aggregate features, such as count and average, can also be represented as summations. The new algorithm can easily handle thousands of variables [65]. In the second algorithm, we apply MCMC within the framework of BP. That is, we use MCMC locally to compute the “hard” messages, while we still compute other messages in analytical forms. This new technique, we call it *local* MCMC, is very general and can be applied to a variety of aggregate features.

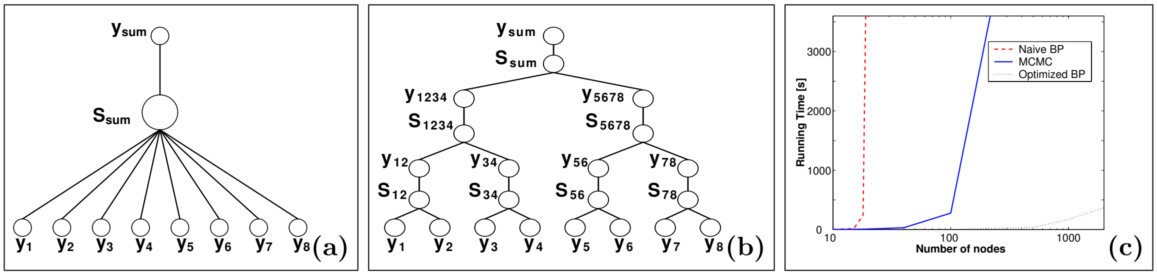
$\mathbf{y}_{sum}$
S_{sum}
$\mathbf{y}_1$ $\mathbf{y}_2$ $\mathbf{y}_3$ $\mathbf{y}_4$ $\mathbf{y}_5$ $\mathbf{y}_6$ $\mathbf{y}_7$ $\mathbf{y}_8$
(a)
$\mathbf{y}_{sum}$
S_{sum}
$\mathbf{y}_{1234}$
S_{1234}
$\mathbf{y}_{5678}$
S_{5678}
$\mathbf{y}_{12}$ $\mathbf{y}_{34}$ $\mathbf{y}_{56}$ $\mathbf{y}_{78}$
S_{12} S_{34} S_{56} S_{78}
$\mathbf{y}_1$ $\mathbf{y}_2$ $\mathbf{y}_3$ $\mathbf{y}_4$ $\mathbf{y}_5$ $\mathbf{y}_6$ $\mathbf{y}_7$ $\mathbf{y}_8$
(b)
Naive BP
MCMC
Optimized BP
Running Time [s]
3000
2000
1000
0
10
100
1000
Number of nodes
(c)

Figure 3.1: (a) Pairwise CRF that represents $\mathbf{y}_{sum} = \sum_{i=1}^{8} \mathbf{y}_i$; (b) Summation tree that represents $\mathbf{y}_{sum} = \sum_{i=1}^{8} \mathbf{y}_i$; (c) Computation time for summation cliques versus the number of nodes in the summation. The S_i's in (a) and (b) are auxiliary nodes to ensure the summation relation

3.3.1 Optimized summation templates using FFT

The aggregate features defined using RMN generate cliques that contain all nodes over which the aggregation is performed. To apply BP algorithm, we first convert the unrolled model into a pairwise CRF by introducing auxiliary variables [115], as shown in Fig. 3.1(a). The potential functions of the auxiliary variables encode the aggregation. Because of the high dimensionality of those aggregate potentials, standard message updates (Eq. (3.4)) often become intractable.

To handle summation cliques with potentially large numbers of addends, our inference dynamically builds a *summation tree*, which is a pairwise Markov network as shown in Fig. 3.1(b). In a summation tree, the leaves are the original addends and each internal node $\mathbf{y}_{jk}$ represents the sum of its two children $\mathbf{y}_j$ and $\mathbf{y}_k$; this sum relation is encoded by an auxiliary node S_{jk}. The state space of S_{jk} consists of the joint (cross-product) state of its neighbors: $\mathbf{y}_j$, $\mathbf{y}_k$, and $\mathbf{y}_{jk}$. It is easy to see that the summation tree guarantees that the root $\mathbf{y}_{sum}$ equals $\sum_{i=1}^{n} \mathbf{y}_i$, where $\mathbf{y}_1$ to $\mathbf{y}_n$ are the leaves of the tree. To define the BP protocol for summation trees, we need to specify two types of messages: an *upward message* from an auxiliary node to its parent (*e.g.*, $m_{S_{12}\mathbf{y}_{12}}$), and a *downward message* from an auxiliary node to one of its two children (*e.g.*, $m_{S_{12}\mathbf{y}_1}$).

Upward message update: Starting with Eq. (3.4), we can update an upward message

$m_{S_{ij}\mathbf{y}_{ij}}$ as follows.

$$
\begin{aligned}
m_{S_{ij}\mathbf{y}_{ij}}(\mathbf{y}_{ij}) &= \sum_{\mathbf{y}_i,\mathbf{y}_j} \phi_S(\mathbf{y}_i,\mathbf{y}_j,\mathbf{y}_{ij})\; m_{\mathbf{y}_i S_{ij}}(\mathbf{y}_i)\; m_{\mathbf{y}_j S_{ij}}(\mathbf{y}_j) \\
&= \sum_{\mathbf{y}_i} m_{\mathbf{y}_i S_{ij}}(\mathbf{y}_i)\; m_{\mathbf{y}_j S_{ij}}(\mathbf{y}_{ij}-\mathbf{y}_i) \qquad (3.11)\\
&= \mathcal{F}^{-1}\left(\mathcal{F}(m_{\mathbf{y}_i S_{ij}}(\mathbf{y}_i))\cdot \mathcal{F}(m_{\mathbf{y}_j S_{ij}}(\mathbf{y}_j))\right) \qquad (3.12)
\end{aligned}
$$

where $\phi_S(\mathbf{y}_i,\mathbf{y}_j,\mathbf{y}_{ij})$ is the potential of S_{ij} encoding the equality $\mathbf{y}_{ij} = \mathbf{y}_i + \mathbf{y}_j$, *i.e.*, $\phi_S(\mathbf{y}_i,\mathbf{y}_j,\mathbf{y}_{ij})$ equals 1 if $\mathbf{y}_{ij} = \mathbf{y}_i + \mathbf{y}_j$ and 0 otherwise. (3.11) follows because all terms not satisfying the equality disappear. Therefore, message $m_{S_{ij}\mathbf{y}_{ij}}$ is the *convolution* of $m_{\mathbf{y}_i S_{ij}}$ and $m_{\mathbf{y}_j S_{ij}}$. (3.12) follows from the *convolution theorem*, which states that the Fourier transform of a convolution is the point-wise product of Fourier transforms [11], where $\mathcal{F}$ and $\mathcal{F}^{-1}$ represent the Fourier transform and its inverse, respectively. When the messages are discrete functions, the Fourier transform and its inverse can be computed efficiently using the Fast Fourier Transform (FFT) [11, 70]. The computational complexity of a summation using FFT is $O(k \log k)$, where k is the maximum number of states in $\mathbf{y}_i$ and $\mathbf{y}_j$.

Downward message update: We also allow messages to pass from sum variables downward to its children. This is necessary if we want to use the belief on sum variables (*e.g.*, knowledge on the count of "DiningOut" activities) to change the distribution of individual variables (*e.g.*, activity labels). From Eq. (3.4) we get the downward message $m_{S_{ij}\mathbf{y}_i}$ as

$$
\begin{aligned}
m_{S_{ij}\mathbf{y}_i}(\mathbf{y}_i) &= \sum_{\mathbf{y}_j,\mathbf{y}_{ij}} \phi_S(\mathbf{y}_i,\mathbf{y}_j,\mathbf{y}_{ij}) m_{\mathbf{y}_j S_{ij}}(\mathbf{y}_j) m_{\mathbf{y}_{ij} S_{ij}}(\mathbf{y}_{ij}) \\
&= \sum_{\mathbf{y}_j} m_{\mathbf{y}_j S_{ij}}(\mathbf{y}_j) m_{\mathbf{y}_{ij} S_{ij}}(\mathbf{y}_i+\mathbf{y}_j) \qquad (3.13)\\
&= \mathcal{F}^{-1}\left(\overline{\mathcal{F}}(m_{\mathbf{y}_j S_{ij}}(\mathbf{y}_j))\cdot \mathcal{F}(m_{\mathbf{y}_{ij} S_{ij}}(\mathbf{y}_{ij}))\right) \qquad (3.14)
\end{aligned}
$$

where (3.13) again follows from the sum relation. Note that the downward message $m_{S_{ij}\mathbf{y}_i}$ turns out to be the *correlation* of messages $m_{\mathbf{y}_j S_{ij}}$ and $m_{\mathbf{y}_{ij} S_{ij}}$. (3.14) follows from the *correlation theorem* [11], which is similar to the convolution theorem except, for correlation, we must compute the *complex conjugate* of the first Fourier transform, denoted as $\overline{\mathcal{F}}$. Again, for discrete messages, (3.14) can be evaluated efficiently using FFT.

At each level of a summation tree, the number of messages (nodes) is reduced by half and the size of each message is doubled. Suppose the tree has n upward messages at the bottom and the maximum size of a message is k . For large summation trees where $n \gg k$, the total complexity of updating the upward messages at all the $\log n$ levels follows now as

$$\sum_{i=1}^{\log n} \frac{n}{2^i} \cdot O\left(2^{i-1} k \log 2^{i-1} k\right) \quad = \quad O\left(\frac{n}{2} \sum_{i=1}^{\log n} \log 2^{i-1}\right) \quad = \quad O(n \log^2 n) \tag{3.15}$$

Similar reasoning shows that the complexity of the downward pass is $O(n \log^2 n)$ as well. Therefore, updating all messages in a summation clique takes $O(n \log^2 n)$ instead of time exponential in n, as would be the case for a non-specialized implementation of aggregation.

We empirically compare our FFT-based BP algorithm for summation cliques with inference based on MCMC and regular BP, using the model and data from [66]. In our experiments, the test accuracies resulting from using the different algorithms are almost identical. Therefore, we only focus on comparing the efficiency and scalability of summation aggregations. We show in Fig. 3.1(c) the running times for the different algorithms as the number of nodes in a summation clique increases. As can be seen, a naive implementation of BP becomes extremely slow for only 20 nodes, MCMC only works for up to a few hundreds nodes, while our algorithm can perform summation for $2,000$ variables within a few minutes.

3.3.2 Combining BP and Local MCMC for Aggregate Features

For summation features, we have developed efficient algorithm using FFT. However, for other aggregate features, this algorithm may not apply. In this section, we present an inference algorithm for complex models with generic aggregate features, by combining BP and MCMC. The rationale is the following: In such complex models, usually most BP messages can be computed efficiently in analytical forms except those involving aggregate features; thus we only need to compute those “hard” messages using MCMC and still compute others messages analytically. The essential part of this new framework is to develop *local* MCMC algorithms for any given aggregate feature. The new algorithm can be much more efficient than BP because it avoids the exponential complexity of computing aggregate messages; it can also be more efficient than traditional MCMC because the local MCMC only needs to deal with a single feature. For example, Gibbs sampling often does not work well for complicated models, but can be efficient enough for single aggregate relations. Furthermore, the modules of local MCMC algorithms can be reused in many different models. Since the number of frequently used aggregate functions is limited, it is possible to develop highly-optimized algorithms for each function.

In the following we explain how to efficiently compute messages using local MCMC. We use Gibbs sampling as an example, but the algorithm can be extended to other MCMC techniques. In Fig. 3.2(a), we show a pairwise CRF piece encoding a certain aggregate feature. During BP, we need to compute the messages from S_{agg} to $\mathbf{y}_{agg}$ and each $\mathbf{y}_i$. Denote $Y = \{\mathbf{y}_1, \ldots, \mathbf{y}_n, \mathbf{y}_{agg}\}$, and for any $\mathbf{y} \in Y$, we can compute the message as:

$$m_{S_{agg}\mathbf{y}}(\mathbf{y}) \quad \propto \sum_{\mathbf{y}' \in Y, \mathbf{y}' \neq \mathbf{y}} \phi(\mathbf{y}_1, \ldots, \mathbf{y}_n, \mathbf{y}_{agg}) \prod_{\mathbf{y}' \in Y, \mathbf{y}' \neq \mathbf{y}} m_{\mathbf{y}' S_{agg}}(\mathbf{y}') \tag{3.16}$$

where $\phi(\mathbf{y}_1, \ldots, \mathbf{y}_n, \mathbf{y}_{agg})$ is the potential encoding the aggregate equality, *i.e.*, $\phi(\mathbf{y}_1, \ldots, \mathbf{y}_n, \mathbf{y}_{agg})$ equals 1 if $\mathbf{y}_{agg} = agg(\mathbf{y}_1, \ldots, \mathbf{y}_n)$ and 0 otherwise. Standard nonparametric BP [102] requires a sampling procedure for each message, *i.e.*, we need to run MCMC $n + 1$ times to get all the messages in this piece of CRF. Fortunately, we can use a trick that requires only one Markov chain for all the messages. The trick works by multiplying $m_{\mathbf{y}S_{agg}}(\mathbf{y})$ on both sides of (3.16), and we get

$$m_{S_{agg}\mathbf{y}}(\mathbf{y}) m_{\mathbf{y}S_{agg}}(\mathbf{y}) \quad \propto \sum_{\mathbf{y}' \in Y, \mathbf{y}' \neq \mathbf{y}} \phi(\mathbf{y}_1, \ldots, \mathbf{y}_n, \mathbf{y}_{agg}) \prod_{\mathbf{y}' \in Y} m_{\mathbf{y}' S_{agg}}(\mathbf{y}') \tag{3.17}$$

Note that, on the right side of (3.17), the terms inside the summation sign are exactly the same for all $\mathbf{y} \in Y$. Therefore, instead of sample each message $m_{S_{agg}\mathbf{y}}(\mathbf{y})$ directly, we can run a single MCMC chain to estimate $m_{S_{agg}\mathbf{y}}(\mathbf{y}) m_{\mathbf{y}S_{agg}}(\mathbf{y})$ for any $\mathbf{y} \in Y$ and then we can compute each message easily.

The algorithm of local Gibbs sampler is describe in Alg. 3.1, which can be easily extended to other MCMC algorithms. Note that because of the deterministic aggregate relation, we

```
    inputs : Messages $m_{\mathbf{y}_{agg}S_{agg}}(\mathbf{y}_{agg})$ and $m_{\mathbf{y}_i S_{agg}}(\mathbf{y}_i), 1 \leq i \leq n$
    output: Messages $m_{S_{agg}\mathbf{y}_{agg}}(\mathbf{y}_{agg})$ and $m_{S_{agg}\mathbf{y}_i}(\mathbf{y}_i), 1 \leq i \leq n$
1.  Initialization: sample $\mathbf{y}_i \sim m_{\mathbf{y}_i S_{agg}}(\mathbf{y}_i), 1 \leq i \leq n$ and set $\mathbf{y}_{agg} = agg(\mathbf{y}_1, \dots, \mathbf{y}_n)$ ;
2.  for $k = 1, \dots, K$ iterations do
3.      for $i = 1, \dots, n$ do
4.          Compute conditional distribution
            $p(\mathbf{y}'_i \mid \mathbf{y}_{-i}) \propto m_{\mathbf{y}_{agg}S_{agg}}(agg(\mathbf{y}_{-i}, \mathbf{y}'_i)) m_{\mathbf{y}_i S_{agg}}(\mathbf{y}'_i)$ ;
5.          Sample $\mathbf{y}_i \sim p(\mathbf{y}'_i \mid \mathbf{y}_{-i})$ ;
6.      end
7.      Set $\mathbf{y}_{agg} = agg(\mathbf{y}_1, \dots, \mathbf{y}_n)$ ;
8.  end
9.  Estimate $m_{S_{agg}\mathbf{y}}(\mathbf{y}) m_{\mathbf{y}S_{agg}}(\mathbf{y}), \mathbf{y} \in \{\mathbf{y}_1, \dots, \mathbf{y}_n, \mathbf{y}_{agg}\}$ by frequency counting ;
10. Compute $m_{S_{agg}\mathbf{y}}(\mathbf{y}) = \frac{m_{S_{agg}\mathbf{y}}(\mathbf{y}) m_{\mathbf{y}S_{agg}}(\mathbf{y})}{m_{\mathbf{y}S_{agg}}(\mathbf{y})}, \mathbf{y} \in \{\mathbf{y}_1, \dots, \mathbf{y}_n, \mathbf{y}_{agg}\}$ ;
```

Algorithm 3.1: Computing aggregate messages using local Gibbs sampling

do not need to sample $\mathbf{y}_{agg}$, but can compute it from other components. At Step 4, the conditional distribution for component $\mathbf{y}_i$ is computed based on other components and the aggregate, which follows from (3.17). Then at Step 5, $\mathbf{y}_i$ is sampled from the conditional distribution. When all $\mathbf{y}_i$ are updated, we compute the value of $\mathbf{y}_{agg}$ at Step 7. After the sampling process, each $m_{S_{agg}\mathbf{y}}(\mathbf{y}) m_{\mathbf{y}S_{agg}}(\mathbf{y})$ is estimate based on the samples, and at the last step we compute each message $m_{S_{agg}\mathbf{y}}(\mathbf{y})$.

To evaluate our algorithm, we apply the algorithm to the model of mobile robot map building [69]. The goal of that project is to enhance metric maps with semantic information about types of objects in an environment, such as door, wall, and others. To do that, line segments are first extracted from laser-range scans and then fed into a classifier. The model takes into account the following evidence:

- Local features, such as the length of a line segment;

- Indentation between neighboring line segments (for example, wall-wall should have small indentations but wall-door should have larger indentations);

- Variance of the door widths in the same hallway, which can be modeled as a zero-mean Gaussian with learned standard deviation;

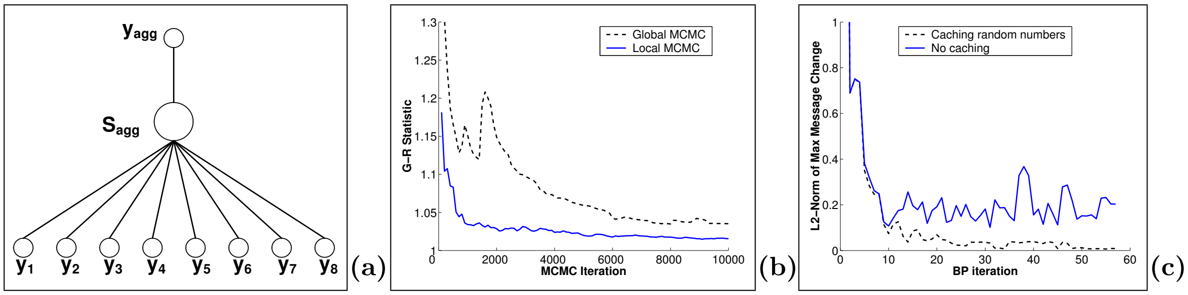

Figure 3.2: (a) A CRF piece in which $\mathbf{y}_{agg}$ is the aggregate of $\mathbf{y}_1, \ldots, \mathbf{y}_8$ and the aggregation is encoded in the potential of auxiliary variable S_{agg}; (b) Convergence comparison of local MCMC with global MCMC (G-R statistics approaching 1 indicates good convergence); (c) Comparison of the inference with and without caching the random numbers.

- Variance of the angles of the wall segments which can also be modeled using a zero-mean Gaussian;

Here the last two features involves aggregate function "variance" and can be implemented using the local MCMC algorithm.

In a preliminary experiment, we compare the convergence rate of the *local* and *global* Gibbs sampling. As shown in Fig. 3.2(b), for local Gibbs sampling, G-R statistics becomes less than 1.05 after a few hundred iterations while for global sampling it takes more than $6,000$ iterations. This is not a surprise because the local Gibbs sampling only involves a single feature, but the global Gibbs sampling takes into account all the features.

One issue of using local MCMC is that the sampling variance could potentially make BP instable. To reduce the sampling variance, we found it very useful to cache the random numbers *locally* and reuse them in later BP iterations. We compare the convergence of BP with and without random number caching. The convergence is measured by the maximal change between the messages before and after each iteration. A typical evolution of maximal changes is shown in Fig. 3.2(c). It is clear that by reusing the random numbers, BP converges much faster to a stable level.

3.4 Summary

The goal of this chapter is to discuss efficient inference algorithms for CRFs and RMNs. Exact inference often becomes intractable for practical models, so we have focused on approximated algorithms. We started with brief introductions to two widely used algorithms: Markov Chain Monte Carlo and (loopy) belief propagation. However, neither of them is efficient enough for models involving aggregate features. In this chapter we presented two optimized algorithms to accelerate the inference with aggregate features. Both algorithms are developed in the framework of belief propagation. For the widely used summation features, we can construct summation trees and apply FFT for message computation at each internal node of the tree. The complexity of the new algorithm is only $O(n \log^2 n)$ instead of exponential in n, where n is the number of variables in a summation. For other generic aggregate features, we proposed to use local MCMC to compute the messages through aggregations. By running sampling only on some portions of a model, the overall performance can be greatly improved.

Chapter 4

TRAINING RELATIONAL MARKOV NETWORKS

In last chapter, we have discussed a variety of inference techniques for conditional random fields (CRF) and relational Markov networks (RMN). In this chapter, we discuss the other task: learning the model parameters. In RMN, the goal of parameter learning is to determine the optimal weights of relational clique templates given the labeled training data. Similar to inference, the learning of RMN starts with instantiating CRFs from the training data, and then searches for the weights so as to optimize a certain criterion. In this chapter, we discuss three different criteria: maximum likelihood (ML), maximum pseudo-likelihood (MPL), and maximum per-label likelihood (as in boosting). The contributions of this chapter include a novel learning algorithm called *virtual evidence boosting*, an algorithm that simultaneously estimates the likelihood of train data and its gradient using MCMC, and empirical comparisons between different learning algorithms.

This chapter starts with the discussion of the ML estimation, which requires running the inference using MCMC or BP. In the second section we explain the MPL estimation. Then we present a new learning algorithm called virtual evidence boosting, which is a general approach for feature selection and parameter estimation for CRF and RMN. Finally we show experimental results on comparing different learning algorithms.

4.1 Maximum Likelihood (ML) Estimation

Given labeled training data $(\mathbf{x}, \mathbf{y})$, the conditional likelihood $p(\mathbf{y} \mid \mathbf{x})$ only depends on the feature weights $\mathbf{w}$, as can be seen in (2.4). From now on we will write the conditional likelihood as $p(\mathbf{y} \mid \mathbf{x}, \mathbf{w})$ to highlight its dependency on $\mathbf{w}$.

A common parameter estimation method is to search for the $\mathbf{w}$ that maximizes this conditional likelihood, or equivalently, that minimizes the *negative log-likelihood*, $-\log p(\mathbf{y} \mid \mathbf{x}, \mathbf{w})$ [58, 104, 66]. To avoid overfitting, one typically imposes a so-called *shrinkage prior* on the weights that keeps weights from getting too large. More specifically, we define the objective function to minimize as the following:

$$\begin{aligned} L(\mathbf{w}) &\triangleq -\log p(\mathbf{y} \mid \mathbf{x}, \mathbf{w}) + \frac{\mathbf{w}^T\mathbf{w}}{2\sigma^2} & (4.1) \\ &= -\mathbf{w}^T \cdot \mathbf{f}(\mathbf{x}, \mathbf{y}) + \log Z(\mathbf{x}, \mathbf{w}) + \frac{\mathbf{w}^T\mathbf{w}}{2\sigma^2} & (4.2) \end{aligned}$$

The rightmost term in (4.1) serves as a zero-mean, Gaussian prior with variance σ^2 on each component of the weight vector. (4.2) follows directly from (4.1) and (2.4). While there is no closed-form solution for minimizing (4.2), it can be shown that (4.2) is *convex* relative to $\mathbf{w}$. Thus, L has a global optimum which can be found using numerical gradient algorithms. The gradient of the objective function $L(\mathbf{w})$ is given by

$$\begin{aligned} \nabla L(\mathbf{w}) &= -\mathbf{f}(\mathbf{x}, \mathbf{y}) + \frac{\nabla Z(\mathbf{x}, \mathbf{w})}{Z(\mathbf{x}, \mathbf{w})} + \frac{\mathbf{w}}{\sigma^2} & (4.3) \\ &= -\mathbf{f}(\mathbf{x}, \mathbf{y}) + \frac{\sum_{\mathbf{y}'} \exp\{\mathbf{w}^T \cdot \mathbf{f}(\mathbf{x}, \mathbf{y}')\}\mathbf{f}(\mathbf{x}, \mathbf{y}')}{Z(\mathbf{x}, \mathbf{w})} + \frac{\mathbf{w}}{\sigma^2} & (4.4) \\ &= -\mathbf{f}(\mathbf{x}, \mathbf{y}) + \sum_{\mathbf{y}'} p(\mathbf{y}' \mid \mathbf{x}, \mathbf{w})\mathbf{f}(\mathbf{x}, \mathbf{y}') + \frac{\mathbf{w}}{\sigma^2} & (4.5) \\ &= -\mathbf{f}(\mathbf{x}, \mathbf{y}) + E_{p(\mathbf{y}' \mid \mathbf{x}, \mathbf{w})}[\mathbf{f}(\mathbf{x}, \mathbf{y}')] + \frac{\mathbf{w}}{\sigma^2} & (4.6) \end{aligned}$$

where (4.4) follows from the definition of partition function, $Z(\mathbf{x}, \mathbf{w}) = \sum_{\mathbf{y}'} \exp\{\mathbf{w}^T \cdot \mathbf{f}(\mathbf{x}, \mathbf{y}')\}$, (4.5) follows from the definition of the conditional likelihood, and in (4.6), the second term is expressed as an expectation over the distribution $p(\mathbf{y}' \mid \mathbf{x}, \mathbf{w})$. Therefore, the gradient is just the difference between the *empirical feature values* $\mathbf{f}(\mathbf{x}, \mathbf{y})$ and the *expected feature values* $E_{p(\mathbf{y}' \mid \mathbf{x}, \mathbf{w})}[\mathbf{f}(\mathbf{x}, \mathbf{y}')]$, plus a prior term. To compute the expected feature values it is necessary to run inference in the CRF using the current weights $\mathbf{w}$. Previous work has shown that straightforward gradient descent often converges slowly, but that modern numerical optimization algorithms, such as conjugate gradient or quasi-Newton techniques, can be much faster [99]. However, these techniques additionally require evaluating the objective values $L(\mathbf{w})$. To compute the objective values in (4.2) is not easy, because the partition function $Z(\mathbf{x}, \mathbf{w})$ requires us to enumerate all the configurations of hidden variables. In this section we describe how to get around this difficulty by using Monte-Carlo approximation or Bethe approximation.

4.1.1 MCMC-based ML Estimation

When MCMC is used for inference, the posterior distribution $p(\mathbf{y} \mid \mathbf{x}, \mathbf{w})$ is approximated using a set of M samples, $\mathbf{y}^{(i)}$, $1 \leq i \leq M$. Then the expected feature values $E_{p(\mathbf{y}'|\mathbf{x},\mathbf{w})}[\mathbf{f}(\mathbf{x}, \mathbf{y}')] \approx \frac{1}{M}\sum_{i=1}^{M} \mathbf{f}(\mathbf{x}, \mathbf{y}^{(i)})$. From (4.6), the gradient can be computed as

$$\begin{aligned} \nabla L(\mathbf{w}) &\approx -\mathbf{f}(\mathbf{x}, \mathbf{y}) + \frac{1}{M}\sum_{i=1}^{M} \mathbf{f}(\mathbf{x}, \mathbf{y}^{(i)}) + \frac{\mathbf{w}}{\sigma^2} \\ &= \frac{1}{M}\sum_{i=1}^{M} \Delta\mathbf{f}^{(i)} + \frac{\mathbf{w}}{\sigma^2} \end{aligned} \tag{4.7}$$

where $\Delta\mathbf{f}^{(i)} = \mathbf{f}(\mathbf{x}, \mathbf{y}^{(i)}) - \mathbf{f}(\mathbf{x}, \mathbf{y})$ is the difference between sampled feature values and the empirical feature values.

As we just said, it is more difficult to evaluate the objective value $L(\mathbf{w})$, which is necessary for advanced optimization techniques. The key idea is that, instead of evaluating the *absolute* values of $L(\mathbf{w})$, we only need to estimate their *relative* values for the purpose of ML estimation. And we can approximate the relative values quite efficiently using Monte Carlo approach [37]. More specifically, $L(\mathbf{w})$ can be approximated relative to $L(\tilde{\mathbf{w}})$, where $\tilde{\mathbf{w}}$ is the *reference weight vector*. We have (see Appendix A.1 for the derivation):

$$L(\mathbf{w}) = L(\tilde{\mathbf{w}}) + \log\left(\frac{1}{M}\sum_{i=1}^{M} \exp\left\{(\mathbf{w} - \tilde{\mathbf{w}})^T \cdot \Delta\tilde{\mathbf{f}}^{(i)}\right\}\right) + \frac{\mathbf{w}^T \cdot \mathbf{w} - \tilde{\mathbf{w}}^T \cdot \tilde{\mathbf{w}}}{2} \tag{4.8}$$

where $\Delta\tilde{\mathbf{f}}^{(i)} = \mathbf{f}(\mathbf{x}, \tilde{\mathbf{y}}^{(i)}) - \mathbf{f}(\mathbf{x}, \mathbf{y})$ is the difference between sampled feature values using $\tilde{\mathbf{w}}$ and the empirical feature values. It can be shown that the best approximation in (4.8) is obtained when $\tilde{\mathbf{w}}$ is near the optimal $\mathbf{w}$ [37]. We should take this into account and use better $\tilde{\mathbf{w}}$ whenever possible.

If we compare Eq. (4.7) and (4.8), we see both require the difference between the sampled feature values and the empirical feature values. But the samples in (4.8) are from

```
    inputs : the given weights $\mathbf{w}$
    output: the objective function value $L(\mathbf{w})$ and its gradient $\nabla L(\mathbf{w})$
    //Evaluate the gradient $\nabla L(\mathbf{w})$
1.  Run MCMC with $\mathbf{w}$ and get $M$ samples from $p(\mathbf{y} \mid \mathbf{x}, \mathbf{w})$ ;
2.  Get feature value difference $\Delta\mathbf{f}^{(i)} = \mathbf{f}(\mathbf{x}, \mathbf{y}^{(i)}) - \mathbf{f}(\mathbf{x}, \mathbf{y})$ for $1 \leq i \leq M$ ;
3.  Compute the gradient $\nabla L(\mathbf{w})$ using Eq. (4.7) ;
    //Evaluate the objective value $L(\mathbf{w})$
4.  if First time calling this function then
5.      $L(\tilde{\mathbf{w}}) = L(\mathbf{w}) = 0$; $\tilde{\mathbf{w}} = \mathbf{w}$ ;
6.      $\Delta\tilde{\mathbf{f}}^{(i)} = \Delta\mathbf{f}^{(i)}$ for $1 \leq i \leq M$ ;
7.  else
8.      Compute $L(\mathbf{w})$ using Eq. (4.8) ;
9.      if $L(\mathbf{w}) < L(\tilde{\mathbf{w}})$ then
10.         $L(\tilde{\mathbf{w}}) = L(\mathbf{w})$; $\tilde{\mathbf{w}} = \mathbf{w}$ ;
11.         $\Delta\tilde{\mathbf{f}}^{(i)} = \Delta\mathbf{f}^{(i)}$ for $1 \leq i \leq M$ ;
12.     end
13. end
```

Algorithm 4.1: MCMC-based algorithm for evaluating objective function and its gradient

the distribution $p(\mathbf{y} \mid \mathbf{x}, \tilde{\mathbf{w}})$ while the samples in (4.7) are from the distribution $p(\mathbf{y} \mid \mathbf{x}, \mathbf{w})$. As we will show, by picking the reference weight vector $\tilde{\mathbf{w}}$ in a specific way and caching the results, we can reuse the samples and simultaneously estimate both the objective value and its gradient .

The algorithm of evaluating objective function and its gradient using MCMC is shown in Alg. 4.1. The algorithm works as a function used by efficient optimization algorithms such as quasi-Newton or conjugate gradient. The input of the algorithm is the weight vector provided by the optimizer and the algorithm returns the estimated objective function and its gradient. To estimate the gradient, we use MCMC sampler to get M samples from the posterior distribution $p(\mathbf{y} \mid \mathbf{x}, \mathbf{w})$ (Step 1) and then calculate the difference between the sampled feature values and the empirical feature values (Step 2). In order to estimate the objective value, we keeps the up-to-now best estimator $\tilde{\mathbf{w}}$, along with $L(\tilde{\mathbf{w}})$ and $\Delta\tilde{\mathbf{f}}^{(i)}(1 \leq i \leq M)$. When the optimizer first calls this function, $\tilde{\mathbf{w}}$ is initialized as $\mathbf{w}$, and both $L(\tilde{\mathbf{w}})$ and $L(\mathbf{w})$ are set as 0 (Step 5). Therefore, all the objective values are relative to the objective value of initial weights. In later iterations, when we find a better $\mathbf{w}$ that makes

$L(\mathbf{w})$ less than $L(\tilde{\mathbf{w}})$, we update $\tilde{\mathbf{w}}$ with the new $\mathbf{w}$ (Step 10 and Step 11). Thus function value estimation becomes very efficient—it re-use the sampled feature values from gradient estimation. Moreover, we can get more accurate estimates as $\tilde{\mathbf{w}}$ approaches closer to the optimal weights, which is important for the optimizer to converge.

4.1.2 BP-based ML Estimation

We can also perform ML estimation using BP inference. Without loss of generality, we only consider the case where the instantiated CRFs are pairwise. At each step of optimization, BP inference gives the posterior distribution for each clique c, $p(\mathbf{y}'_c \mid \mathbf{x})$ (in Eq. (3.6) and Eq. (3.7)). Thus we get the expected feature values as

$$E_{p(\mathbf{y}'|\mathbf{x},\mathbf{w})}\left[\mathbf{f}(\mathbf{x},\mathbf{y}')\right] \;=\; \sum_{c\in\mathcal{C}} \mathbf{f}_c(\mathbf{x},\mathbf{y}'_c)p(\mathbf{y}'_c|\mathbf{x}) \tag{4.9}$$

where $\mathcal{C}$ denotes all the cliques in a CRF and $\mathbf{f}_c$ is the feature values counted on clique c. We can then compute the gradient using (4.6).

To approximate the objective value $L(\mathbf{w})$, we can use Bethe method [117]. Specifically, we approximate the partition function Z as

$$-\log Z \approx U_{Bethe} - H_{Bethe}, \tag{4.10}$$

where U_{Bethe} is called *Bethe average energy* and H_{Bethe} is called *Bethe entropy*, and they are computed as

$$U_{Bethe} \;=\; -\sum_{c\in\mathcal{C}}\sum_{\mathbf{y}'_c} p(\mathbf{y}'_c \mid \mathbf{x})\left(\mathbf{w}^T \cdot \mathbf{f}_c(\mathbf{x},\mathbf{y}'_c)\right),$$

and

$$H_{Bethe} \;=\; -\sum_{c\in\mathcal{C}}\sum_{\mathbf{y}'_c} p(\mathbf{y}'_c \mid \mathbf{x})\log p(\mathbf{y}'_c \mid \mathbf{x}) + \sum_{i=1}^{N}(d_i - 1)\sum_{y'_i} p(y'_i \mid \mathbf{x})\log p(y'_i \mid \mathbf{x}),$$

where i ranges over all the variables and d_i is the degree for variable i.

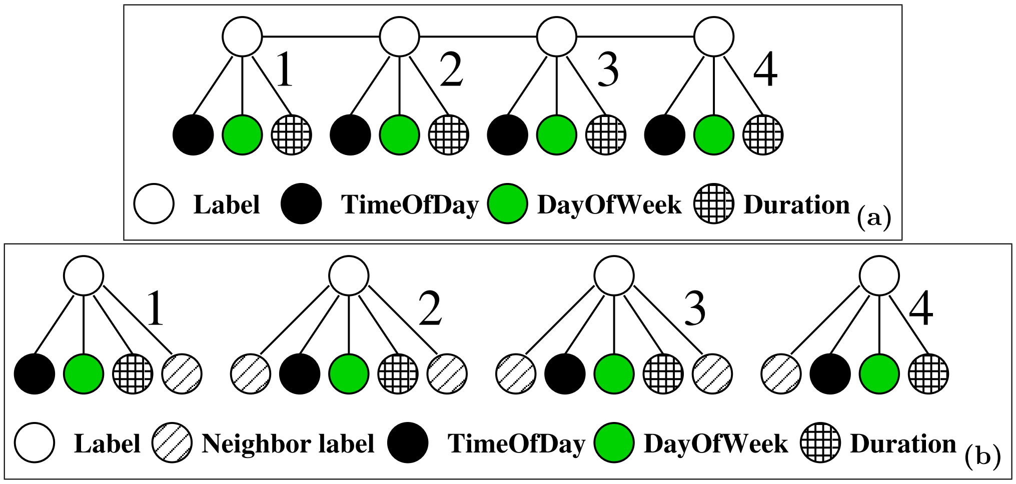

Figure 4.1: (a) Original CRF for learning; (b) Converted CRF for MPL learning by copying the true labels of neighbors as local evidence.

After we have an estimate of the partition function Z, we can approximate the objective values using (4.2). When the instantiated CRFs have no loops, the Bethe method gives the exact value of the objective values and thereby in theory the ML learning converges to the global optimum. When the CRFs do have loops, the Bethe method only gives approximated result; therefore, the learning may not converge to the optimum, or may not converge (even when the BP inference converges).

4.2 Maximum Pseudo-Likelihood (MPL) Estimation

A key assumption in traditional machine learning algorithms is the *independence* between hidden labels. RMN and CRF break this assumption by considering the mutual influence between labels. This breakthrough greatly enhances the expressiveness and flexibility, however, at a cost of more expensive learning. As discussed in last section, ML learning requires running an inference procedure at each iteration of the optimization, which can be very expensive even for approximated algorithms. To circumvent this cost, another learning algorithm was developed that instead maximizes the *pseudo-likelihood* of the training data (MPL) [9].

To give some intuitions on how MPL works, let's start with the CRF example discussed in Chapter 2. We show the model structure again in Fig. 4.1(a). MPL converts the original CRF to a CRF as shown in Fig. 4.1(b), where the *true* labels of neighbors (known during learning) are copied as local attributes. By doing this, the structure of the CRF is significantly simplified — it becomes a set of separated chunks where each chunk has only one hidden variable. MPL estimation is essentially the ML estimation on this simplified model. Specifically, MPL maximizes the following *pseudo-likelihood*:

$$pl(\mathbf{y} \mid \mathbf{x}, \mathbf{w}) \triangleq \prod_{i=1}^{n} p(y_i \mid \mathrm{MB}(y_i), \mathbf{w}) \tag{4.11}$$

Here, $\mathrm{MB}(y_i)$ is the Markov blanket of variable y_i, which contains the immediate neighbors of y_i in the CRF graph (note that the value of each node is known during learning). Thus, the pseudo-likelihood is the product of all the *local likelihoods*, $p(y_i \mid \mathrm{MB}(y_i), \mathbf{w})$. By representing the local likelihoods as log-linear combinations of features, we can rewrite the pseudo-likelihood as

$$pl(\mathbf{y} \mid \mathbf{x}, \mathbf{w}) = \prod_{i=1}^{n} \frac{1}{Z(\mathrm{MB}(y_i), \mathbf{w})} \exp\left\{\mathbf{w}^T \cdot \mathbf{f}(y_i, \mathrm{MB}(y_i))\right\}, \tag{4.12}$$

where $\mathbf{f}(y_i, \mathrm{MB}(y_i))$ is the local feature values involving variable y_i, and $Z(\mathrm{MB}(y_i), \mathbf{w}) = \sum_{y_i'} \exp\left\{\mathbf{w}^T \cdot \mathbf{f}(y_i', \mathrm{MB}(y_i'))\right\}$ is the *local* normalizing function. Therefore, computing pseudo-likelihood is much more efficient than computing likelihood $p(\mathbf{y}|\mathbf{x}, \mathbf{w})$, because pseudo-likelihood only requires computing local normalizing functions and avoids computing the global partition function $Z(\mathbf{x}, \mathbf{w})$.

Similar to ML, in practice we minimize the negative log-pseudo-likelihood plus a shrinkage prior, and the objective function becomes

$$\begin{aligned} PL(\mathbf{w}) &\triangleq -\log pl(\mathbf{y} \mid \mathbf{x}, \mathbf{w}) + \frac{\mathbf{w}^T\mathbf{w}}{2\sigma^2} && (4.13)\\ &= -\sum_{i=1}^{n} \log p(y_i \mid \mathrm{MB}(y_i), \mathbf{w}) + \frac{\mathbf{w}^T\mathbf{w}}{2\sigma^2} && (4.14)\\ &= \sum_{i=1}^{n} \left(-\mathbf{w}^T \cdot \mathbf{f}(y_i, \mathrm{MB}(y_i)) + \log Z(\mathrm{MB}(y_i), \mathbf{w})\right) + \frac{\mathbf{w}^T\mathbf{w}}{2\sigma^2} && (4.15) \end{aligned}$$

$PL(\mathbf{w})$ is a convex function (think $PL(\mathbf{w})$ as the ML objective function in the simplified model) and we can apply gradient-based algorithms to find $\mathbf{w}$ that minimizes $PL(\mathbf{w})$. The gradient of $PL(\mathbf{w})$ can be computed as

$$\nabla PL(\mathbf{w}) \;=\; \sum_{i=1}^{n} \Big(-\mathbf{f}(y_i, \mathrm{MB}(y_i)) + E_{p(y_i'|\mathrm{MB}(y_i),\mathbf{w})}\left[\mathbf{f}(y_i', \mathrm{MB}(y_i))\right]\Big) + \frac{\mathbf{w}}{\sigma^2}. \qquad (4.16)$$

As we can see, (4.16) can be expressed as the difference between empirical feature values and expected feature values, similar to (4.6). However, the key difference is that (4.16) can be evaluated very efficiently without running a complete inference procedure.

MPL has been shown to perform well in several domains [56, 95]. However, it is possible that the results of MPL differ significantly from the results of ML [37] and no general guidance has been given on when MPL can be safely used.

Finally, readers may notice that the simplified model as in Fig. 4.1(b) cannot be used for inference, since it assumes that the hidden states $\mathbf{y}$ are known.

4.3 Virtual Evidence Boosting

Boosting is a general approach for supervised learning and has been successfully applied in a lot of domains [29, 31]. Given the training data $(\mathbf{x}_1, \mathbf{y}_1)$, ..., $(\mathbf{x}_N, \mathbf{y}_N)$, where $\mathbf{x}_i$ is an observation vector and $\mathbf{y}_i$ is the label, boosting works by sequentially learning a set of weak classifiers and combining them for final decisions. Can we apply boosting to CRFs? At the first look, the answer seems to be no, since the boosting algorithms assume the *independence* between training examples but in CRFs the labels are dependent. However, we can overcome this difficulty by borrowing the idea of MPL; that is, we cut an instantiated CRF into individual patches (see Fig. 4.1(b)), and use these patches as training instances for boosting. Based on this idea, we introduce a novel learning algorithm, called *virtual evidence boosting* (VEB) [63], which combines boosting and CRF. The key difference to MPL, however, is that in the new algorithm the neighbor labels are not treated as observed, but as virtual evidence. This avoids over-estimating the neighborhood dependencies, as often happens to MPL.

VEB is a general approach for feature selection and parameter estimation in CRFs and

RMNs. This approach is able to

- simultaneously perform feature selection and parameter estimation;
- select compatible features between labels and thus learn *dependency structures* in the relational data;
- handle both discrete and continuous observations;
- and select various features in a *unified* and *efficient* manner, by simply running one iteration of BP and performing feature counting at each boosting iteration.

To develop the algorithm, we extend the standard boosting algorithms so that the input observations are either virtual evidences in the form of likelihood values or deterministic quantities.

4.3.1 Extending Boosting to Handle Virtual Evidence

While traditional boosting algorithms assume observation values be deterministic, in this section we extend them with *virtual evidence* [86], *i.e.*, an observation could have a distribution over its domain rather than a single, observed value. Specifically, we generalize the LogitBoost algorithm [31], which directly handles probabilities and is closely related to random field models. For simplicity, we will only explain LogitBoost and our extension for the binary classification case, *i.e.*, $\mathbf{y}_i \in \{0, 1\}$, but both can be easily extended to multi-class problems [31].

LogitBoost algorithm

LogitBoost works by minimizing the negative per-label-log-likelihood:

$$L(F) = -\sum_{i=1}^{N} \log p(\mathbf{y}_i) \tag{4.17}$$

where F refers to the *ensemble* of weak learners, *i.e.*, $F(\mathbf{x}) = \sum_{m=1}^{M} f_m(\mathbf{x})$, and $p(\mathbf{y}_i)$ is a short notation that represents the posterior probability of a true label *conditioned* on its evidences. We have

$$p(\mathbf{y}_i) = \begin{cases} \frac{e^{-F(\mathbf{x}_i)}}{e^{F(\mathbf{x}_i)}+e^{-F(\mathbf{x}_i)}} & \text{if } \mathbf{y}_i = 0; \\ \frac{e^{F(\mathbf{x}_i)}}{e^{F(\mathbf{x}_i)}+e^{-F(\mathbf{x}_i)}} & \text{if } \mathbf{y}_i = 1. \end{cases} \tag{4.18}$$

where we assume without loss of generality that ensembles are reverse for $\mathbf{y}_i = 1$ and 0. It is easy to identify the consistency between (4.18) and the logistic regression models, in which $e^{F(\mathbf{x}_i)}$ and $e^{-F(\mathbf{x}_i)}$ represent the *potentials* for $\mathbf{y}_i = 1$ and 0, respectively.

LogitBoost minimizes the objective function (4.17) respect to F using *Newton steps*. Given the current ensemble F, the next weak learner in a Newton step is obtained by solving the weighted least-square-error (WLSE) problem [31]:

$$f_m(\mathbf{x}) \quad = \quad \underset{f}{\operatorname{argmin}} \sum_{i=1}^{N} \alpha_i \left(f(\mathbf{x}_i) - z_i \right)^2 \tag{4.19}$$

where $\alpha_i = p(\mathbf{y}_i)(1 - p(\mathbf{y}_i))$ and $z_i = \frac{\mathbf{y}_i - 0.5}{p(\mathbf{y}_i)}$ are the *weight* and *working response* for sample i, respectively.

Extension with virtual evidence

To extend the LogitBoost with virtual evidence, we denote the training data as $(\mathbf{ve}(\mathbf{x}_1), \mathbf{y}_1)$, $\ldots$, $(\mathbf{ve}(\mathbf{x}_N), \mathbf{y}_N)$, where each virtual evidence $\mathbf{ve}(\mathbf{x}_i)$ is a given distribution over the observation domain $\{1, \ldots, X\}$ [1]. We again aim to minimize the negative per-label-log-likelihood, defined in (4.17). However, the computation of the posterior probability $p(\mathbf{y}_i)$ has to take the virtual evidence into account:

$$p(\mathbf{y}_i) = \begin{cases} \frac{\sum_{\mathbf{x}_i=1}^{X} \mathbf{ve}(\mathbf{x}_i) e^{-F(\mathbf{x}_i)}}{\sum_{\mathbf{x}_i=1}^{X} \mathbf{ve}(\mathbf{x}_i) e^{F(\mathbf{x}_i)} + \sum_{\mathbf{x}_i=1}^{X} \mathbf{ve}(\mathbf{x}_i) e^{-F(\mathbf{x}_i)}} & \text{if } \mathbf{y}_i = 0; \\ \frac{\sum_{\mathbf{x}_i=1}^{X} \mathbf{ve}(\mathbf{x}_i) e^{F(\mathbf{x}_i)}}{\sum_{\mathbf{x}_i=1}^{X} \mathbf{ve}(\mathbf{x}_i) e^{F(\mathbf{x}_i)} + \sum_{\mathbf{x}_i=1}^{X} \mathbf{ve}(\mathbf{x}_i) e^{-F(\mathbf{x}_i)}} & \text{if } \mathbf{y}_i = 1. \end{cases} \tag{4.20}$$

where $\sum_{\mathbf{x}_i=1}^{X} \mathbf{ve}(\mathbf{x}_i) e^{\pm F(\mathbf{x}_i)}$ computes the *expected potentials* given the virtual evidence.

To determine the next weak learner $f_m(\mathbf{x})$, we modify the LogitBoost error criterion

[1] Here virtual evidence is always a discrete distribution, which is enough for our purpose of training CRFs with discrete hidden states.

```
inputs : training data $(\mathbf{ve}(\mathbf{x}_i), \mathbf{y}_i)$, $\mathbf{x}_i \in \{1, \ldots, X\}$ and $\mathbf{y}_i \in \{0, 1\}$, $1 \leq i \leq N$, and
         $F = 0$
output: $F$ that approximately minimizes Eq. (4.17)
1. for $m = 1, 2, \cdots, M$ do
2.     for $i = 1, 2, \cdots, N$ do
3.         Compute the likelihood $p(\mathbf{y}_i)$ using Eq. (4.20);
4.         Compute the weight $\alpha_i = p(\mathbf{y}_i)(1 - p(\mathbf{y}_i))$;
5.         Compute the working response $z_i = \frac{\mathbf{y}_i - 0.5}{p(\mathbf{y}_i)}$;
6.     end
7.     Obtain "best" $f_m(\mathbf{x})$ by solving Eq. (4.21);
8.     Update $F(\mathbf{x}) = F(\mathbf{x}) + f_m(\mathbf{x})$ ;
9. end
```

Algorithm 4.2: Extending LogitBoost with virtual evidence

(4.19) by taking the expectation w.r.t. the virtual evidence:

$$\begin{aligned} f_m(\mathbf{x}) &= \underset{f}{\operatorname{argmin}} \sum_{i=1}^{N} \alpha_i E \left(f(\mathbf{x}_i) - z_i \right)^2 \\ &= \underset{f}{\operatorname{argmin}} \sum_{i=1}^{N} \sum_{\mathbf{x}_i=1}^{X} \alpha_i \mathbf{ve}(\mathbf{x}_i) \left(f(\mathbf{x}_i) - z_i \right)^2 , \end{aligned} \tag{4.21}$$

where α_i and z_i can be computed as in LogitBoost, using $p(\mathbf{y}_i)$ obtained from (4.20). It can be shown that by taking the expectation we are essentially performing Newton steps for optimization (see Appendix A.2 for the derivation).

The algorithm is described in Alg. 4.2, which constructs F in M iterations. Within each iteration, the algorithm first formulates the WLSE problem (line 2 to 6), and then solves it to obtain the next weak learner (line 7). When $\mathbf{ve}(\mathbf{x})$ is a deterministic value, Eq. (4.20) becomes (4.18) and Eq. (4.21) becomes (4.19); thus we get exactly the original LogitBoost algorithm. So our extension with virtual evidence is a generalization of the original LogitBoost and is able to handle deterministic evidence as well.

4.3.2 Virtual Evidence Boosting

Our extension to boosting allows us to consistently learn both local features (with deterministic evidence) and compatible features (with virtual evidence). Note that as we select more features, we must also update the virtual evidence accordingly; this can be efficiently done using the BP procedure. VEB is a very general technique: It can handle both continuous and discrete observations, and can be used in CRFs with arbitrary structures. We will explain VEB in the context of binary classification; the algorithm can be readily extended to the cases of multi-class labels, and we have done that for our experiments.

The algorithm

Intuitively, virtual evidence is closely related to the *messages* in BP inference: both influence the posterior distributions of hidden labels. To build the quantitative relationship between them, consider the simple case where a label $\mathbf{y}_i$ only receives a message from its only neighbor, $\mathbf{y}_k$. Thus

$$p(\mathbf{y}_i) \quad \propto \quad \sum_{\mathbf{y}_k} \prod_{j \in n(k) \setminus i} m_{jk}(\mathbf{y}_k) e^{\pm F(\mathbf{y}_k)}, \tag{4.22}$$

where $n(k) \setminus i$ denotes k's neighbors other than i, $m_{jk}(\mathbf{y}_k)$ is the message from $\mathbf{y}_j$ to $\mathbf{y}_k$ during BP, and $e^{\pm F(\mathbf{y}_k)}$ is the pairwise potential between $\mathbf{y}_i$ and $\mathbf{y}_k$ (the sign depends on $\mathbf{y}_i = 1$ or 0). To make (4.22) consistent with (4.20) on computing the probability, we define the virtual evidence from $\mathbf{y}_k$ to $\mathbf{y}_i$ as:

$$\mathbf{ve}_i(\mathbf{y}_k) \quad \triangleq \quad \beta \prod_{j \in n(k) \setminus i} m_{jk}(\mathbf{y}_k), \tag{4.23}$$

where β is used for normalization.

Now we are ready to apply extended LogitBoost into CRFs. The VEB algorithm is described in Alg. 4.3, which is similar to Alg. 4.2. However, while in Alg. 4.2 the virtual evidences remain unchanged, they are updated via BP at each iteration of VEB (line 2). For efficiency, the algorithm does not have to run BP to its convergence. In our experiments, we run it only for one iteration and it works well.

```
inputs : CRFs with labels $\mathbf{y}_1, \ldots, \mathbf{y}_N$, $\mathbf{y}_i \in \{0, 1\}$, and its observations $\mathbf{x}_1, \ldots, \mathbf{x}_N$,
         and $F = 0$
output: Learned $F$
1. for $m = 1, 2, \cdots, M$ do
2.     Run BP with the current $F$ to obtain marginal probability $p(\mathbf{y}_i)$ and virtual
       evidence $\mathbf{ve}_i(\mathbf{y}_k)$ ;
3.     for $i = 1, 2, \cdots, N$ do
4.         Compute the weight $\alpha_i = p(\mathbf{y}_i)(1 - p(\mathbf{y}_i))$;
5.         Compute the working response $z_i = \frac{\mathbf{y}_i - 0.5}{p(\mathbf{y}_i)}$;
6.     end
7.     Obtain a weak learner $f_m$ by solving the WLSE problem (see Section 4.3.2 for
       details) ;
8.     Update $F = F + f_m$ ;
9. end
```

Algorithm 4.3: Training CRFs using VEB

Feature selection in VEB

In step 7 of Alg. 4.3, the "best" weak learner f_m is found by solving the WLSE problem with respect to α and z. In this section, we discuss how to formulate weak learners for CRFs and solve the WLSE problem efficiently. Note that since a weak learner in CRFs is a certain kind of combination of features, the algorithm is essentially performing feature selection. In this paper we only consider weak learners that are linear combinations of features and involve one single type of local attribute or neighbor [2]. Specifically, we consider three different cases: when the weak learner involves a continuous attribute, a discrete attribute, or a neighbor relationship. While the first two cases can be treated just like in regular LogitBoost, we apply extended boosting for the neighbor relationships to handle virtual evidences, with the evidences provided by BP.

- For a **continuous attribute $\mathbf{x}^{(k)}$**, the weak learner is a linear combination of decision stump features:

$$f(\mathbf{x}^{(k)}) \quad = \quad w_1 \delta(\mathbf{x}^{(k)} \geq h) + w_2 \delta(\mathbf{x}^{(k)} < h),$$

[2] Complex weak learners, such as decision trees involving different attributes, can also be learned in similar ways.

where h is the threshold, and w_1 and w_2 are the feature weights. We get their (approximately) optimal values by solving the WLSE problem in (4.19). Specifically, h is determined using some heuristic, *e.g.*, to maximize the information gain. Then we compute the optimal w_1 and w_2 analytically by setting the first-order partial derivative of the square error equal to zero. Thus we get

$$\begin{aligned} w_1 &= \frac{\sum_{i=1}^{N} \alpha_i z_i \delta(\mathbf{x}_i^{(k)} \geq h)}{\sum_{i=1}^{N} \alpha_i \delta(\mathbf{x}_i^{(k)} \geq h)} \\ w_2 &= \frac{\sum_{i=1}^{N} \alpha_i z_i \delta(\mathbf{x}_i^{(k)} < h)}{\sum_{i=1}^{N} \alpha_i \delta(\mathbf{x}_i^{(k)} < h)} \end{aligned} \tag{4.24}$$

- Given a **discrete attribute** $\mathbf{x}^{(k)} \in \{1, \cdots, D\}$, the weak learner is expressed as

$$f(\mathbf{x}^{(k)}) = \sum_{d=1}^{D} w_d \delta(\mathbf{x}^{(k)} = d),$$

where w_d is the weight for feature $\delta(\mathbf{x}^{(k)} = d)$, an indicator function. The optimal weights can be calculated similarly as:

$$w_d = \frac{\sum_{i=1}^{N} \alpha_i z_i \delta(\mathbf{x}_i^{(k)} = d)}{\sum_{i=1}^{N} \alpha_i \delta(\mathbf{x}_i^{(k)} = d)} \tag{4.25}$$

- Given a certain type of **neighbor** and corresponding virtual evidence $\mathbf{ve}_i(\mathbf{y}_k)$, we write the weak learner as the weighted sum of two indicator functions (compatible features):

$$f(\mathbf{y}_k) = \sum_{d=0}^{1} w_d \delta(\mathbf{y}_k = d).$$

Solving the WLSE problem with virtual evidence, as in (4.21), we get the optimal weights:

$$w_d = \frac{\sum_{i=1}^{N} \alpha_i z_i \mathbf{ve}_i(\mathbf{y}_k = d)}{\sum_{i=1}^{N} \alpha_i \mathbf{ve}_i(\mathbf{y}_k = d)} \tag{4.26}$$

We can unify the expressions (4.24), (4.25), and (4.26) for computing optimal feature weights as follows:

$$w_d = \frac{\sum_{i=1}^{N} \alpha_i z_i c_{di}}{\sum_{i=1}^{N} \alpha_i c_{di}} \tag{4.27}$$

where c_{di} is the count of feature d counted in data instance i (assume we have cut CRFs into individual patches). c_{di} can be 0 and 1 for local features, or a real number between 0 and 1 for virtual evidence. It can also be greater than 1 if we allow parameter sharing within an instance, for example, when a node is connected with more than one neighbor of the same type. Thus in our approach parameter estimation is solved by simply performing *feature counting*, which makes the whole algorithm very efficient.

So far, we have explained how the algorithm determines the optimal parameters in a weak learner, but it must also determine the "best" weak learner. To accomplish that, the algorithm enumerates all possible weak learners, computes the optimal parameters and corresponding square error for each of them, and then picks the one which has the least square error overall. It is important to notice that the algorithm typically first picks reliable local attributes since virtual evidences are close to uniform at the beginning, then after some iterations it starts picking compatible features as virtual evidences provide more information.

4.4 Comparison of Learning Algorithms

In the section, we compare the performance of different algorithms. We perform experiments using both synthetic data and a dataset collected for real applications.

4.4.1 Synthetic Data

Virtual evidence boosting vs. boosted random fields

VEB is similar to boosted random fields (BRF) presented by Torralba *et al.* [110]: both run boosting and BP alternately, and both can be used for feature selection. However, BRF assumes the graphs are densely connected and thereby each individual message is not very informative. Based on this assumption, they approximate the compatibility weak learner as a linear function of beliefs. In contrast, VEB does not require any assumption about the connectivity structure and formulates the compatibility weak learner differently. This difference is significant because although their assumption is often true for the vision applications discussed in [110], it may be invalid for many other applications. In this experiment, we examine the performance of VEB and BRF as the dependencies between nodes get stronger.

The synthetic data is generated using a first-order Markov chain with binary labels. To emphasize the difference on learning compatible features, we intentionally use weak observation models: each label is connected to 50 binary observations and the conditional probabilities in the observation models are uniformly sampled from the range $[0.45, 0.55]$. We set the transition probabilities (from label 0 to 0 and from label 1 to 1) from 0.5 to 0.99. For each given transition and observation model, we generate 10 chains and each has 2,000 labels. We then perform leave-one-out cross-validation using a linear-chain CRF: train the model using 9 chains, test on the remaining one, and repeat for different combinations. We additionally run the experiments several times by randomly generating different observation models.

We run VEB as well as BRF for 50 iterations, and in each iteration we run one iteration of BP. The running durations of both algorithms are very similar, so we only compare the accuracies. The accuracies are calculated based on the MAP inference sequence. The average accuracies using VEB and BRF and their confidence intervals are shown in Fig. 4.2(a). It is clear that when the compatible dependencies are not strong (transition probabilities range from 0.5 to 0.8), both methods give very similar accuracies. However, as the dependencies get stronger (from 0.9 to 0.99), VEB dramatically outperforms BRF, mainly because the weak interaction assumption underlying BRF does not hold any more.

Feature selection in complex models

Standard training techniques, such as ML and MPL, can be inefficient and prone to overfitting because of the lack of feature selection. In this section we compare ML and MPL

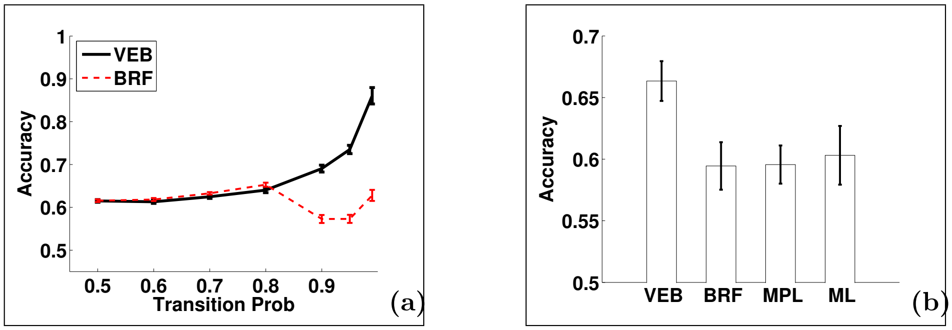

Figure 4.2: Classification accuracies in experiments using synthetic data, where the error bars indicate 95% confidence intervals. (a) VEB vs. BRF when the transition probabilities (pairwise dependencies) turn from weak to strong. (b) Comparison of different learning algorithms for feature selection.

with VEB which performs feature selection explicitly. In ML and MPL learning, we use a shrinkage prior with zero mean and unit variance to avoid overfitting.

Many real sequential data have long-range dependencies, which can be modeled using high-order Markov models. However in practice it is often impossible to know the exact order, so people may have to use Markov models that have longer dependencies than actual data. In this experiment, we simulate this scenario by generating synthetic data using a high-order Markov model, whose transition probability $p(y_n \mid y_{1:n-1}) = p(y_n \mid y_{n-k})$, where k is a constant (the observation model is similar as the one in the previous experiment). That is, a label y_n only depends on one past label y_{n-k}, but the value of k is unknown to the CRF model. Specifically, we pick k from 1 to 5, and we set the transition probability $p(y_n \mid y_{n-k})$ as 0.9 if $y_n = y_{n-k}$ and 0.1 otherwise. For a given k, we generate ten 2,000-long chains and perform leave-one-out cross-validation. We repeat the experiment for different k and compute the average.

Since the exact value of k is unknown to the CRF model, we generate a densely-connected CRF that has connections between each pair of nodes whose distance is less than or equal to 5; then the CRF is trained using different algorithms. In our experiments, VEB can reliably identify the correct values of k, *i.e.*, picking only pairwise features whose distance is k or multiples of k. Although BRF also performs feature selection and structure learning, it does not perform as well as VEB. The average classification accuracies are shown in Fig. 4.2(b).

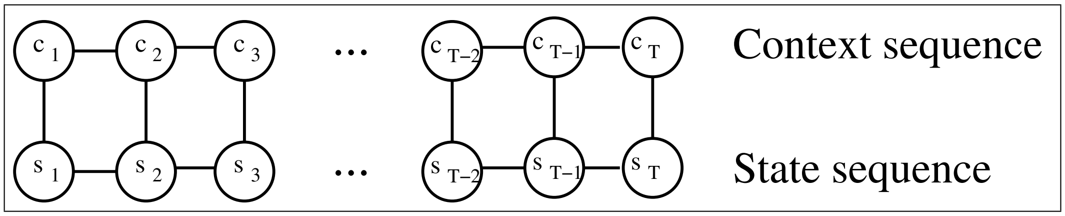

Figure 4.3: The CRF model for simultaneously inferring motion states and spatial contexts (observations are omitted for simplicity).

Because VEB can robustly extract the sparse structures, it significantly outperforms other approaches. As to the running time, VEB, BRF, and MPL are all quite efficient; each training takes only tens of seconds. In contrast, the training using ML takes about 20 minutes.

4.4.2 Real Data for Recognizing Motions and Spatial Contexts

Subramanya *et al.* [101] proposed a model for simultaneously recognizing motion states (*e.g.*, stationary, walking, running, driving, and going up/down stairs) and spatial contexts (*e.g.*, indoors, outdoors, vehicle) from wearable sensors. They train local features using AdaBoost and incorporate the boosted classifiers as observation into a HMM that infers jointly the states and contexts. Their data set consists of 12 episodes and about 100,000 labels. In our experiment, we perform the same task with the same data set, but using a CRF instead of HMM. As shown in Fig. 4.3, the CRF captures the pairwise relations between states and contexts. One difficulty in this experiment is that learning algorithms must be able to handle *continuous* sensor data. Although VEB can handle continuous observations directly, doing that in ML and MPL is not straightforward. The performance of ML and MPL is terrible if we simply use the continuous measurements as feature values. We try two tricks to circumvent this difficulty. One is to learn decision stumps for all observations, using the heuristics as in VEB. The other is to use boosting (*e.g.*, LogitBoost in our experiment) to select a set of decision stump features and these decision stumps are then fed into ML and MPL for weight estimation.

We perform leave-one-out cross-validation using different learning approaches. In such

Table 4.1: Accuracy for inferring states and contexts

Training algorithm	Average overall accuracy and confidence interval
VEB	$88.8 \pm 4.4\%$
MPL + all observations	$72.1 \pm 3.9\%$
MPL + boosting	$70.9 \pm 6.5\%$
HMM + AdaBoost	$85.8 \pm 2.7\%$

huge and loopy CRFs, ML becomes completely intractable and does not finish in two days. MPL and VEB take about 2 hours for training. The overall average accuracies are shown in Table 4.4.2. Our VEB clearly outperforms MPL, as well as the result in the original paper.

4.5 Summary

In this chapter we discussed three algorithms for training CRFs and RMNs: maximum likelihood (ML), maximum pseudo-likelihood (MPL), and virtual evidence boosting (VEB).

ML has been most widely used for training CRFs. However, ML requires running the inference at each iteration of the optimization and can be very expensive even for approximated inference algorithms, such as MCMC and BP. Moreover, when using approximated inference, the learning procedure could converge to suboptimal results or even diverge. In contrast, MPL is usually very efficient. However, no general guidance has been given on when MPL can be safely used. Indeed MPL has been observed to over-estimate the dependency parameters in some experiments. In addition, neither ML nor MPL performs feature selection and neither of them is able to adequately handle continuous observations. Compared with ML and MPL, VEB performs feature selection explicitly and can handle continuous observations directly. In our experiments using both synthetic and real data, it significantly outperforms other alternatives.

Another promising approach is max-margin Markov network [105], which extends support vector machines (SVM) to CRFs. The comparison between VEB and max-margin Markov network is a very interesting piece of future work.

Chapter 5
EXTRACTING PLACES AND ACTIVITIES FROM GPS TRACES

From Chapter 2 to Chapter 4, we described a powerful probabilistic framework that is flexible to encode complicated relations and at the same time supports efficient inference and learning. In this chapter, we discuss the application of the framework onto *location-based activity recognition* [65, 66, 67]. Given a sequence of GPS data collected by a person, our goal is to recognize the high-level activities in which a person is engaged over a period of many weeks, and to further determine the relationship between activities and locations that are important to the user. For example, we want to segment a user's day into everyday activities such as "working," "visiting," "travel," and to recognize and label significant places that are associated with one or more activity, such as "workplace," "friend's house," "user's bus stop." The information of activities and significant places is very useful for context-aware services. Such activity logs can also be used as an automated personal diary, or collected from a group of users for large-scale studies of human behavior across time and space for disciplines such as urban studies and sociology [17].

Previous approaches to automated activity and place labeling suffer from design decisions that limit their accuracy and flexibility:

Restricted activity models: Previous approaches to location-based activity recognition have rather limited models of a person's activities. Ashbrook and colleagues [3] only reason about moving between places, without considering different types of places or different routes between places. In the context of indoor mobile robotics, Bennewitz *et al.* [7] showed how to learn different motion paths between places. However, their approach does not model different types of places and does not estimate the user's activities when moving between places.

Inaccurate place detection: Virtually all previous approaches address the problem of determining a person's significant places by assuming that a geographic location is significant if and only if the user spends at least θ minutes there, for some fixed threshold θ [3, 64, 39, 7]. In practice, unfortunately, there is no threshold that leads to a satisfying detection of all significant locations. For instance, locations such as the place where the user drops off his children at school may be visited only briefly, and so would be excluded when using a high threshold θ. A low threshold, on the other hand, would include too many insignificant locations, for example, a place where the user waited at a traffic light. Such detection errors can only be resolved by taking additional context information into account, such as the user's current activity.

In this chapter we present a novel, unified approach to automated activity and place labeling which overcomes these limitations. Our approach is based on the framework of RMN and the key features of our system are:

- It achieves *high accuracy in detecting significant places* by taking a user's context into account when determining which places are significant. This is done by simultaneously estimating a person's activities over time, identifying places that correspond to significant activities, and labeling these places by their types. As a result, our approach does not rely on arbitrary thresholds regarding the time spent at a location or on a pre-specified number of significant places.

- It creates a *rich interpretation of a user's data*, including modes of transportation as well as activities performed at particular places. It allows different kinds of activities to be performed at the same location, and vice-versa.

- This complex estimation task requires *efficient, approximate inference and learning algorithms*. Our system performs inference using belief propagation (BP), and parameter learning is done using maximum pseudo-likelihood (MPL). In order to efficiently reason about aggregations, we apply the optimized algorithm described in Section 3.3.

Although the main content of this chapter is activity recognition using GPS data, the framework is general enough to model indoor activities. In this chapter we also present

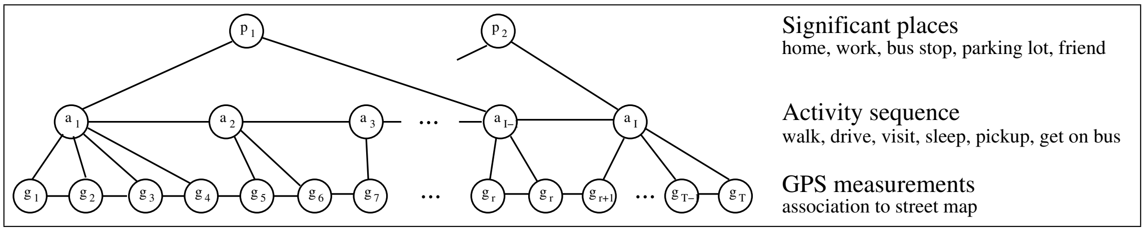

Figure 5.1: The concept hierarchy for location-based activity recognition. For each day of data collection, the lowest level typically consists of several thousand GPS measurements, the next level contains around one thousand discrete activity cells, and the place level contains around five places.

preliminary results of indoor activity recognition from audio, acceleration, and light sensor data.

This chapter is organized as follows. We begin with modeling the problem of location-based activity recognition using the framework of RMN. In the next section, we explain the inference, especially how we handle instance uncertainty. Then, we present experimental results on real-world data that demonstrate significant improvement in coverage and accuracy over previous work. Finally we show the results of indoor activity recognition.

5.1 Relational Activity Model

The basic concept underlying our activity model is shown in Fig. 5.1. Each circle in the model indicates an object such as a GPS measurement, an activity, or a significant place. The edges illustrate probabilistic dependencies between these objects. The relational schema is shown in Fig. 5.2.

GPS measurements are the input to our model — a typical trace consists of approximately one GPS reading per second, each reading includes a *timestamp* and the corresponding *coordinates* in the 2D space. We segment a GPS trace in order to generate a discrete sequence of activity nodes at the next level of the model (see Fig. 5.1). If a street map is available, then we perform the segmentation by associating the GPS readings to a discretized version of the streets in the map (in our experiments we used 10m for discretization). See Fig. 5.6(a) for an example of street association.

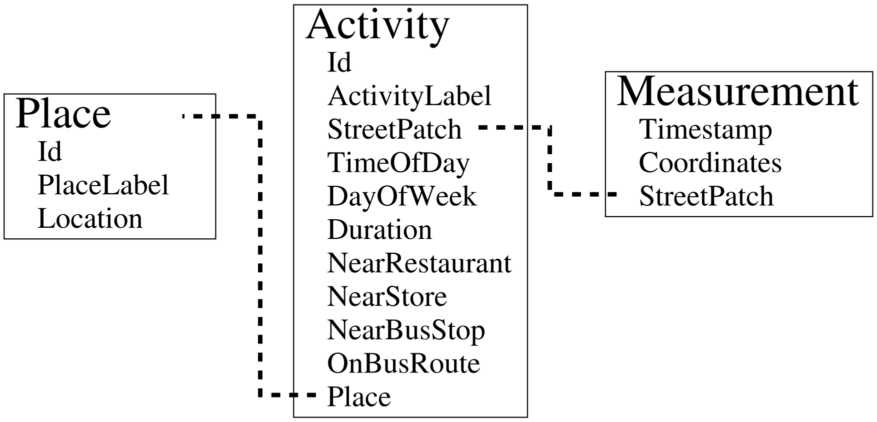

Figure 5.2: The relational schema of location-based activity recognition. Dash lines indicate the references between classes.

Activities are estimated based on spatially segmented GPS trace, as illustrated in Fig. 5.1. Put differently, our model labels a person's activity whenever she passes through or stays at a 10m patch of the environment. We distinguish two main groups of activities, *significant activities* and *navigation activities*. Significant activities are typically performed while the user is at some significant locations, such as work, leisure, sleep, visit, drop off / pickup, getting on/off the bus, or getting into/out of the car. Activities related to navigation are walking, driving car, and riding bus. To determine activities, our model relies on temporal features associated with each activity node such as duration and time of day, and on geographic information such as whether a location is near restaurant or store.

Significant places are those locations that play a significant role in the activities of a person. Such places include a person's home and work place, the bus stops and parking lots the person typically uses, the homes of friends, stores the person frequently shops in, and so on. Note that our model allows different types of activities to occur at the same significant place. For example, at a friend's home, the activity could be visiting or picking up friend. Furthermore, due to signal loss and noise in the GPS readings, the same significant place can comprise multiple, different locations.

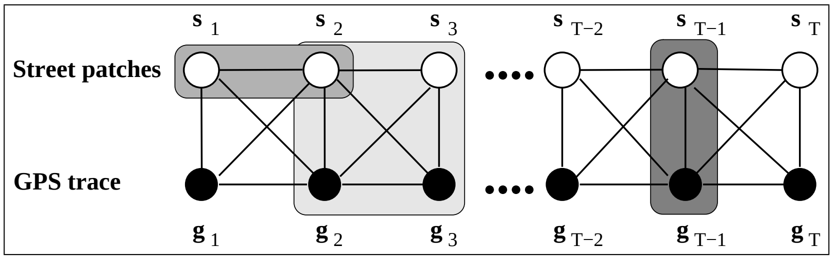

Figure 5.3: CRF for associating GPS measurements to street patches. The shaded areas indicate different types of cliques: from the left, they are smoothness clique, temporal consistency clique, and GPS noise clique.

5.1.1 GPS to Street Map Association

As mentioned above, we segment GPS traces by grouping consecutive GPS readings based on their spatial relationship. Without a street map, this segmentation can be performed by simply combining all consecutive readings that are within a certain distance from each other (10m in our implementation). However, it might be desirable to associate GPS traces to a street map, for example, in order to relate locations to addresses in the map. Street maps are represented by graph structures, where one edge typically represents a city block section of a street, and a vertex is an intersection between streets [64].

To jointly estimate the GPS to street association and the trace segmentation, we associate each GPS measurement to a 10m patch on a street edge. The associated *street patch* indicates the street, the patch location, and the moving direction. As shown in Fig. 5.6(a) in Section 5.3, GPS traces can deviate significantly from the street map, which is mostly because of measurement errors and inaccuracies in street maps. One straightforward way to performing this association is to snap each GPS reading to the nearest street patch. However, such an approach would clearly give wrong results in situations such as the one shown in Fig. 5.6(a). To generate a consistent association, we construct a RMN that takes into account the spatial relationship between GPS measurements and street patches. Specifically, based on the schema in Fig. 5.2, the RMN defines the following relational clique templates.

- GPS noise and map uncertainty are considered by cliques whose features measure the squared distance between a GPS measurement and the center of the street patch it is associated with. The SQL query of the template is

SELECT StreetPatch s_t**, Coordinates** g_t
FROM Measurement .

The corresponding feature function is defined as

$$\mathbf{f}_{\mathrm{m}}(g_t, s_t) \quad = \quad \frac{||g_t - s_t.\mathrm{location}||^2}{\sigma^2}$$

where g_t is the location of the t-th GPS reading, s_t is the index of one of the street patches in the vicinity of g_t, s_t.location (not shown in the schema) denotes the central location of street patch s_t, and σ is used to control the scale of the distance (note that this feature function corresponds to a Gaussian noise model for GPS measurements). The feature $\mathbf{f}_{\mathrm{m}}$ is shared for the potential functions of all cliques connecting GPS readings and their street patches (one such clique is shown as the dark shaded area in Fig. 5.3).

- Temporal consistency is ensured by four node cliques that compare the spatial relationship between consecutive GPS readings and the spatial relationship between their associated street patches (light shaded area in Fig. 5.3). The more similar these relationships, the more consistent the association. This comparison is done via a template defined as

  SELECT m1.StreetPatch s_t**, m2.StreetPatch** s_{t+1}**,**
  m1.Coordinates g_t**, m2.Coordinates** g_{t+1}
  FROM Measurement m1, Measurement m2
  WHERE m1.Timestamp + 1 = m2.Timestamp

  and a feature function that compares the vectors between GPS readings and associated patches:

$$\mathbf{f}_{\mathrm{t}}(g_t, g_{t+1}, s_t, s_{t+1}) \quad = \quad \frac{||(g_{t+1} - g_t) - (s_{t+1}.\mathrm{location} - s_t.\mathrm{location})||^2}{\sigma^2}$$

  Here, s_t and s_{t+1} are the indices of street patches associated at two consecutive timestamps.

- Smoothness cliques prefer traces that do not switch frequently between different streets. To model this preference, we use binary features that test whether consecutive patches are on the same street and in the same direction. Note that in our model each street patch has a direction, either up or down the street, so we can define the template as:

  SELECT m1.StreetPatch s_t, m2.StreetPatch s_{t+1}

  FROM Measurement m1, Measurement m2

  WHERE m1.Timestamp + 1 = m2.Timestamp ,

  and

$$\mathbf{f}_\mathrm{S}(s_t, s_{t+1}) \;=\; \delta(s_t.\mathrm{street}, s_{t+1}.\mathrm{street}) \cdot \delta(s_t.\mathrm{direction}, s_{t+1}.\mathrm{direction})$$

  where $\delta(u, v)$ is the indicator function which equals 1 if $u = v$ and 0 otherwise.

The structure of the instantiated CRF is shown in Fig. 5.3. The values of each s_t range over the street patches in the map that are within a certain distance of the GPS reading g_t. Using the feature functions defined above, this conditional distribution can be written as

$$p(s_{1:T} | g_{1:T}) \;=\; \frac{1}{Z(\mathbf{x})} \exp \left\{ \sum_{t=1}^{T} \mathbf{w}_\mathrm{m} \cdot \mathbf{f}_\mathrm{m}(g_t, s_t) + \sum_{t=1}^{T-1} \mathbf{w}_\mathrm{t} \cdot \mathbf{f}_\mathrm{t}(g_t, g_{t+1}, s_t, s_{t+1}) + \sum_{t=1}^{T-1} \mathbf{w}_\mathrm{S} \cdot \mathbf{f}_\mathrm{S}(s_t, s_{t+1}) \right\},$$

where $\mathbf{w}_\mathrm{m}, \mathbf{w}_\mathrm{t}$ and $\mathbf{w}_\mathrm{S}$ are the corresponding weights of the features. During inference, the CRF uses the above features to estimate distributions over s_t.

5.1.2 Extracting and Inferring Activities

Our system estimates a person's activities based on the segmented GPS traces, which corresponds to generating and labeling the second level of the hierarchy (see Fig. 5.1). Here we have the problem of *instance uncertainty* since the set of activity nodes is unknown beforehand. As discussed in Section 2.2.2, we can handle this uncertainty using the extended RMN model. To specify the generation of activity nodes, we define the following RMN template:

INSERT INTO Activity (StreetPatch, TimeOfDay, DayOfWeek, Duration)

```
SELECT StreetPatch, TimestampToTimeOfDay(MIN(Timestamp)),
  TimestampToDayOfWeek(MIN(Timestamp)), MAX(Timestamp)-MIN(Timestamp)
FROM BEST(1) Measurement
GROUP CONSECUTIVELY BY StreetPatch .
```

This template instantiates the activities using the MAP sequence of the street patches. Fig. 5.6(a) illustrates the MAP association of a GPS trace to a map. Such an association also provides a unique segmentation of the GPS trace. This is done by simply combining consecutive GPS readings that are associated to the same street patch. Each segment of consecutive measurements generates an instance of activity. The temporal information of each activity can be extracted from the group of measurements. For example, the TimeOfDay of an activity is obtained from the starting timestamp, MIN(Timestamp), and its duration is just the temporal length of the segment, MAX(Timestamp)-MIN(Timestamp). Each activity entity also includes geographical information (not shown in the SQL), such as NearRestaurant, NearStore, NearBusStop, and OnBusRoute, which is extracted from geographic databases using the coordinates of the street patch.

After extracting the activity instances, we define relational clique templates that connect the labels of activities with all sources of evidence. These sources of evidence include:

- Temporal information such as time of day, day of week, and duration of the stay. These measures are discretized in order to allow more flexible feature functions. For example, time of day can be *Morning*, *Noon*, *Afternoon*, *Evening*, or *Night*. The instantiated cliques connect each activity node to one of the solid nodes in the CRF shown in Fig. 5.4. And the features are binary indicator functions, one for each possible combination of temporal feature and activity. For instance, the following function returns 1 if the activity is work and the time of day is morning, and 0 otherwise: $\mathbf{f}(a_i, d_i) = \delta(a_i, Work) \cdot \delta(d_i, Morning)$.

- Average speed through a segment, which is important for discriminating different transportation modes. The speed value is also discretized and indicator features are

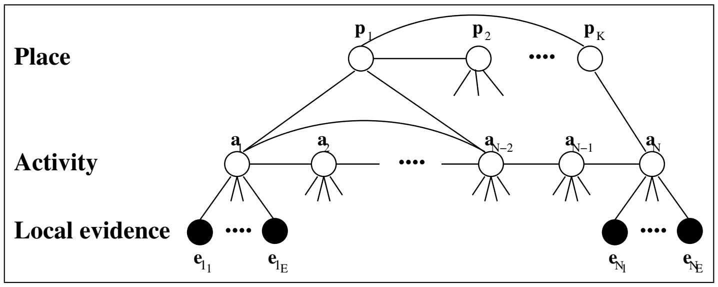

Figure 5.4: CRF for labeling activities and places. Each activity node a_i is connected to E observed local evidence nodes e_{i_j}. Local evidence comprises information such as time of day, duration, and geographic knowledges. Place nodes p_1 to p_K are generated based on the activities inferred at the activity level. Each place is connected to all activity nodes that are within a certain distance.

used, similar to temporal information. This discretization has the advantage over a linear feature function that multi-modal velocity distributions can be modeled.

- Information extracted from geographic databases, such as whether a patch is on a bus route, whether it is close to a bus stop, and whether it is near a restaurant or grocery store. Again, we use indicator features to incorporate this information.

- Additionally, each activity node is connected to its neighbors using the following template:

  SELECT a1.ActivityLabel a_i**, a2.ActivityLabel** a_{i+1}

  FROM Activity a1, Activity a2

  WHERE a1.Id + 1 = a2.Id .

  The corresponding features measure compatibility between types of activities at neighboring nodes in the trace. For instance, it is extremely unlikely to get on the bus at one location and drive a car at the neighboring location right afterwards. The feature function is $\mathbf{f}(a_i, a_{i+1}) = \delta(a_i, OnBus) \cdot \delta(a_{i+1}, Car)$, where a_i and a_{i+1} are specific activities at two consecutive activity nodes. The weight of this feature should be a negative value after supervised learning, thereby giving a labeling that contains this combination a low probability.

The instantiated CRF encoding all these features is shown as the lower levels of Fig. 5.4

without the nodes of places.

5.1.3 Extracting and Labeling Significant Places

Our model also aims at determining those places that play a significant role in the activities of a person, such as home, workplace, friends' home, grocery stores, restaurants, and bus stops. Such *significant places* comprise the upper level of the CRF shown in Fig. 5.4. However, since these places are unknown a priori, we must additionally *detect* a person's significant places. Again we encounter the problem of instance uncertainty. To handle this problem, we define the following template:

INSERT INTO Place (Location)
SELECT Cluster(StreetPatch)
FROM BEST(1) Activity
WHERE IsSignificant(ActivityLabel).

From the MAP sequence of the activity labels, this template looks for all the significant activities using a filter function IsSignificant(). Then all the street patches of significant activities are clustered and the set of clusters is added into the set of significant places.

After we get the set of significant places, we define the following templates in order to infer place types:

- The activities that occur at a place strongly indicate the type of the place. For example, at grocery stores people mainly do shopping, and at a friends' home people either visit or pick up / drop off friend. Our template captures the dependencies between the place labels and the activity labels:

  SELECT a.ActivityLabel a_i**, p.PlaceLabel** p_j
  FROM Activity a, Place p
  WHERE a.Place = p.Id,

  which generates a clique between each place label and each activity label in its vicinity, as shown in Fig. 5.4. For each combination of type of place and type of activity, we then have an indicator feature, such as

$$\mathbf{f}(p_j, a_i) \quad = \quad \delta(p_j, Store) \cdot \delta(a_i, Shopping)$$

- A person usually has only a limited number of different homes or work places. To use this knowledge to improve labeling places, we add two additional templates that count the number of different homes and work places. These counts provide soft constraints that bias the system to generate interpretations that result in reasonable numbers of different homes and work places. For example, the template for count of homes is

  SELECT COUNT(*)
  FROM Place
  WHERE PlaceLabel = Home,

  and the feature is simply the count, which could make the likelihood of labels decrease exponentially as the count increases. Note that these templates can generate very large cliques in the unrolled CRF. This is because we must build a clique for all the place nodes in order to count the number of homes or workplaces.

5.2 Inference

Given the structure of instantiated CRF, the inference is rather straightforward: we run BP to get MAP configuration of all the labels. To make the inference efficient with large aggregate cliques, we apply the optimized BP algorithm described in Section 3.3. However, we have the problem of structure uncertainty because activity nodes and place nodes are not given a priori. To handle such uncertainty, we construct the CRF in three steps. In the **first** step, the GPS trace is segmented as discussed in Section 5.1.1: segmentation of a trace is performed by either clustering consecutive GPS readings that are nearby or associating the GPS trace to a discretized street map using the CRF shown in Fig. 5.3. In the **second** step, the activity nodes are generated based on the MAP segmentation, as discussed in Section 5.1.2. However, since significant places are not yet known at this stage, the instantiated CRF contains no place nodes. MAP inference is then performed in this restricted CRF so as to determine the MAP activity sequence. Then in the **third**

```
inputs : GPS trace $\langle g_1, g_2, \ldots, g_T \rangle$
output: MAP activity sequence $\mathbf{a}^*$ and significant places $\mathbf{p}^*$
//Generate activity segments and local evidence by grouping consecutive GPS readings
$(\langle a_1, \ldots, a_N \rangle, \langle e_{1_1}, e_{1_2}, \ldots, e_{1_E}, e_{2_1}, \ldots, e_{N_E} \rangle) = \text{segmentation}(\langle g_1, g_2, \ldots, g_T \rangle)$ ;
//Generate CRF without places (lower two levels in Fig. 5.4)
$\text{CRF}_0 = \text{instantiate\_crf}(\langle\ \rangle, \langle a_1, \ldots, a_N \rangle, \langle e_{1_1}, e_{1_2}, \ldots, e_{1_E}, e_{2_1}, \ldots, e_{N_E} \rangle)$ ;
${\mathbf{a}^*}_0 = \text{MAP\_inference}(\text{CRF}_0)$ ;          // Determine MAP sequence of activities
i = 0 ;
repeat
    i = i + 1 ;
    //Generate places by clustering significant activities
    $\langle p_1, \ldots, p_K \rangle_i = \text{generate\_places}({\mathbf{a}^*}_{i-1})$
    //Generate complete CRF with instantiated places
    $\text{CRF}_i = \text{instantiate\_crf}(\langle p_1, \ldots, p_K \rangle_i, \langle a_1, \ldots, a_N \rangle, \langle e_{1_1}, e_{1_2}, \ldots, e_{1_E}, e_{2_1}, \ldots, e_{N_E} \rangle)$
    //Perform MAP inference in complete CRF
    $\langle {\mathbf{a}^*}_i, {\mathbf{p}^*}_i \rangle = \text{MAP\_inference}(\ \text{CRF}_i)$
until ${\mathbf{a}^*}_i = {\mathbf{a}^*}_{i-1}$ ;
$\mathbf{a}^* = {\mathbf{a}^*}_i$ ;
$\mathbf{p}^* = {\mathbf{p}^*}_i$ ;
```

Algorithm 5.1: Detecting and labeling activities and places

step, the MAP activity sequence is used to extract a set of significant places. As discussed in Section 5.1.3, this is done by classifying individual activities in the sequence into whether or not they belong to a significant place. For instance, while walking, driving car, or riding bus is not associated to significant places, working or getting on or off the bus indicates a significant place. Each instance at which a *significant activity* occurs generates a place node. Because a place can be visited multiple times within a sequence, we perform clustering and merge duplicate places into the same place node. Thus we have instantiated the complete CRF model as shown in Fig. 5.4, and we are able to do inference to obtain the labels for both activities and significant places. However, because the complete CRF has a different structure than the restricted CRF, it might generate a different MAP activity sequence. If this is the case, the third step is repeated until the activity sequence does not change. In our experiments we observed that this algorithm converges very quickly, typically after only two iterations. The complete iterative algorithm is shown in Alg. 5.1.

5.3 Experimental Results

In our experiments we evaluate how well our system can *extract* and *label* a person's activities and significant places. Furthermore, we demonstrate that it is feasible to learn models from data collected by a set of people and then apply this model to another person. That is, our system can recognize a person's activities without requiring any manual labeling of that person's data.

We collected GPS data traces from four different persons, approximately six days of data per person. Each trace consisted of roughly 40,000 GPS measurements, resulting in about 9,000 segments. We then manually labeled all activities and significant places in these traces [1]. We used leave-one-out cross-validation for evaluation, that is, learning was performed based on the data collected by three persons and the learned model was evaluated on the fourth person. We used maximum pseudo-likelihood (MPL) for learning, which took, on a regular PC less than one minute to converge on the training data collected by three persons. For each evaluation, we used the algorithm described in Alg. 5.1, which typically extracted the MAP activities and places from a one week trace within one minute of computation. When a street map was used, the association between GPS trace and street map at Step 1 in Alg. 5.1 took additional four minutes.

5.3.1 Example Analysis

The different steps involved in the analysis of a GPS trace are illustrated in Fig. 5.5. The second panel (b) shows the GPS trace snapped to 10m patches on the street map. This association is performed by Step 1 of the algorithm given in Alg. 5.1, using the CRF discussed in Section 5.1.1. The visited patches along with local information such as time of day or duration are used to generate the activity CRF. This is done by Step 2 in Alg. 5.1, generating the activity level of Fig. 5.4. MAP inference in this CRF determines one activity for each patch visit, as shown in panel (c) of Fig. 5.5 (Step 3 of the algorithm). Note that this example analysis misses the get off bus activity at the left end of the bus trip. The significant

[1] Even though we performed the manual labeling as thoroughly as possible, we might have "missed" some significant places and activities. This might result in a slightly lower false negative rate than reported here.

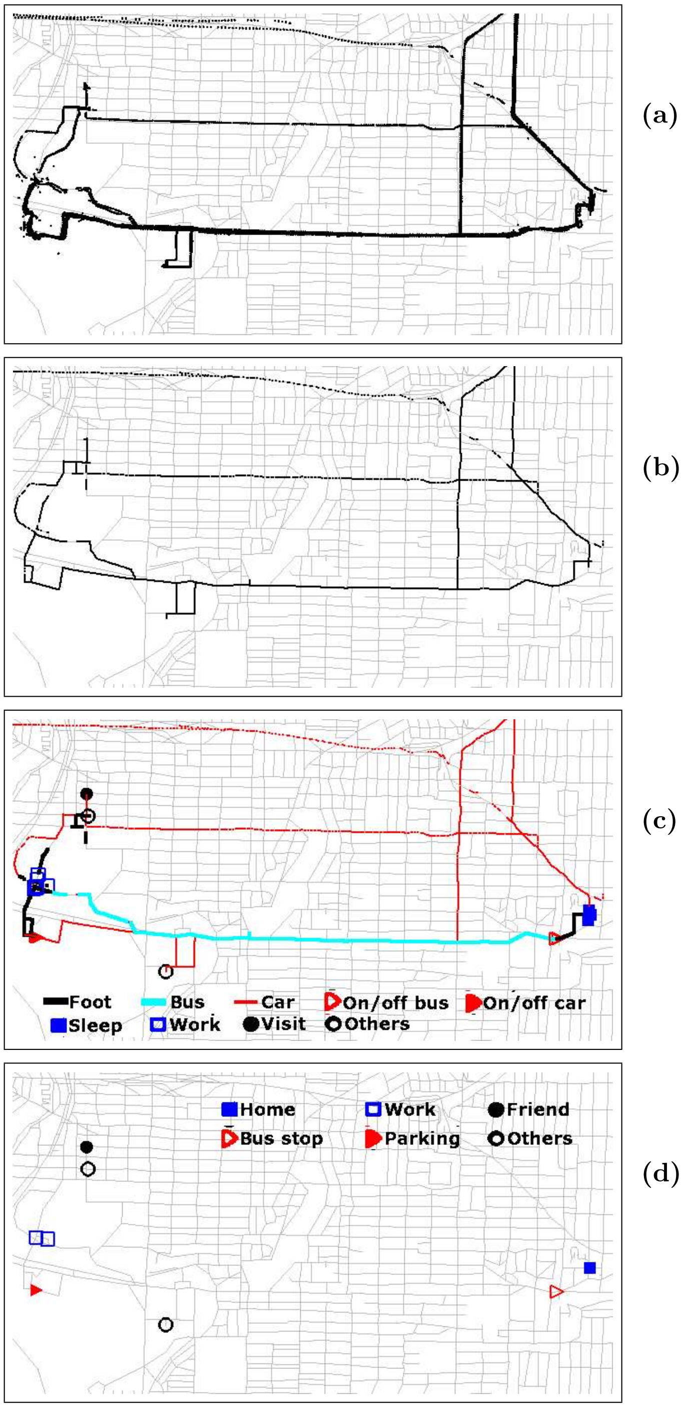

Figure 5.5: Illustration of inference on part of a GPS trace, the area of size 2km x 1km is visited several times. (a) The raw GPS data has substantial variability due to sensor noise. (b) GPS trace snapped to 10m street patches, multiple visits to the same patch are plotted on top of each other. (c) Activities estimated for each patch. (d) Places generated by clustering significant activities, followed by a determination of place types.

Table 5.1: Summary of a typical day based on the inference results.

Time	Activity and transportation
8:15am - 8:34am	Drive from home$_1$ to parking lot$_2$, walk to workplace$_1$;
8:34am - 5:44pm	Work at workplace$_1$;
5:44pm - 6:54pm	Walk from workplace$_1$ to parking lot$_2$, drive to friend$_3$'s place;
6:54pm - 6:56pm	Pick up/drop off at friend$_3$'s place;
6:56pm - 7:15pm	Drive from friend$_3$'s place to other place$_2$;
9:01pm - 9:20pm	Drive from other place$_2$ to friend$_1$'s place;
9:20pm - 9:21pm	Pick up/drop off at friend$_1$'s place;
9:21pm - 9:50pm	Drive from friend$_1$'s place to home$_1$;
9:50pm - 8:22am	Sleep at home$_1$.

activities in the MAP sequence are clustered and additional place nodes are generated in a new CRF (Step 7 and Step 8 in Alg. 5.1). MAP inference in this CRF provides labels for the detected places, as shown in Fig. 5.5(d). The algorithm repeats generation of the CRFs until the MAP activity sequence does not change any more. In all experiments, this happens within the first four iterations of the algorithm.

Fig. 5.6(a) provides another example of the quality achieved by our approach to snapping GPS traces to street maps. Note how the complete trace is snapped consistently to the street map. Table 5.1 shows a typical summary of a person's day provided by the MAP sequence of activities and visited places. Note that the system determines where significant places are, how the person moves between them, and what role the different places play for this person.

5.3.2 Extracting Significant Places

In this experiment we compare our system's ability to detect significant places to the results achieved with a widely-used approach that applies a time threshold to determine whether or not a location is significant [3, 42, 64, 66, 39]. Our model was trained on data collected by three persons and tested on the fourth person. For the threshold method, we generated results for different thresholds from 1 minute to 10 minutes. The data contained 21 significant places. Fig. 5.6(b) shows the false positive and false negative rates achieved with

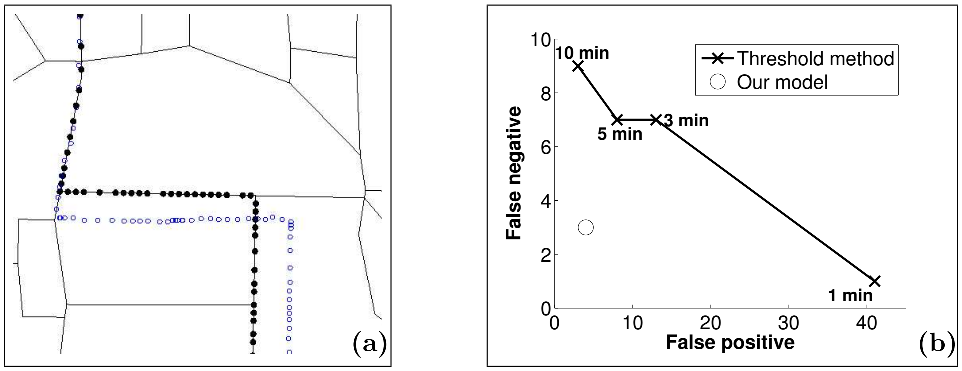

Figure 5.6: (a) GPS trace (gray circles) and the associated street patches (black circles) on the street map (lines). (b) Comparison of accuracies on extracting significant places.

the two approaches. As can seen, our approach clearly outperforms the threshold method. Any fixed threshold is not satisfactory: low thresholds have many false negatives, and high thresholds result in many false positives. In contrast, our model performs much better: it only generates 4 false positives and 3 false negatives.

5.3.3 Labeling Places and Activities

The confusion matrices given in Table 5.2 and Table 5.3 summarize the results achieved with our system on the cross-validation data. Table 5.2 shows activity estimation results on the significant activities. An instance was considered false positive (FP) if a significant activity was detected when none occurred; it was considered false negative (FN) if a significant activity occurred but was labeled as non-significant such as walking. The results are given with and without taking the detected places into account. More specifically, without places are results achieved by CRF$_0$ generated by Step 3 of the algorithm in Alg. 5.1, and results with places are those achieved after model convergence. When the results of both approaches are identical, only one number is given; otherwise, the first number gives results achieved with the complete model. The table shows two main results. First, the accuracy of our approach is quite high (86.0%), especially when considering that the system was evaluated on only one week of data and was trained on only three weeks of data collected by different persons. Second, performing joint inference over activities and places increases the quality

Table 5.2: Activity confusion matrix of cross-validation data with (left values) and without (right values) considering places for activity inference.

Truth	Inferred labels							FN
	Work	Sleep	Leisure	Visit	Pickup	On/off car	Other	
Work	12 / 11	0	0 / 1	0	0	0	1	0
Sleep	0	21	1	2	0	0	0	0
Leisure	2	0	20 / 17	1 / 4	0	0	3	0
Visiting	0	0	0 / 2	7 / 5	0	0	2	0
Pickup	0	0	0	0	1	0	0	2
On/Off car	0	0	0	0	1	13 / 12	0	2 / 3
Other	0	0	0	0	0	0	37	1
FP	0	0	0	0	2	2	3	-

Table 5.3: Confusion matrix of place detection and labeling.

Truth	Inferred labels					FN
	Work	Home	Friend	Parking	Other	
Work	5	0	0	0	0	0
Home	0	4	0	0	0	0
Friend	0	0	3	0	2	0
Parking	0	0	0	8	0	2
Other	0	0	0	0	28	1
FP	0	0	1	1	2	-

of inference. The reason for this is that a place node connects all the activities occurring in its spatial area so that these activities can be labeled in a more consistent way.

Finally, the confusion matrix shown in Table 5.3 summarizes the results achieved on detecting and labeling significant places. As can be seen, the approach commits zero errors in labeling the home and work locations of the persons used for testing. The overall accuracy in place detection and labeling is 90.6%.

Table 5.4: Average accuracy for indoor activities

Training algorithm	Average accuracy
VEB	94.1%
ML + all observations	87.7%
ML + boosting	88.5%
MPL + all observations	87.9%
MPL + boosting	88.5%

5.4 Indoor Activity Recognition

So far we have discussed activity recognition using GPS data. Since GPS does not work indoors, it is impossible to recognition finer-grained activities, such as computer usage, lunch, meeting at a workplace. However, because our framework is very general, we can recognize indoor activities by applying the same technique to other sensors. In this section we present preliminary results of our experiments. The CRF model in this case is simply a linear chain, so the BP inference is very efficient and gives exact results. However, because there are a large number of continuous observations in the sensor data, parameter learning using ML or MPL does not work well. Therefore, we apply virtual evidence boosting (VEB) for this task, which performs feature selection explicitly and can handle continuous features naturally.

In this experiment, one person collected audio, acceleration, and light sensor data as he stayed indoors using the hardware described in [60]. The total length of the data set is about 1,100 minutes, recorded over a period of 12 days. The goal is to recognize the person's major indoor activities including computer usage, meal, meeting, TV watching and sleeping. We segmented the data into one-minute chunks and manually labeled the activity at each minute for the purpose of supervised learning and testing. For each chunk of data, we computed 315 features values, which included energy in various frequency bands of the signal, autocorrelation, and different entropy measures, *etc.* These features were fed into the CRF as observations and a linear chain CRF is created per day. We evaluated our algorithm using leave-one-day-out cross-validation. Since the person performs different activities in different days, the accuracies can vary significantly from day to day. So we only compare the overall average accuracy of VEB with ML and MPL. Because ML and MPL cannot handle continuous features directly, we used the two tricks mentioned in Section 4.4.2. The results are shown in Table 5.4, in which VEB is about 5% to 6% better than ML and MPL, no matter how they incorporated the continuous observations.

5.5 Summary

In this chapter we have developed a novel approach to performing location-based activity recognition. In contrast to existing techniques, our approach uses one consistent framework for both the extraction and the labeling of a person's activities and significant places, as well as the low-level segmentation. Our model is able to take many sources of evidence into account in order to detect and label the significant places of a person. Furthermore, once these places are determined, they help to better recognize activities occurring in their vicinity. Therefore, by capturing complex relations between the activities and the high level context, our approach can create a rich and consistent interpretation of a user's data with high accuracy. Our experiments based on traces of GPS data showed that our system significantly outperforms existing approaches, both in expressiveness and in accuracy. Moreover, both inference and learning can be done very efficiently.

Our technique is very general and can be readily applied to other tasks of activity recognition. In our preliminary experiments, we presented promising results of indoor activity recognition from multi-modal sensors. In particular we showed that using virtual evidence boosting for feature selection and parameter estimation can significantly outperform our learning algorithms such as maximum likelihood and maximum pseudo-likelihood.

Chapter 6

LEARNING AND INFERRING TRANSPORTATION ROUTINES

In previous chapters, our task was to recognize different types of activities and significant places from GPS data, which is essentially a supervised classification problem. However, as we discussed in Chapter 1, the techniques of classification may not be suitable for all location-based services. In this chapter, we describe a dynamic Bayesian network that captures a user's daily movement patterns between places. Instead of to learn the discriminative features, we aim to understand the transition patterns at all levels of transportation routines and to make accurate prediction at real time [64, 68]. Specifically, our system is able to

- Robustly track and predict a user's location even with loss of GPS signals or in the presence of other sources of noise;
- Infer at real time a user's mode of transportation (*i.e.*, traveling by foot, car, or bus) and predict when and where she will change modes;
- Predict her future movements, both in the short term (Will the user turn left at the next street corner?) and in terms of distant goals (Is she going to work?);
- Infer when a user has deviated from her ordinary routine, and in some cases explicitly infer that a user has made an error, such as boarding the wrong bus to get to the doctor.

We are motivated in this work by the development of personal guidance systems to help cognitively-impaired individuals move safely and independently through their community. This technology also supports many other applications, such as *customized* "just in time" information services for presenting relevant bus schedules and traffic information based on routes.

Our approach is based on a hierarchical Markov model trained to model a user with data collected by a small portable GPS unit. The model is compactly represented by a dynamic Bayesian network, and inference is efficiently performed using Rao-Blackwellized particle filtering both for the low level sensor integration and for the higher levels of the hierarchical model.

The main research contribution in this chapter is a demonstration of efficient inference and the development of unsupervised learning algorithms for the hierarchical predictive models of transportation routines. Previous work has described inference in hierarchical models [14] and learning non-hierarchical transportation models [84], but our work is the first to combine these techniques. A second research contribution is in unifying this model with detecting *novel* and *erroneous* behavior [85].

This chapter is organized as follows. In the next section, we provide an overview of the hierarchical activity model, followed by a description of inference and learning algorithms. Then we present experimental results and an end-to-end implementation of these techniques called "Opportunity Knocks."

6.1 Hierarchical Activity Model

We estimate a person's activities using the three level dynamic Bayesian network model shown in Fig. 6.1. The individual nodes in such a temporal graphical model represent different components of the state space and the arcs indicate dependencies between the nodes [21, 77]. Temporal dependencies are represented by arcs connecting the two time slices $k-1$ and k. The highest level of the model, the novelty mode, indicates whether the user is currently behaving normally, doing something novel, or making a transportation error. The second level of the model represents two concepts: the person's next goal (*e.g.*, her workplace) and the user's current trip segment. A trip segment is a route with a single transportation mode, which can be concatenated with other trip segments to form a plan for transiting between goals. The person's instantaneous transportation mode, location, and velocity are estimated from the GPS sensor measurements at the lowest level of the model.

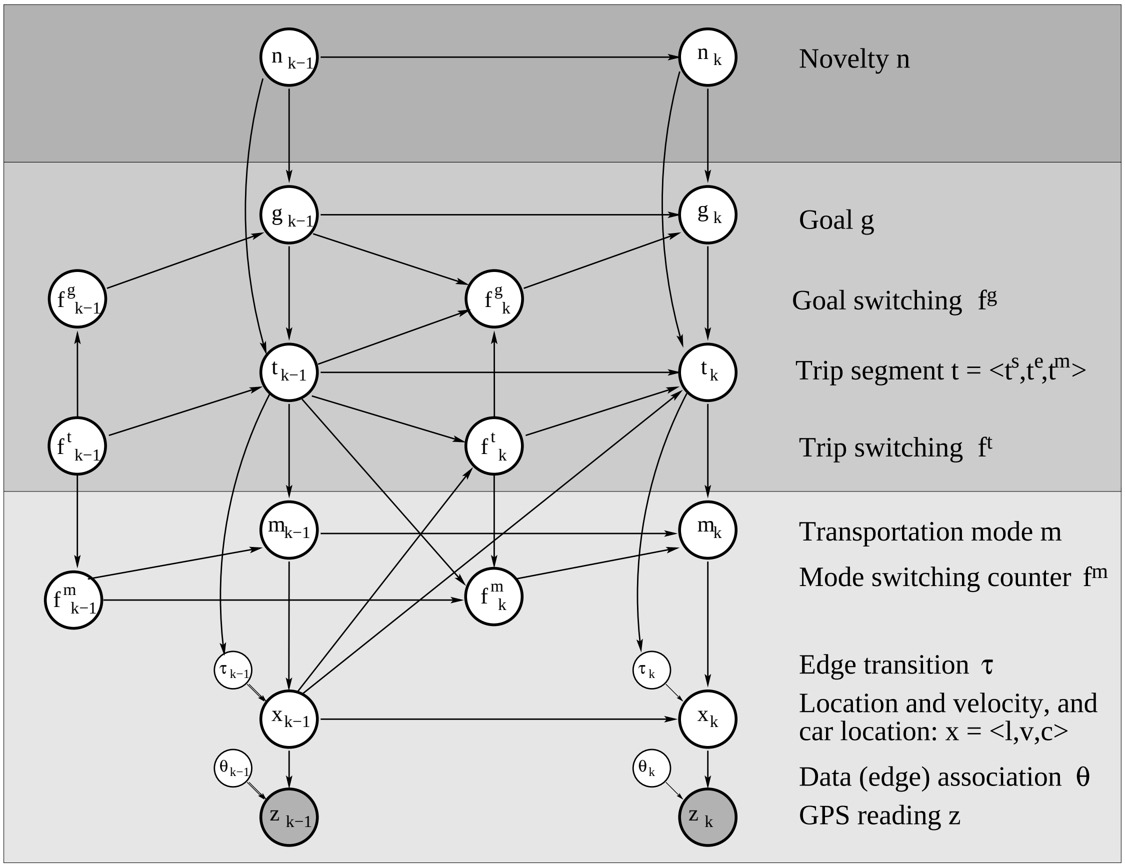

Figure 6.1: Hierarchical activity model representing a person's outdoor movements during everyday activities. The upper level is used for novelty detection, and the middle layer estimates the user's goal and the trip segments he or she is taking to get there. The lowest layer represents the user's mode of transportation, speed, and location. Two time slices, k and $k-1$, are shown.

6.1.1 Locations and transportation modes

We denote by $x_k = \langle l_k, v_k, c_k \rangle$ the location (l_k) and velocity (v_k) of the person, and the location of the person's car (c_k) (subscripts k indicate discrete time). A key point of our representation is that we constrain all locations to be on a street map. Thus, locations (both l_k and c_k) can be represented using a *directed* graph $G = (V, E)$ whose edges correspond to streets or footpaths and whose vertices correspond to intersections. A location is determined by an edge and distance pair. The edge corresponds to a street, with a given direction either up or down the street, and the distance is the distance from the start vertex of the edge.

The direction of velocity v_k is identical to the direction of the edge. The location of the person at time k depends on his previous location, l_{k-1}, the velocity, v_k, and the transition, τ_k. Vertex transitions τ_k model the decision a person makes when moving over a vertex in the graph, corresponding to an intersection on the street map. The domain of τ_k is the set of outgoing neighbors of the current edge; for example, the user could turn right, left, or not at all when transiting a street intersection. (For simplicity we assume here the person never performs U-turns to reverse moving direction on a street. In our implementation we allow U-turns with a fixed small probability and the detail is omitted here.)

GPS sensor measurements, z_k, are generated by the person carrying a GPS sensor. Since measurements are simply points in continuous xy-coordinates, they have to be "snapped" onto an edge in the graph structure. The edge to which a specific measurement is "snapped" to is estimated by the association variable θ_k. Note that θ_k is picked from the edges close to z_k (*e.g.*, within 50 meters from z_k) *independently* from the edge of location l_k.

Both the motion model, $p(l_k \mid l_{k-1}, v_k, \tau_k)$, and the sensor model, $p(z_k \mid l_k, \theta_k)$ are represented as (conditional) Gaussian models, as we will describe in Section 6.2.

The transportation mode m_k can take on four different values BUS, $FOOT$, CAR, and $BUILDING$. Similar to [84], these modes influence the velocity, v_k, which is picked from a Gaussian mixture model. For example, the $FOOT$ mode draws velocities only from the Gaussian representing walking speeds, while BUS and CAR modes draw velocities from Gaussian distributions representing both high and low velocities. $BUILDING$ is a special mode that occurs only when the GPS signal is lost for significantly long time, corresponding to the assumption that the person is indoors and not moving.

Finally, the location of the car only changes when the person is in the car and thus in CAR mode, in which case the car location is set to the person's location. If the person is not in CAR mode, the car's location affects whether a person can switch into the CAR mode. (For these experiments we assume that the user only rides in her own car. The approach could be generalized to distinguish "car travel as driver" and "car travel as passenger.")

6.1.2 Trip segments

A trip segment is defined by its start location, t_k.`start`, end location, t_k.`end`, and the mode of transportation, t_k.`mode`, the person uses during the segment. For example, a trip segment models information such as "the user boards the bus at location t_k.`start`, rides the bus to location t_k.`end`, and then debarks". In addition to transportation mode, a trip segment predicts the route on which the person gets from t_k.`start` to t_k.`end`. This route is not specified through a deterministic sequence of edges on the graph, but rather through transition probabilities on the graph. These probabilities provide a prediction of the person's change in direction when reaching an intersection, or equivalently, when crossing a vertex in the graph. This dependency is indicated by the arc from t_k to τ_k.

The transfer between modes and trip segments is handled by the switching nodes f_k^m and f_k^t, respectively. The Boolean trip switching node f_k^t is set to true whenever the person reaches the end location t_k.`end` of the current trip segment. In this case, the trip segment is allowed to switch with the constraint that the start location of the next segment is identical to the end location of the current segment. The next trip segment is chosen according to the segment transition conditioned on the current goal g_k as well as the car location c_{k-1} (indicated using the link from x_{k-1} to t_k). Once the next trip segment is active, the person still has to change mode of transportation. This does not happen instantaneously, since, for example, a person has to wait for the bus even though he already reached the bus stop (and thus entered the bus trip segment). This semi-Markov property of delayed mode switching is modeled by the node f_k^m, which is a counter that measures the time steps until the next transportation mode is entered. The counter is initialized by the next trip segment, then decremented until it reaches a value of zero, which triggers the mode switch. [1]

6.1.3 Goals

A goal represents the current target location of the person. Goals include locations such as the person's home, workplace, the grocery store, and locations of friend's homes. The goal

[1] This semi-Markov mode switch may be handled more efficiently by using fixed lag smoothing and observing when significant velocity changes are made.

of the person can only change when the person reaches the end of a trip segment. This is facilitated by a goal switching node f_k^g which is true only when the trip switching node f_k^t is true and the end of the current trip segment t_k is identical to the goal g_k. If the goal switches, the next goal is chosen according to a learned goal-to-goal transition model.

6.1.4 Novelty

At the highest level is a boolean variable n_k, indicating whether a user's behavior is consistent with historical patterns. Different values of n_k instantiate different parameters for the lower part of the model.

When a user is behaving normally, $n_k = false$, the hierarchical model functions as described up to this point and the parameters are trained using historical data. When a user's behavior is novel, $n_k = true$, the goal and the trip segment are set to a distinguished value "UNKNOWN" and as a consequence the parameters of the lowest layer of the model (*i.e.*, transportation mode transitions and edge transitions) are switched to their untrained values: An "UNKNOWN" goal and trip segment does not provide any information about the direction that a user will go when she gets to an intersection, or ways in which she will change modes of transportation. The model that is instantiated in this way is referred to as a *flat* model because there is no influence of high level model elements on the inference at the street level. A flat model respects basic intuitions about changing transportation modes and moving on a street map, but is not influenced by long-term goals such as where and how the user is getting home from work. Instead the flat model utilizes straightforward Markov transition probabilities in the lowest level of Fig. 6.1 analogous to [84].

6.2 Inference

After we have defined the structure of the model and assumed values for the transition parameters (parameter estimation will be discussed in the next section), we must develop efficient algorithms to infer the distribution of hidden variables at real time given a sequence of GPS readings. In this section, we first focus on the estimation of locations and modes of transportation. For simplicity, we present a version of this algorithm that does not apply switching nodes and waiting time counters. These concepts will be discussed in the context of the hierarchical model, which additionally estimates a person's high level goals, trip segments, and novelty.

6.2.1 Flat Model

First we will explain the estimation of locations and transportation modes using a *flat* model. This is the model shown in Fig. 6.1 with the top two levels removed. Note that removing the top levels may introduce additional direct dependencies in the lowest level. For instance, we must add arcs from x_{k-1} to m_k, τ_k, and f_k^m. Remember our system tracks people's locations on a street map. Because street maps have a complex structure and the estimation problem contains a variety of continuous (locations, velocities) and discrete states (edge transition, transportation mode, *etc.*), exact inference is intractable. Instead, we rely on Rao-Blackwellized particle filters for inference in the flat model [25]. In our case, the Rao-Blackwellized particle filter combines particle filters with Kalman filters. Particle filters [24, 107] and Kalman filters [107, 6] are two widely-used techniques for state tracking in dynamic systems. The goal of state tracking is to estimate the posterior distribution, $p(s_k \mid z_{1:k})$, at each time step k, where s_k represents the set of state variables at k and $z_{1:k}$ is the sequence of observations up to time k. In this section, we will first briefly describe the particle filters and Kalman filters in general, and then discuss the application of these techniques in our flat model.

Particle filters

Particle filters represent posterior distributions over the state space with temporal sets, S_k, of n weighted samples:

$$S_k \;=\; \{s_k^{(i)}, w_k^{(i)} \mid 1 \leq i \leq N\}$$

Here $s_k^{(i)}$ is a sample (or state), and $w_k^{(i)}$ is a non-negative numerical factor called an *importance weight*. The basic particle filter updates the posterior according to the following sampling procedure, often referred to as sequential importance sampling with re-sampling (SISR, see also [24, 107]).

- **Sampling:** Draw n samples, $s_{k-1}^{(i)}$, from the previous set and generate n new samples, $s_k^{(i)}$, using the *proposal distribution*, $q(s_k \mid s_{k-1}^{(i)}, z_k)$

- **Importance sampling:** Assign each sample an importance weight $w_k^{(i)}$ as

$$w_k^{(i)} \;\propto\; w_{k-1}^{(i)} \, \frac{p(z_k \mid s_k^{(i)}) p(s_k^{(i)} \mid s_{k-1}^{(i)})}{q(s_k^{(i)} \mid s_{k-1}^{(i)}, z_k)} \tag{6.1}$$

- **Re-sampling:** Multiply / discard samples by drawing samples with replacement according to the distribution defined through the importance weights $w_k^{(i)}$.

It is often convenient to choose the proposal distribution to be the prediction as

$$q(s_k \mid s_{k-1}^{(i)}, z_k) \;=\; p(s_k \mid s_{k-1}^{(i)}) \tag{6.2}$$

By substituting (6.2) into (6.1), we get

$$w_k^{(i)} \;\propto\; w_{k-1}^{(i)} \, p(z_k \mid s_k^{(i)}) \tag{6.3}$$

Kalman filters

Kalman filtering [107, 6] represents beliefs by a unimodal Gaussian distribution, $\mathcal{N}(s_k; \mu_k, \Sigma_k)$, where μ_k and Σ_k are the mean and the variance, respectively. At each time step, Kalman filters update these Gaussian beliefs by two steps: a *prediction step* followed by a *correction step.*

In the prediction step, Kalman filters predict the state distribution based on the previous belief $\mathcal{N}(s_{k-1}; \mu_{k-1}, \Sigma_{k-1})$ and the system dynamics $p(s_k \mid s_{k-1})$. Under the assumption that the state at time k is a linear function of the previous state with additive Gaussian noise, the system dynamics can be represented by another Gaussian $\mathcal{N}(s_k; A_t s_{k-1}, R_t)$, where A_t is the dynamics matrix and R_t is the covariance of the Gaussian noise. The prediction is a convolution of these two Gaussians and thus the result is also a Gaussian over the state space:

$$\mathcal{N}(s_k; \widehat{\mu}_k, \widehat{\Sigma}_k) \quad = \quad \int \mathcal{N}(s_k; A_t s_{k-1}, R_t)\, \mathcal{N}(s_{k-1}; \mu_{k-1}, \Sigma_{k-1})\, \mathrm{d}s_{k-1} \tag{6.4}$$

Here, $\langle \widehat{\mu}_k, \widehat{\Sigma}_k \rangle$ denote the parameters defining the *predictive belief* at time k, that is, the belief before the observation z_k is considered. The parameters can be computed in closed form as

$$\begin{aligned} \widehat{\mu}_k &= A_t \mu_{k-1} \\ \widehat{\Sigma}_k &= A_t \Sigma_{k-1} A_t^T + R_t. \end{aligned} \tag{6.5}$$

In the correction step, the most recent measurement z_k is used to adjust the prediction $\mathcal{N}(s_k; \widehat{\mu}_k, \widehat{\Sigma}_k)$. If we assume that sensor measurements z_k are linear functions of the state s_k, with added Gaussian noise, then the sensor model $p(z_k \mid s_k)$ is the Gaussian $\mathcal{N}(z_k; C_k s_k, Q_k)$. Here the matrix C_k maps states to observations and Q_t is the covariance of the observation noise. The posterior belief is again a Gaussian

$$\mathcal{N}(s_k; \mu_k, \Sigma_k) \quad \propto \quad \mathcal{N}(z_k; C_t s_k, Q_k)\, \mathcal{N}(s_k; \widehat{\mu}_k, \widehat{\Sigma}_k) \tag{6.6}$$

with

$$\begin{aligned} \mu_k &= \widehat{\mu}_k + K_k\, (z_k - C_t\, \widehat{\mu}_k) \\ \Sigma_k &= (1 - K_k C_k)\, \widehat{\Sigma}_k \end{aligned} \tag{6.7}$$

where $K_k = \widehat{\Sigma}_k C_k^T / (C_k \widehat{\Sigma}_k C_k^T + Q_k)$ is the so-called *Kalman gain.*

Rao-Blackwellized particle filters for estimation in the flat model

The main advantage of Kalman filters is their computational efficiency. This efficiency, however, comes at the cost of restricted representation power because Kalman filters only apply to (approximately) linear systems that can be described by unimodal distributions. While particle filters can be applied to arbitrary, non-linear systems, they are less efficient than

Kalman filters. The key idea of Rao-Blackwellized particle filters (RBPF) is to combine both representations, thereby leveraging the efficiency of Kalman filters and the representational power of particle filters. RBPFs have been applied with great success to various state estimation problems, including robot mapping [76, 73], tracking [24, 57, 98], and system monitoring [20, 74].

In our approach, we estimate the posterior over the location of the person and the car, and the complete histories of the other parts of the state space, conditioned on $z_{1:k}$, the sequence of GPS measurements observed so far. As we will see, the estimation of these histories is necessary for the derivation of the filter, but implementations of the RBPF typically keep track of the current state only. The following factorization of the posterior forms the basis for our Rao-Blackwellized particle filter:

$$\begin{aligned} & p(c_k, l_k, m_{1:k}, v_{1:k}, \tau_{1:k}, \theta_{1:k} \mid z_{1:k}) \\ = \quad & p(c_k \mid l_k, m_{1:k}, v_{1:k}, \tau_{1:k}, \theta_{1:k}, z_{1:k}) \\ & p(l_k \mid m_{1:k}, v_{1:k}, \tau_{1:k}, \theta_{1:k}, z_{1:k}) \, p(m_{1:k}, v_{1:k}, \tau_{1:k}, \theta_{1:k} \mid z_{1:k}) \end{aligned} \tag{6.8}$$

This factorization separates the state space of our estimation problem into three parts. From right to left, the first part contains histories over the transportation mode $m_{1:k}$, velocity $v_{1:k}$, edge transition $\tau_{1:k}$, and edge association $\theta_{1:k}$, which are represented by the samples in a particle filter. The second part is the location of the person l_k on the graph, which is estimated using Kalman filters conditioned on the samples. The third part represents the car location which, as we will show, is a function of the person's location.

Each particle of the flat RBPF has the following form:

$$s_k^{(i)} = \left\langle \langle \xi_k^{(i)}, \Xi_k^{(i)} \rangle, \langle \mu_k^{(i)}, \Sigma_k^{(i)} \rangle, \, m_{1:k}^{(i)}, v_{1:k}^{(i)}, \tau_{1:k}^{(i)}, \theta_{1:k}^{(i)} \right\rangle, \tag{6.9}$$

where $\langle \xi_k^{(i)}, \Xi_k^{(i)} \rangle$ and $\langle \mu_k^{(i)}, \Sigma_k^{(i)} \rangle$ represent the mean and variance of the car location and person location estimates, respectively. Here we present a memory efficient version of the RBPF algorithm that only stores the most recent states. Whenever a new GPS measurement arrives, the RBPF draws a particle $s_{k-1}^{(i)}$ from the previous sample set. The updated particles are then generated in three steps, evaluating (6.8) from right to left: First, the state histories are expanded by sampling the most recent states. Second, the person's location estimate is updated using a Kalman filter update conditioned on the measurement and the sampled values. Finally, the car location is updated conditioned on these estimates.

Sampling step

The updated histories $m_{1:k}^{(i)}, v_{1:k}^{(i)}, \tau_{1:k}^{(i)}$, and $\theta_{1:k}^{(i)}$ are generated by expanding $s_{k-1}^{(i)}$'s histories via sampling the states at time k and attaching them to the existing histories. First, the transportation mode $m_k^{(i)}$ is sampled from $p(m_k^{(i)} \mid m_{k-1}^{(i)}, \mu_{k-1}^{(i)}, \xi_{k-1}^{(i)})$ and then attached to the particle's mode history $m_{1:k-1}^{(i)}$ to generate $m_{1:k}^{(i)}$. Mode transitions take information about bus routes and the person's car into account. For instance, whenever the person's location $\mu_{k-1}^{(i)}$ was near a bus stop and the previous mode was `FOOT`, then $m_k^{(i)}$ switches to `BUS` with a small probability. Similarly, the person can only switch into the `CAR` mode if he was near the car location $\xi_{k-1}^{(i)}$.

Once the transportation mode is sampled, the motion velocity $v_k^{(i)}$ is sampled from a mixture of Gaussians which is conditioned on the mode. The value of the next edge transition variable $\tau_k^{(i)}$ is sampled based on the previous position of the person and a learned transition model. This is used in case the mean of the location estimate reaches an intersection. The edge association variable $\theta_k^{(i)}$ "snaps" the GPS reading to a street in the map. To sample $\theta_k^{(i)}$, we first determine the distance between the measurement, z_k, and the different streets in the vicinity. The probability of "snapping" z_k to one of these streets is then computed from this distance. These assignments are crucial for the Kalman filter update described next.

Kalman filter step

After the RBPF generated all the sampled histories of a particle, that is,

$$s_k^{(i)} = \left\langle \langle \_, \_ \rangle, \langle \_, \_ \rangle, m_{1:k}^{(i)}, v_{1:k}^{(i)}, \tau_{1:k}^{(i)}, \theta_{1:k}^{(i)} \right\rangle ,$$

it then generates the missing location estimate $\langle \mu_k^{(i)}, \Sigma_k^{(i)} \rangle$ by updating the Kalman filter conditioned on the already sampled values. To elaborate, let us rewrite the second term on the right hand side of (6.8):

$$\begin{aligned} & p(l_k \mid m_{1:k}^{(i)}, v_{1:k}^{(i)}, \tau_{1:k}^{(i)}, \theta_{1:k}^{(i)}, z_{1:k}) \\ = \quad & p(l_k \mid \langle \mu_{k-1}^{(i)}, \Sigma_{k-1}^{(i)} \rangle, m_k^{(i)}, v_k^{(i)}, \tau_k^{(i)}, \theta_k^{(i)}, z_k) \qquad (6.10) \\ \propto \quad & p(z_k \mid l_k, \theta_k^{(i)}) \int p(l_k \mid v_k^{(i)}, \tau_k^{(i)}, l_{k-1}^{(i)})\, \mathcal{N}(l_{k-1}^{(i)}; \mu_{k-1}^{(i)}, \Sigma_{k-1}^{(i)})\, \mathrm{d}l_{k-1}^{(i)} \qquad (6.11) \end{aligned}$$

(6.10) follows from the fact that the Gaussian estimate $\langle \mu_{k-1}^{(i)}, \Sigma_{k-1}^{(i)} \rangle$ of the person's location is a sufficient statistic for all observations up to time $k-1$, when conditioned on the particle's histories over the other parts of the state space. The justification of this step is the key reason for estimating histories rather than only the most recent states. Equation (6.11) now follows by applying Bayes rule and the independences in our estimation problem (cf. Fig. 6.1). It represents a standard recursive Bayes filter update rule; see [107, 6] for details. The prior probability is given by the Gaussian of the previous Kalman filter estimate. Conditioned on the already sampled values $\theta_k^{(i)}, v_k^{(i)}$, and $\tau_k^{(i)}$, (6.11) reduces to a standard Kalman filter update.

In the prediction step, the traveled distance is predicted using the sampled Gaussian velocity component. The prediction, $\langle \widehat{\mu}_k^{(i)}, \widehat{\Sigma}_k^{(i)} \rangle$, results then from shifting and convolving the previous estimate by the predicted motion, thereby implementing the integration in (6.11) via the Kalman update (6.5). This prediction step is straightforward if the person stays on the same edge of the graph. If she transits over a vertex of the graph, then the next edge is given by the previously sampled edge transition ${\tau_k}^{(i)}$ (see upper panel in Fig. 6.2). To simplify computation, only the predicted mean $\widehat{\mu}_k^{(i)}$ is used to determine whether the person switches edges. In our experience this approximation is accurate enough for location tracking.

In the correction step, the predicted estimate $\langle \widehat{\mu}_k^{(i)}, \widehat{\Sigma}_k^{(i)} \rangle$ is corrected based on the most recent GPS measurement z_k, using (6.7). Intuitively, this correction compares the predicted mean $\widehat{\mu}_k^{(i)}$ with the location of z_k and shifts the mean toward the measurement (under

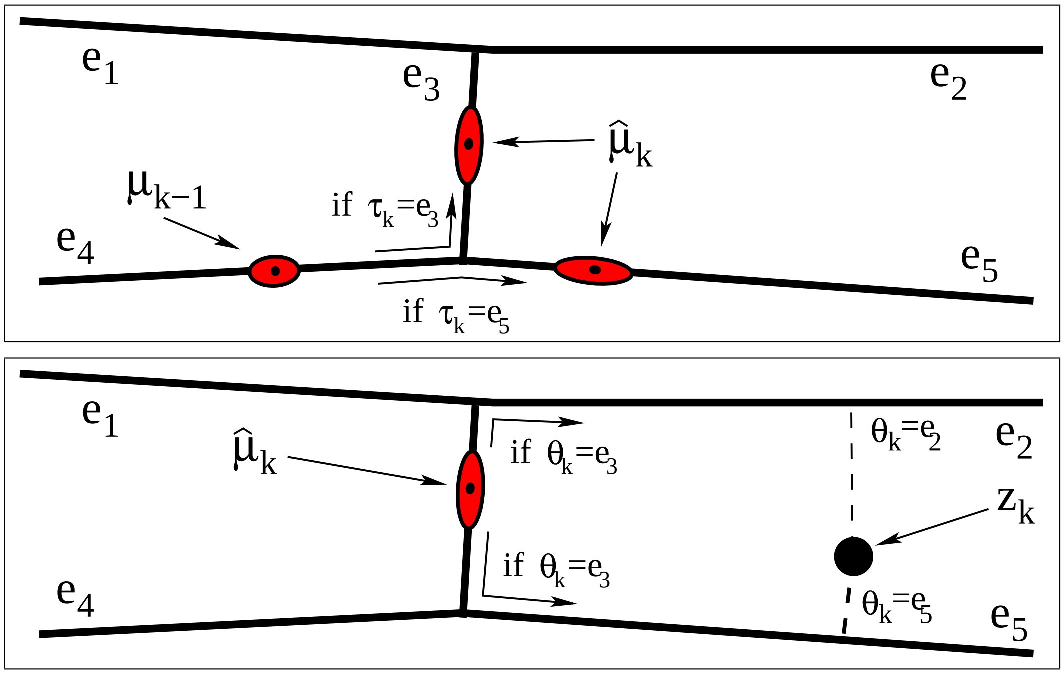

Figure 6.2: Kalman filter prediction (upper panel) and correction (lower panel) on a street graph. The previous belief is located on edge e_4. When the predicted mean transits over the vertex, then the next location can be either on e_3 or e_5, depending on the sampled edge transition τ_k. In the correction step (lower panel), the continuous coordinates of the GPS measurement, z_k, are between edges e_2 and e_5. Depending on the value of the edge association, θ_k, the correction step moves the estimate up-wards or down-wards.

consideration of the uncertainties). The correction step for one Gaussian is illustrated in the lower panel of Fig. 6.2. Because we restrict the location estimates to the graph, we "snap" the GPS measurements onto the graph. The already sampled value of the edge association variable $\theta_k^{(i)}$ uniquely determines to which edge the reading is snapped. After a GPS measurement is snapped onto one of the edges, we find the shortest path on the graph between the $\widehat{\mu}_k^{(i)}$ and the snapped measurement using the standard A* search algorithm. Then we can apply a one-dimensional Kalman filtering correction step and get the posterior location estimate $\langle {\mu_k}^{(i)}, {\Sigma_k}^{(i)} \rangle$.

Finally, the car location is updated. We rewrite the first term of the factorization in

(6.8) as

$$
\begin{aligned}
&p(c_k \mid l_k, v_{1:k}, m_{1:k}, \theta_{1:k}, \tau_{1:k}, z_{1:k}) \\
&= \begin{cases} \delta(l_k - c_k) & \text{if } m_k = \texttt{CAR} \\ \delta(c_{k-1} - c_k)\, p(c_{k-1} \mid l_{k-1}, v_{1:k-1}, m_{1:k-1}, \theta_{1:k-1}, \tau_{1:k-1}, z_{1:k-1}) & \text{otherwise} \end{cases}
\end{aligned}
\tag{6.12}
$$

where $\delta(x)$ is the Dirac delta function that returns infinity if $x = 0$ and zero otherwise. (6.12) is based on the assumption that the person is always using the same vehicle and that nobody else moves the vehicle. As a result, if the person is in the car, then the car location is set to the person's location. Otherwise, the car location is the same as in the previous time step.

Importance weights

After all components of each particle are generated, the importance weights of the particles need to be updated using Equation (6.1). In our case, the sampling steps do not consider the most recent observation z_k and the proposal distribution is identical to (6.2), resulting in importance weights proportional to the observation likelihood:

$$
\begin{aligned}
w_k^{(i)} &\propto w_{k-1}^{(i)}\, p(z_k \mid s_k^{(i)}) && (6.13) \\
&= w_{k-1}^{(i)}\, p(z_k \mid \langle \xi_{k-1}^{(i)}, \Xi_{k-1}^{(i)} \rangle, \langle \mu_{k-1}^{(i)}, \Sigma_{k-1}^{(i)} \rangle, m_{1:k}^{(i)}, v_{1:k}^{(i)}, \tau_{1:k}^{(i)}, \theta_{1:k}^{(i)}) && (6.14) \\
&= w_{k-1}^{(i)}\, \mathcal{N}(z_k;\ \widehat{\mu}_k^{(i)}, \widehat{\Sigma}_k^{(i)} + Q_k) && (6.15)
\end{aligned}
$$

This observation likelihood is computed based on each particle's sampled values, as given in (6.13). The likelihood can be computed in closed form from the Kalman filter correction step [107]. In the case of GPS readings, the likelihood of a measurement is given by a Gaussian with mean at the predicted location $\widehat{\mu}_k^{(i)}$ and variance given by the predicted location uncertainty $\widehat{\Sigma}_k^{(i)}$ plus measurement noise Q_k, as given in (6.15).

```
inputs : Sample set $S_{k-1} = \{\langle s_{k-1}^{(i)}, w_{k-1}^{(i)}\rangle \mid 1 \le i \le N\}$ and observation $z_k$
output: Current sample set: $S_k = \{\langle s_k^{(i)}, w_k^{(i)}\rangle \mid 1 \le i \le N\}$
1.  $S_k = \emptyset$ ;                                                      // Initialize
2.  for $i = 1, \ldots, N$ do
3.      Sample $m_k^{(i)} \sim p(m_k^{(i)} \mid m_{k-1}^{(i)}, \mu_{k-1}^{(i)}, \xi_{k-1}^{(i)})$ ;      // Sample transportation mode
4.      Sample $v_k^{(i)} \sim p(v_k^{(i)} \mid m_k^{(i)})$;                               // Sample velocity
5.      Sample $\tau_k^{(i)} \sim p(\tau_k^{(i)} \mid \mu_{k-1}^{(i)}, m_k^{(i)})$ ;          // Sample decision at next vertex
6.      Sample $\theta_k^{(i)} \sim p(\theta_k^{(i)} \mid z_k)$ ;                        // Sample GPS to edge association
7.      Compute $\langle \mu_k^{(i)}, \Sigma_k^{(i)}\rangle$ conditioned on $\langle \mu_{k-1}^{(i)}, \Sigma_{k-1}^{(i)}\rangle$, $v_k^{(i)}$,$\tau_k^{(i)}$, $\theta_k^{(i)}$, and $z_k$ ;
8.      if $m_k^{(i)} = \texttt{CAR}$ then $\langle \xi_k^{(i)}, \Xi_k^{(i)}\rangle := \langle \mu_k^{(i)}, \Sigma_k^{(i)}\rangle$ ;         // Car moves with person
9.      else $\langle \xi_k^{(i)}, \Xi_k^{(i)}\rangle := \langle \xi_{k-1}^{(i)}, \Xi_{k-1}^{(i)}\rangle$ ;                // Car does not move
10.     $w_k^{(i)} = w_{k-1}^{(i)}\, \mathcal{N}(z_k;\, \widehat{\mu}_k^{(i)}, \widehat{\Sigma}_k^{(i)} + Q_k)$ ;          // Kalman filter likelihood
11.     $S_k = S_k \cup \{\langle s_k^{(i)}, w_k^{(i)}\rangle\}$ ;                        // Insert into sample set
12. end
13. Multiply / discard samples in $S_k$ based on normalized weights ;
```

Algorithm 6.1: RBPF for flat model

RBPF algorithm for the flat model

The algorithm **RBPF_Flat** is summarized in Alg. 6.1. The algorithm accepts as inputs a sample set representing the previous belief and the most recent GPS measurement. For each particle, the algorithm first samples the transportation mode in Step 3. The sampling distribution models that a person can only get on or off a bus when she is near a bus stop, and she can only get into the car when she is near the location where the car is parked. Then, the algorithm samples the velocity conditioned on the mode, the motion decision at the next vertex, and the association of the GPS reading to an edge in the street map (Step 4 to Step 6).

Then, in Step 7, the Gaussian estimate of the person's location is updated using Kalman filtering. Step 8 and Step 9 set the car location accordingly. The weight of each particle is determined in Step 10, based on the Kalman filter estimate of the person's location. After inserting each particle into the sample set, the algorithm performs resampling based on the importance weights. Resampling with minimal variance can be implemented efficiently (constant time per sample) using a procedure known as deterministic selection [51, 2] or stochastic universal sampling [5].

6.2.2 Hierarchical Model

Up to this point, we have described state estimation in a “flat” model, that is, a model that does not reason about a person’s goals, trip segments, and novelty. We will now describe how to extend the RBPF for the flat model so as to estimate the posterior over the complete hierarchical model shown in Fig. 6.1. To additionally model goals, trip segments, novelty, and improved mode switching, we add the corresponding components to each particle of the RBPF [2]:

$$s_k^{(i)} = \left\langle n_k^{(i)}, \langle g_k^{(i)}, t_k^{(i)} \rangle, f_k^{g(i)}, \langle \xi_k^{(i)}, \Xi_k^{(i)} \rangle, \langle \mu_k^{(i)}, \Sigma_k^{(i)} \rangle, v_k^{(i)}, m_k^{(i)}, f_k^{m(i)}, f_k^{t(i)}, \theta_k^{(i)}, \tau_k^{(i)} \right\rangle \tag{6.16}$$

Here each $\langle g_k^{(i)}, t_k^{(i)} \rangle$ is a *discrete distribution* over goals and trip segments. These distributions are estimated using exact inference conditioned on the sampled values, just like exact Kalman filtering is performed for the location estimates $\langle \mu_k^{(i)}, \Sigma_k^{(i)} \rangle$ in the flat model. Boolean variable $n_k^{(i)}$ represents whether or not the person is currently following an expected route, where the expectation is based on historical data. The values $f_k^{g(i)}$, $f_k^{t(i)}$, and $f_k^{m(i)}$ represent sampled information about switching between goals, trip segments, and transportation modes, respectively.

RBPF algorithm for the hierarchical model

Alg. 6.2 summarizes one update step of the algorithm **RBPF_Hierarchical**, which implements Rao-Blackwellized particle filtering for the complete model except novel behavior. We omit a full derivation of this algorithm; it is similar to the derivation of **RBPF_Flat** and to Rao-Blackwellized inference for abstract hidden Markov models, with which our model shares the high-level structure [12].

The algorithm accepts as inputs the sample set representing the previous belief and the most recent measurement. In order to be able to sample the switching nodes conditioned on

[2] For simplicity we omit the histories of sampled values. Similar to the case of flat model, those histories are necessary for deriving the algorithm, but do not have to be stored during implementation.

```
inputs : Sample set $S_{k-1} = \{\langle s_{k-1}^{(i)}, w_{k-1}^{(i)} \rangle \mid 1 \leq i \leq N\}$ and observation $z_k$
output: Current sample set: $S_k = \{\langle s_k^{(i)}, w_k^{(i)} \rangle \mid 1 \leq i \leq N\}$
$S_k = \emptyset$ ;                                                                // Initialize
for $i = 1, \ldots, N$ do
    Sample $(\tilde{g}_{k-1}^{(i)}, \tilde{t}_{k-1}^{(i)}) \sim p(g_{k-1}^{(i)}, t_{k-1}^{(i)})$ ;          // Draw goal and trip segment
    if $\mu_{k-1}^{(i)} = \tilde{t}_{k-1}^{(i)}$.end then $f_k^{t(i)} := true$ ;        // Just reached end of trip segment?
    else $f_k^{t(i)} := false$ ;
    if $f_k^{t(i)} = true$ and $\tilde{g}_{k-1}^{(i)} = \tilde{t}_{k-1}^{(i)}$.end then $f_k^{g(i)} := true$ ;   // Goal reached?
    else $f_k^{g(i)} := false$ ;
    if $f_k^{t(i)} = true$ then
        $f_k^{m(i)} \sim \mathrm{Uniform}[0, \text{max-waiting-time}]$ ;           // Sample when to switch mode
    else $f_k^{m(i)} := f_{k-1}^{m(i)} - 1$ ;
    Compute $p(\hat{g}_k^{(i)}, \hat{t}_k^{(i)} \mid f_k^{g(i)}, f_k^{t(i)}, g_{k-1}^{(i)}, t_{k-1}^{(i)}, \xi_{k-1}^{(i)})$ ;
    Sample $(\tilde{g}_k^{(i)}, \tilde{t}_k^{(i)}) \sim p(\hat{g}_k^{(i)}, \hat{t}_k^{(i)})$ ;                // Draw goal and trip segment
    if $f_k^{m(i)} = 0$ then $m_k^{(i)} = \tilde{t}_k^{(i)}$.mode ;                    // Change transportation mode?
    else $m_k^{(i)} = m_{k-1}^{(i)}$ ;
    Sample $v_k^{(i)} \sim p(v_k^{(i)} \mid m_k^{(i)})$ ;                                   // Sample velocity
    Sample $\tau_k^{(i)} \sim p(\tau_k^{(i)} \mid \mu_{k-1}^{(i)}, \tilde{t}_k^{(i)})$ ;                   // Sample decision at next vertex
    Sample $\theta_k^{(i)} \sim p(\theta_k^{(i)} \mid z_k)$ ;                              // Sample GPS to edge association
    Compute $\langle \mu_k^{(i)}, \Sigma_k^{(i)} \rangle$ conditioned on $\langle \mu_{k-1}^{(i)}, \Sigma_{k-1}^{(i)} \rangle$, $v_k^{(i)}$,$\tau_k^{(i)}$, $\theta_k^{(i)}$, and $z_k$ ;
    if $m_k^{(i)} = CAR$ then $\langle \xi_k^{(i)}, \Xi_k^{(i)} \rangle := \langle \mu_k^{(i)}, \Sigma_k^{(i)} \rangle$ ;          // Car moves with person
    else $\langle \xi_k^{(i)}, \Xi_k^{(i)} \rangle := \langle \xi_{k-1}^{(i)}, \Xi_{k-1}^{(i)} \rangle$ ;                  // Car does not move
    Compute $p(g_k^{(i)}, t_k^{(i)} \mid m_k^{(i)}, \tau_k^{(i)}, \hat{g}_k^{(i)}, \hat{t}_k^{(i)})$
    $w_k^{(i)} = w_{k-1}^{(i)} \, \mathcal{N}(z_k;\ \widehat{\mu}_k^{(i)}, \widehat{\Sigma}_k^{(i)} + Q_k)$ ;                // Update particle weight
    $S_k = S_k \cup \{\langle s_k^{(i)}, w_k^{(i)} \rangle\}$;                                  // Insert into sample set
end
Multiply / discard samples in $S_k$ based on normalized weights
```

Algorithm 6.2: RBPF for hierarchical model

the high-level nodes, the algorithm first samples a goal / trip segment combination from the previous distribution (Step 3). Then, Step 4 tests whether the previous location reached the end of the trip segment. In our implementation, this test returns true if $\mu_{k-1}^{(i)}$ just entered the edge of $\tilde{t}_{k-1}^{(i)}.\texttt{end}$. The goal switching node $f_k^{g(i)}$ is set to true if the end of the trip segment is reached and the trip segment ends in the goal location (Step 6). The time period until the transportation mode on the new trip segment is switched, is sampled in Step 9, and decremented in Step 10. This semi-Markov mode switching enables the RBPF to model non-exponential waiting times between, for example, reaching a bus stop and getting on the bus. We found that this technique is far more robust than a straightforward approach that samples a mode switch at every iteration.

Then, in Step 11, the distribution over goals and trip segments is projected forward conditioned on the sampled switching nodes as well as the car location $\xi_{k-1}^{(i)}$. Similar to Step 3, a goal / trip segment combination is sampled from the predicted distribution in Step 12. If the transportation mode switching counter reaches zero, then $m_k^{(i)}$ is set to the mode of the sampled trip segment (Step 13). Step 15 through Step 20 correspond exactly to Step 4 through Step 9 in the flat model, with a key difference in Step 16: While the flat model samples the transition $\tau_k^{(i)}$ at the next intersection solely based on the location $\mu_{k-1}^{(i)}$ and $m_k^{(i)}$, the hierarchical model takes the current trip segment $\tilde{t}_k^{(i)}$ into account. Thus, the hierarchical model can have different transition probabilities at an intersection depending on the trip segment the person is following. As we will show in the experimental results, this additional dependency leads to greatly improved predictive capabilities.

The distribution over goals and trip segments is updated in Step 21. The sampled transition $\tau_k^{(i)}$ plays an important role in this update, since it indicates in which direction the person is moving. Similarly, the sampled transportation mode $m_k^{(i)}$ indicates transitions between trip segments. After each particle is weighted and inserted into the sample set, the algorithm finishes with the resampling step.

```
   inputs : Sample set $S_{k-1} = \{\langle s_{k-1}^{(i)}, w_{k-1}^{(i)} \rangle \mid 1 \leq i \leq N\}$ and observation $z_k$
   output: Current sample set: $S_k = \{\langle s_k^{(i)}, w_k^{(i)} \rangle \mid 1 \leq i \leq N\}$
1. $S_k = \emptyset$ ;                                                    // Initialize
2. for $i = 1, \ldots, N$ do
3.     Sample $n_k^{(i)} \sim p(n_k^{(i)} \mid n_{k-1}^{(i)})$ ;                              // Novel behavior?
4.     if $n_k^{(i)} = true$ then $\langle s_k^{(i)}, w_k^{(i)} \rangle :=$ RBPF_Flat($\langle s_{k-1}^{(i)}, w_{k-1}^{(i)} \rangle$) ;
5.     else $\langle s_k^{(i)}, w_k^{(i)} \rangle :=$ RBPF_Hierarchical($\langle s_{k-1}^{(i)}, w_{k-1}^{(i)} \rangle$) ;
6. end
7. Multiply / discard samples in $S_k$ based on normalized weights;
```

Algorithm 6.3: RBPF for novelty detection

Detecting novel behavior

In order to distinguish novel from expected behavior, we compare the predictive capabilities of a model that is not trained for a specific user and a model with goals, trip segments, and transition probabilities trained on data collected by the specific user (see Section 6.3). The idea behind this approach is that if the person behaves as expected based on his history, then the trained model is able to much better predict the person's motion. If the user follows a novel route or commits an error, then the untrained model is more predictive, since it is not biased toward any specific route.

This approach can be implemented naturally within our RBPF technique. To do so, we sample the node $n_k^{(i)}$ and, if $n_k^{(i)} = false$, a particle is associated with a trained model. When $n_k^{(i)} = true$, the particle is updated using an untrained model. As a result, while particles with $n_k^{(i)} = false$ are strongly biased toward following routes and transportation routines the user has visited in the training data, particles with $n_k^{(i)} = true$ have no user-specific preferences for certain motion directions or modes of transportation. The algorithm **RBPF_Novelty**, shown in Alg. 6.3, implements novelty detection.

Step 3 samples a particle's novelty. Switching from $n_{k-1}^{(i)} = false$ to $n_k^{(i)} = true$ indicates that the person just left the routes expected by the learned model. Switching from *true* to *false* models the situation when the person gets back onto a known route. The probability for these two cases is significantly lower than the probability of remaining in the previous novelty mode. If the sampled novelty is *true*, then the particle is updated using the untrained, flat RBPF algorithm in Step 4. Here, we choose the flat model since it supports unbiased motion more naturally and efficiently than a hierarchical model with uniform transitions. If the novelty is $false$, then the particle is updated using a hierarchical model that is trained on historical data collected by the user (Step 5). Finally, if the novelty mode switches from $n_{k-1}^{(i)} = true$ to $n_k^{(i)} = false$, we re-initialize the distribution over goals and trip segments to uniform.

The resulting technique is able to detect when a user deviates from a known route and when she returns to a previously used route. The interpretation of the novelty, however, depends on the context: it could mean user errors (*e.g.*, taking a wrong bus) or deliberate novel behavior (*e.g.*, driving to a new place). In some cases, we may want to explicitly estimate the probability of an error. This can be done by combining two factors: the probability of novelty and the probability of an error given a novel behavior, as the following:

$$P(\text{Error}) \quad = \quad P(n_k = true)P(\text{Error} \mid n_k = true) \tag{6.17}$$

When the true goal is unknown (as we have assumed so far), $P(n_k = true)$ is estimated by sampling as we have discussed, and $P(\text{Error} \mid n_k = true)$ is a user-dependent parameter that we set manually: for people who seldom make mistakes, we could choose its value as 0, while for people with cognitive disabilities, the value should be set much higher.

When the user's *true* intention is known, we can integrate the knowledge into our inference and predict errors more accurately. It is possible for the system to know where the user is going, for example, if the user asks for directions to a destination, if a care-giver or job coach indicates the "correct" destination, or if the system has access to a location enabled date-book (see Section 6.5 for an example). In these cases, $P(n_k) = true$ in (6.17) can be estimated similarly to the previous case; the difference is that we now *clamp* the supplied value of the goal and/or trip segment in the learned model. If the user has specified the goal, then $P(\text{Error} \mid n_k = true)$ should be set close to 1, *i.e.*, if a user follows a novel route while heading toward a familiar goal, there is a strong probability that he is making an error.

6.3 Learning

Learning the hierarchical model of a given user includes two procedures. The first is to identify the possible sets of goals and trip segments, which comprise the range of the variables g_k and t_k in the hierarchical model shown in Fig. 6.1. This corresponds to finding the set of significant places including frequently-used bus stops and parking areas. We can identify those significant places robustly using the techniques discussed in Chapter 5. In this section, we discuss the second task — estimating the transition matrices at all levels of the hierarchical model, including the transition matrix between the goals, the transition matrix between the trip segments given a goal, and the street transition matrix within a trip segment. The street transition matrices in a flat model can be estimated similarly (see [84] for details).

Given the GPS data collected by a person moving through the community, one way of learning the transition parameters is to require the person to keep a diary for several weeks of their transportation routines in order to create a supervised training set. Then we can estimate the transition matrices by simply counting the corresponding transitions and normalizing the counts. However, it is extremely hard in practice to obtain the labeled training data, and thus we want to estimate those parameters in an *unsupervised manner* without any manual labels. A general approach for solving such learning problems is the well-known Expectation-Maximization (EM) algorithm [22, 94]. EM solves such problems by iterating between an Expectation step (E-step) and a Maximization step (M-step). In a nutshell, each E-step estimates expectations (distributions) over the transition counts using the GPS observations along with the current estimate of the model parameters. Then in the M-step the model parameters are updated using the expectations obtained in the E-step. The updated model is then used in the next E-step to obtain more accurate estimates of the hidden transition counts. EM theory tells us that in each iteration the estimation of the parameters will be improved and it will eventually converge to a local optimum.

A brief description of the learning algorithm is shown in Alg. 6.4. In Step 1, all the transition parameters are initialized: $p(g_{i'} \mid g_i)$ is initialized as uniform, $p(t_{j'} \mid t_j, g_i)$ is also a uniform distribution given $t_{j'}.\texttt{start} = t_j.\texttt{end}$, and similarly $p(e_{k'} \mid e_k, t_j)$ is initialized as

```
   inputs : GPS trace $z_k$, set of goals $g_1, \ldots, g_I$, set of trip segments $t_1, \ldots, t_J$, and set
            of streets $e_1, \ldots, e_K$
   output:  Estimated transition matrices between goals $p(g_{i'} \mid g_i)$, trip segments
            $p(t_{j'} \mid t_j, g_i)$, and streets $p(e_{k'} \mid e_k, t_j)$, $1 \leq i, i' \leq I$, $1 \leq j, j' \leq J$,
            $1 \leq k, k' \leq K$
1. Initialize all the transition parameters;
2. repeat
       //E-step:
3.     Perform forward filtering pass using current estimate of transition parameters;
4.     Perform backward filtering pass using current estimate of transition parameters;
5.     Obtain smoothed transition counts by combining forward and backward passes;
       //M-step:
6.     Updated transition parameters based on smoothed transition counts in the E-step;
7. until transition parameters converge
```

Algorithm 6.4: Transition parameter estimation in hierarchical model using EM

uniform for all the outgoing streets of e_k.

Then in the E-step (Step 3 through Step 5), both the forward filtering pass and a backward (in time) filtering path are performed using the current estimate of the parameters [84, 108]. The forward filtering pass uses the Rao-Blackwellised particle filter shown in Alg. 6.2 (transition parameters are used in Step 11, Step 16, and Step 21). The backward filtering pass is very similar to the forward pass except the GPS readings are played in a reverse order. The transition parameters for the backward pass can be computed from the normal (forward) transition parameters using Bayes rules. The expected transition counts are smoothed by combining the results from forward and backward passes, and these smoothed counts are used in the M-step (Step 6) to update the transition parameters [84, 94].

Our approach is in fact a direct extension of the Monte Carlo EM algorithm [114]. The only difference is that we allow particles to evolve with time. It has been shown that when the number of particles n is large enough, Monte Carlo EM estimation converges to the theoretical EM estimation [62].

In addition to the user specific transition parameters our model requires the specification of other parameters, such as motion velocity model and the GPS sensor model. The motion velocity is modeled as a mixture of Gaussians from which velocities are drawn at random.

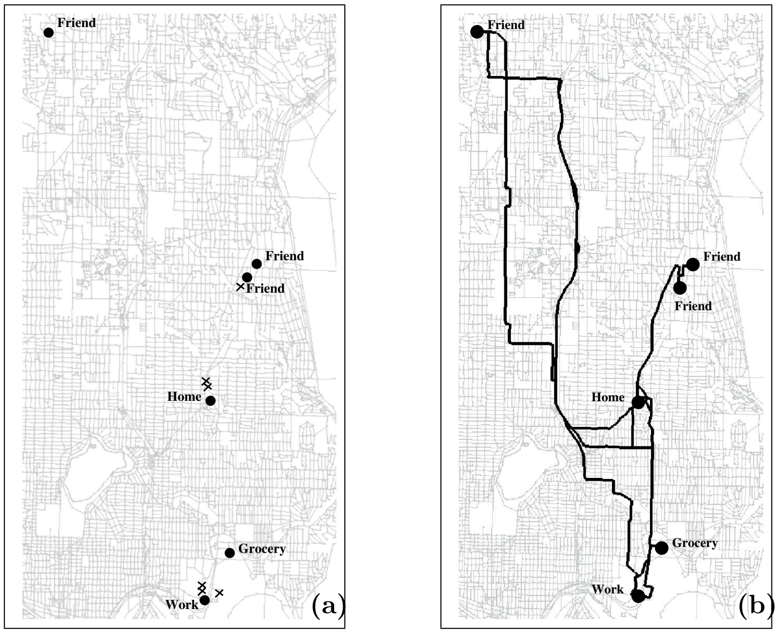

Figure 6.3: (a) Street map along with goals (dots) learned from 30 days of data. Learned trip switching locations are indicated by cross marks. (b) Most likely trajectories between goals obtained from the learned transition matrices. Text labels were manually added.

The probabilities of the mixture components depend on the current motion mode and can be learned beforehand using data labeled with the correct mode of motion [84]. The GPS sensor noise is modeled as a Gaussian with a fixed variance. Our system does not currently learn the parameters associated with novelty detection. This would entail learning the likelihood of a user making an error versus doing something novel, and is beyond the scope of this work.

6.4 Experimental Results

To validate our model, we collected 60 days of GPS data from one person wearing a small GPS unit. We used the first 30 days for learning and the second 30 days for testing.

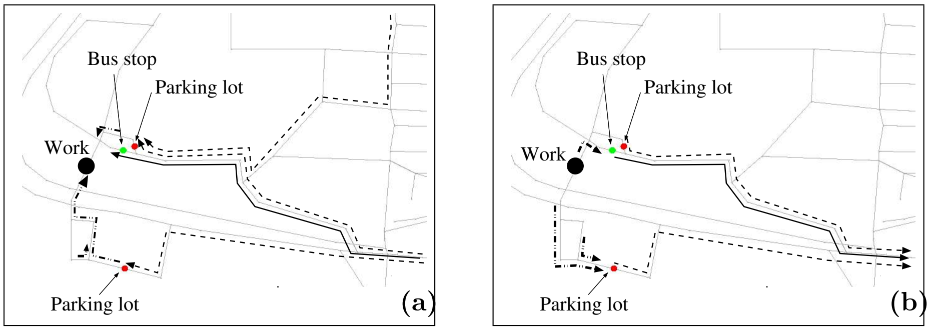

Figure 6.4: Close up of the area around the workplace. (a) Shown are edges that are connected by likely transitions (probability above 0.75), given that the goal is the workplace (dashed lines indicate car mode, solid lines bus, and dashed-dotted lines foot). (b) Learned transitions in the same area conditioned on home being the goal.

6.4.1 Activity Model Learning

The learning was done without manual labeling. The system precisely identifies the subject's six most common transportation goals and all frequently used bus stops and parking lots, as shown in Fig. 6.3 (a). In this experiment, goals are those locations where the person spent more than an hour in total, and bus stops and parking lots are determined using 0.85 as the transition threshold . After recognizing the goals and transfer locations, parameter learning estimates the transition matrices at all levels of the model. Using those transition matrices, we can extract the most likely trajectories on the street map between pairs of the goals, as shown in Fig. 6.3 (b).

Fig. 6.4 shows a close up display of the area near the workplace. The learned results clearly show the common routes using different modes of transportation, as well as the usual bus stops and parking lots.

6.4.2 Empirical Comparison to Other Models

The hierarchical model is very expressive and able to answer many useful queries. For example, many applications need to query the probability of a given goal. In this section we present results comparing the goal prediction performance of our hierarchical model with a flat model [84] and a second-order Markov model (2MM) trained on sequences of goals [3].

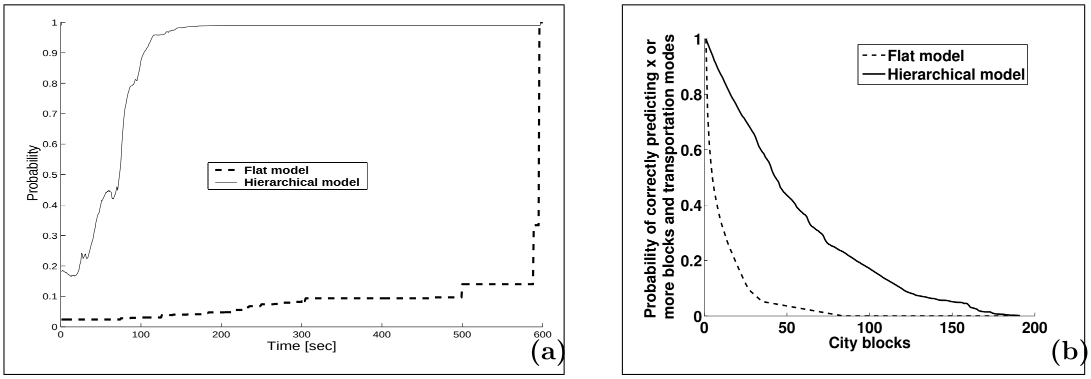

Figure 6.5: Comparison of flat model and hierarchical model. (a) Probability of the true goal (workplace) during an episode from home to work, estimated using the flat and the hierarchical model. (b) Location and transportation mode prediction capabilities of the learned model.

The flat model is basically a first-order Markov model over the street blocks. Thus, in order to calculate the probability of a goal, one must calculate the sum over all possible paths to the goal, which is intractable if the goal is far away. A reasonable approximation is to compute the probability of the most likely path to the goal. Fig. 6.5(a) compares the result of such a query on the probability of the goal being the workplace during an episode of traveling from home to work. As one can see, the hierarchical model quickly assigns a high probability to the true goal, while the estimate from the flat model is meaningless until the user is near the goal. In [84], the flat model is also used to predict the street blocks and transportation modes in the future. As shown in Fig. 6.5(b), the prediction capability of the hierarchical model is much better than that of the flat model. For instance, in 50% of the cases, the flat model is able to correctly predict the motion and transportation mode of the person for 5 city blocks, while the hierarchical model can predict correctly for 43 blocks.

The 2MM model introduced in [3] is a second-order Markov model that only reasons about transitions between goal locations. Since this model ignores GPS measurements collected during transit between goals, it cannot refine the goal prediction as a person moves to a goal. To show the difference in performance, we labeled the 30 days of test data with the true goals and computed the prediction accuracy using the 2MM and our hierarchical model, which was learned using the same training data. The average prediction

Table 6.1: Comparison of goal predictions using 2MM and hierarchical model

	Avg. accuracy at given time			
Model	beginning	25%	50%	75%
2MM	0.69	0.69	0.69	0.69
Hierarchical model	0.66	0.75	0.82	0.98

accuracies at the beginning of each trip and after 25%, 50%, and 75% of each trip was completed are listed in Table 6.1. At the beginning, our model predicts the next goal using first-order transition matrices; it performs only slightly worse than the 2MM. However, by integrating real time measurements, our predictions become much more accurate while 2MM's estimates remain the same.

6.4.3 Error Detection

Another important feature of our model is the capability to differentiate normal, erroneous, and deliberately novel activities.

Whenever a true destination is known, the system can *clamp* it as the user's goal, g_k, in the hierarchical model, estimate the novelty probability and then compute the error probability using Equation (6.17). To evaluate the effect of clamping on our model's ability to detect errors we conducted two experiments. In each experiment, we calculated the probabilities of normal behavior and user errors over time and compared the results (see Fig. 6.6).

In the first experiment, the user had notified the system that the true destination was going home; however, the user took an incorrect bus toward one of his friend's houses. Both the correct bus route and the incorrect bus route had been learned during training. For the first 700 seconds, the wrong bus route coincided with the correct one and both the clamped and unclamped inference engines believed that the user was in normal mode, *i.e.*, $n_k = false$ (see Fig. 6.6(a and b)). But when the incorrect bus took a turn at time 700 that the user had never taken *to get home*, the probability of errors in the model with the goal clamped to home dramatically jumped (see Fig. 6.6(a)). In contrast, the unclamped

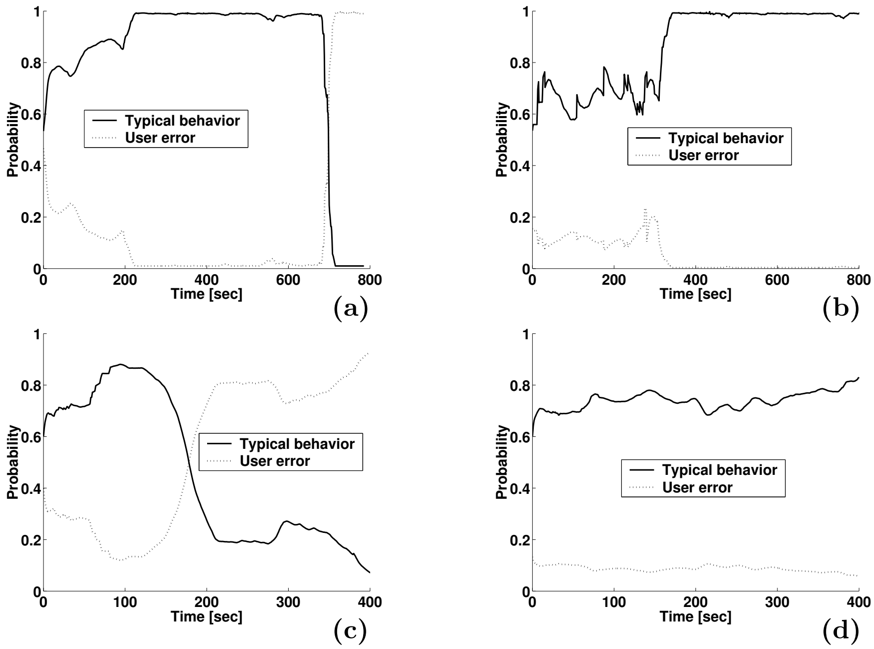

Figure 6.6: The probabilities of typical behavior vs. user errors in two experiments (when no goals are clamped, the prior ratio of typical behavior, user error and deliberate novel behavior is 3:1:2; when a goal is clamped, the probability of deliberately novel behavior is zero): (a) Bus experiment with a clamped goal; (b) Bus experiment with an unclamped goal; (c) Foot experiment with a clamped goal; (d) Foot experiment with an unclamped goal.

model could not conclude that the user was making an error because the user, while on the wrong bus route to get home, was on a bus route consistent with going to other familiar goals (see Fig. 6.6(b)).

In the second experiment, the user left his office and then proceeded to walk in a direction away from his normal parking spot. When the destination was not specified (see Fig. 6.6(d)), the tracker had a fairly steady level of confidence in the user's path (there were many previously observed paths from his office consistent with the observed data). However, when the destination was specified (see Fig. 6.6(c)), the system initially inferred that the behavior was consistent with walking toward the parking lot, and then, as the user began to turn away at time 125, the tracker started doubting the success of the user's intentions. The tracker's confidence in the user's success correspondingly dropped.

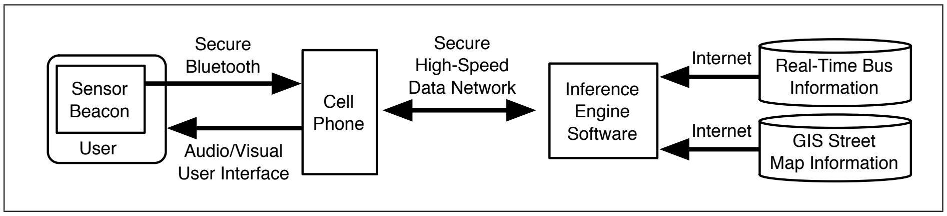

Figure 6.7: The client-server architecture of Opportunity Knocks

6.5 Application: Opportunity Knocks

Our motivation for developing these techniques was grounded in the observation that for many individuals, mobility in the community means using public transportation. However, public transportation can be daunting for anyone who is born with below average cognitive abilities or whose cognitive abilities have begun to decline. If impaired individuals had effective compensatory cognitive aids to help them use public transportation, their independence and safety would improve, they would have new opportunities for socialization and employment, and stress on their families and care givers would be reduced.

Based on the techniques we have discussed, we developed a ubiquitous computing system, called “Opportunity Knocks” (OK) [85], in order to explore the feasibility of just such a cognitive aid. This system targets mentally retarded individuals and individuals with traumatic brain injury, who are generally high functioning but unable to use public transportation due to short-term confusion or memory lapses. The name of our system is derived from the desire to provide our users with a source of computer generated opportunities from which they can learn more efficient transportation routes, and correct simple errors before they become dangerous errors. When the system has determined that an especially important opportunity has made itself available, it plays a sound like a door knocking to get the user’s attention.

Our system has a client-server architecture, as shown in Fig. 6.7. The client side consists of a cell phone and a GPS sensor beacon which communicates position information to the phone via Bluetooth technology. The cell phone transmits GPS readings and user queries to a server through a wireless (GPRS) data network. On the server side, the learning and inference engine integrates the user information with map and bus information, and sends inference results or suggestions back to the client side.

In the experiment, explained in Fig. 6.8 and Fig. 6.9, a user with our device boarded a bus to get home after carrying the system with them for 1 month (a similar scenario to Fig. 6.6(a, b), but with different data). Unfortunately, the user boarded the wrong bus, which shared the first part of the bus route in common with the correct bus. OK detected the mistake and guided the user back on track. The top of each panel in the figures display a representation of the reasoning process that the inference engine is undertaking. The center portion of each panel displays what the user interface displayed at each stage of the experiment, and the bottom portion holds a text description of the frame.

6.6 Summary

We have described the foundations and experimental validation of a hierarchical model that can learn and infer a user's daily movements and use of different modes of transportation. The model can be learned using unlabeled data, and online inference can be efficiently performed. Our results showed that the approach can provide predictions of movements to distant goals, and support a simple and effective strategy for detecting novel events that may indicate user errors. Based on this technique, we implemented a system called "Opportunity Knocks" that is able to help cognitively impaired people use public transit independently and safely.

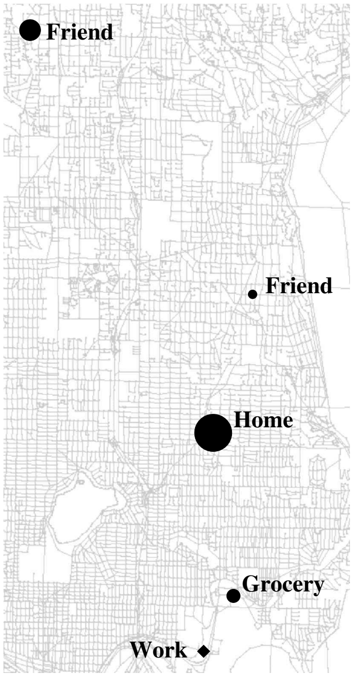

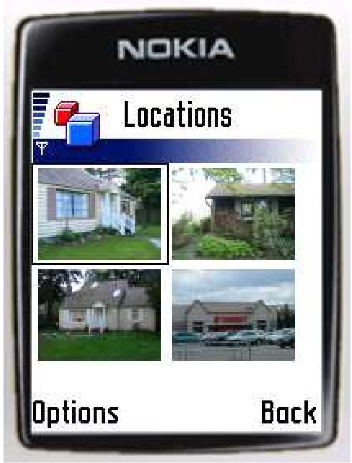

This frame shows the user at work when the system identified the most likely destinations. Circle areas correspond to relative likelihood. The phone displayed images of the most likely destinations left to right, top to bottom: home, friend 1, friend 2, grocery store.

1

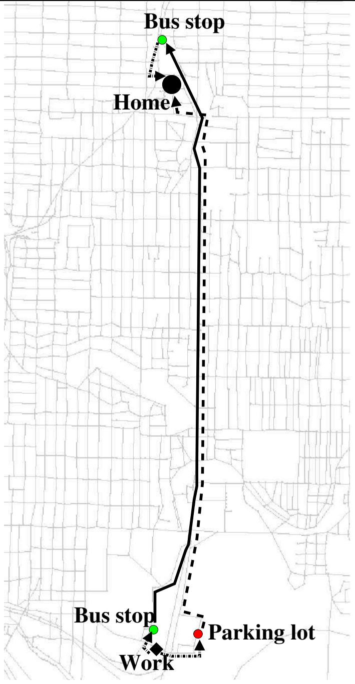

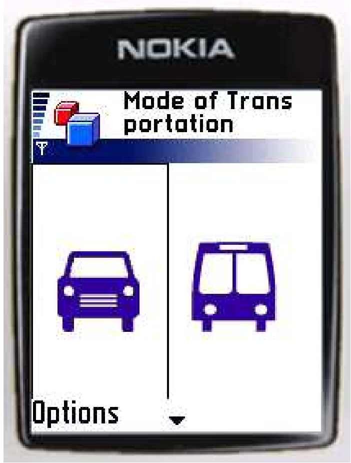

After the user indicated that he'd like to go home, the system identified two routes that he usually takes, a bus route shown in solid lines and a car route shown in dashed lines. The system asked the user which way he would like to proceed.

2

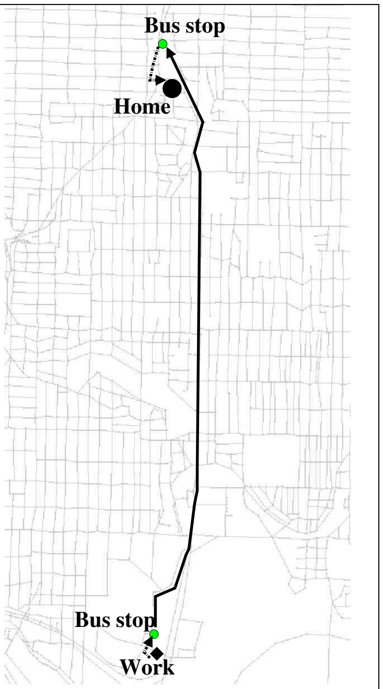

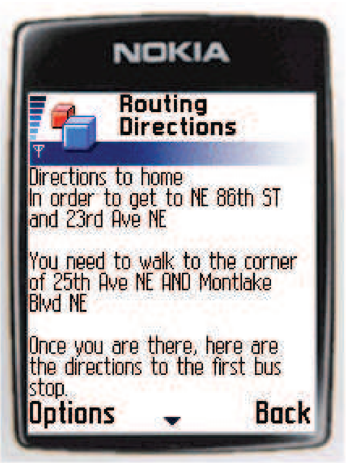

Routing Directions

Directions to home
In order to get to NE 86th ST and 23rd Ave NE

You need to walk to the corner of 25th Ave NE AND Montlake Blvd NE

Once you are there, here are the directions to the first bus stop.

Options Back

The user selected the bus route and *OK* presented a text description of the learned route. The user proceeded to the bus stop, and boarded a bus. The bus that the user boarded however was going to his friend's house, a familiar, but incorrect route considering the expressed intention to go home.

3

Figure 6.8: An experiment using Opportunity Knocks (Part I)

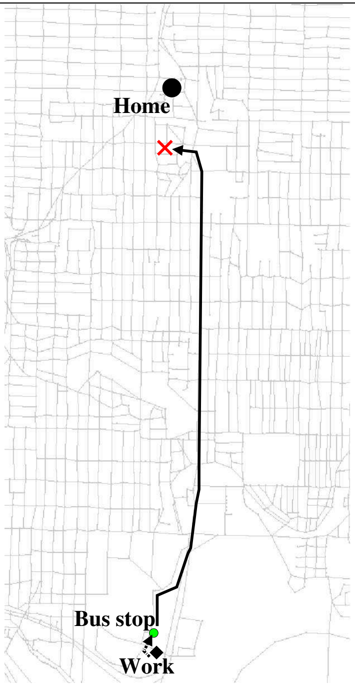

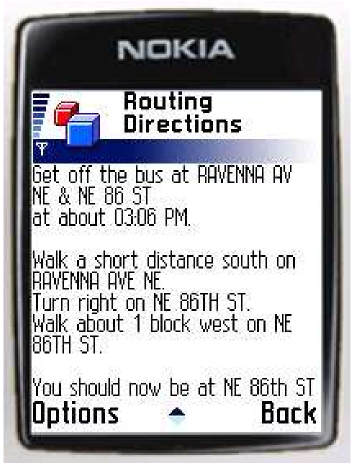

Get off the bus at RAVENNA AV NE & NE 86 ST at about 03:06 PM.

Walk a short distance south on RAVENNA AVE NE.
Turn right on NE 86TH ST.
Walk about 1 block west on NE 86TH ST.

You should now be at NE 86th ST

The system was unable to identify that the user was on the wrong bus because the routes coincided for the first portion of the bus ride. Before getting to the correct bus stop for going home, the system observed that the user had departed from the expected trip segment and turned west.

4

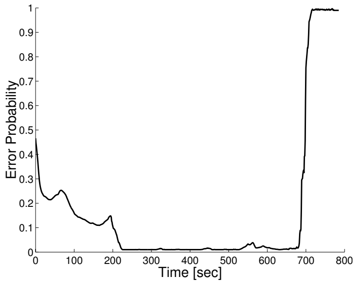

This graph shows how the system reasons about errors. When the error probability rises above 50% confidence, the system believes an abnormal condition exists. *OK* waits until a clamped curve breaks 80% confidence before alerting.

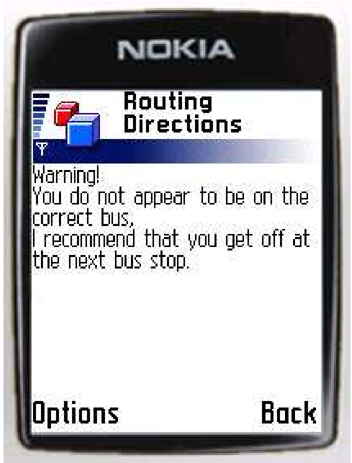

Warning!
You do not appear to be on the correct bus,
I recommend that you get off at the next bus stop.

When the bus diverted from the correct route, the system identified the behavior condition as an error. This was possible *even though* the user was on a frequently taken route. In response it proactively made its door knocking alert noise and showed a corresponding message

5

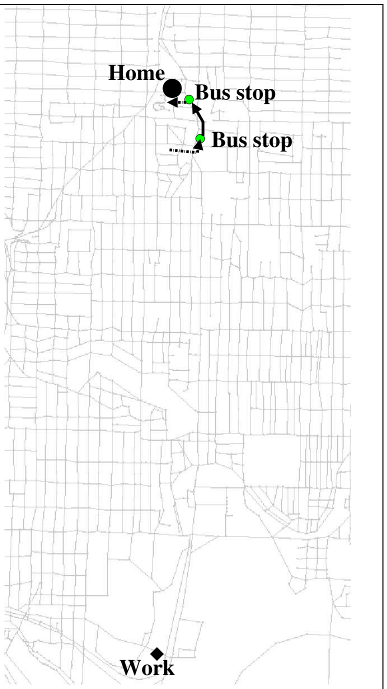

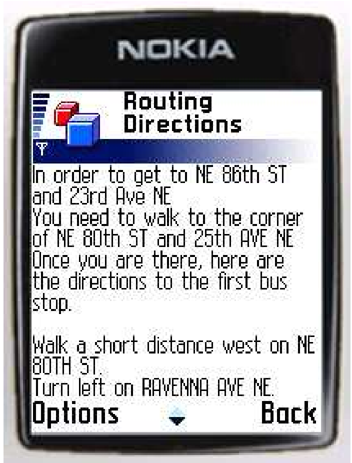

In order to get to NE 86th ST and 23rd Ave NE
You need to walk to the corner of NE 80th ST and 25th AVE NE
Once you are there, here are the directions to the first bus stop.

Walk a short distance west on NE 80TH ST.
Turn left on RAVENNA AVE NE.

Once off the incorrect bus, the user reselects home as the destination. This time OK queries a real-time bus planning system for a route home. The user is directed to walk back to the arterial road and catch a different bus that is going the correct way.

6

Figure 6.9: An experiment using Opportunity Knocks (Part II)

Chapter 7

INDOOR VORONOI TRACKING

In last chapter, we described a person's transportation routines using a DBN model, whose parameters are customized based on GPS data collected by the person. We applied Rao-Blackwellised particle filters for inference and EM algorithm for unsupervised learning. In this chapter, we apply similar approach to learning people's movement patterns in indoor environments.

The first difficulty for indoor environments is the ineffectiveness of GPS; thus we have to resort to other tracking techniques. The indoor location estimation has gained a lot of attention in the robotics community [27, 97, 55]. Most existing approaches to people tracking rely on laser range-finders [27, 8, 97] or cameras [55]. A key advantage of these sensors is their location accuracy. Unfortunately, they usually do not provide information about the identity of people. Over the last years, especially in the ubiquitous computing community, people have started to equip indoor environments with networks of sensors that are capable of providing information about a person's location and identity [113, 4]. Such sensors, however, have the disadvantage that they provide only relatively coarse location information in practice. In addition to being corrupted by noise, such sensors provide measurements at low frame rates only. In this chapter, we discuss a robust approach for location estimation using such sparse and noisy sensor data.

Another difficulty is that we do not have street maps available indoors, which play a important role in our outdoor models. To overcome this difficulty, we track the locations of people on (generalized) Voronoi graphs [16] of indoor environments (see Fig. 7.2(a) for an example). Thus we can naturally represent typical human motion along the main axes of the free space. The estimated trajectories on the Voronoi graph help us to bridge the gap between continuous sensor data and discrete, abstract models of human motion behavior. Surprisingly, such an approximation can also improve the tracking accuracy in the case of

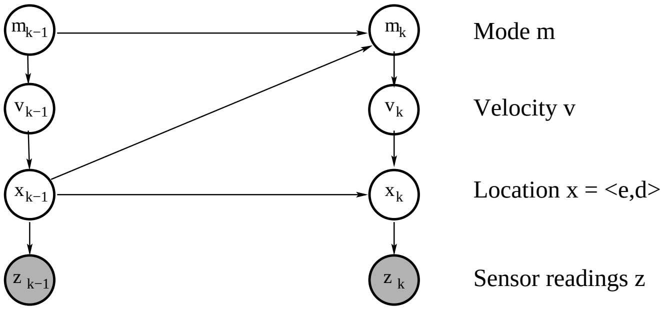

Figure 7.1: DBN model of the Voronoi tracking

sparse and noisy sensor data, as we will show in the experiments.

This chapter is organized as follows. we first present a DBN model for indoor location tracking. Although the motion model is similar to outdoor case, the sensor model is very different. Then we briefly explain the inference and learning algorithms. Finally, we will show experimental results of Voronoi tracking.

7.1 Voronoi Tracking

We define a Voronoi graph $G = (V, E)$ by a set V of vertices v_i and a set E of directed edges e_j. Roughly speaking, Voronoi graph of an environment is the skeleton of the free space. Fig. 7.2(a) shows the Voronoi graph representing the Intel Research Lab Seattle, our indoor testing environment. Note that this graph results from manual pruning of the original Voronoi graph [16] and that for clarity only the undirected version of the graph is shown.

Similar to outdoor GPS tracking and the inference of modes of transportation, we construct a DBN model, as shown in Fig. 7.1. From the top of the model, $m_k \in \{\text{stopped}, \text{moving}\}$ indicates the current motion mode of the object, which depends on the previous mode m_{k-1} and previous edge e_{k-1}. Intuitively, places such as offices should have higher stopping probabilities and hallways should have lower stopping probabilities. Therefore, by learning the mode transition probabilities at each edge, we can have some idea of the different types of places. The next level is velocity. If $m_k = \text{stopped}$, then $v_k = 0$; otherwise v_k is governed by a Gaussian distribution whose mean and variance are manually set based on ordinary

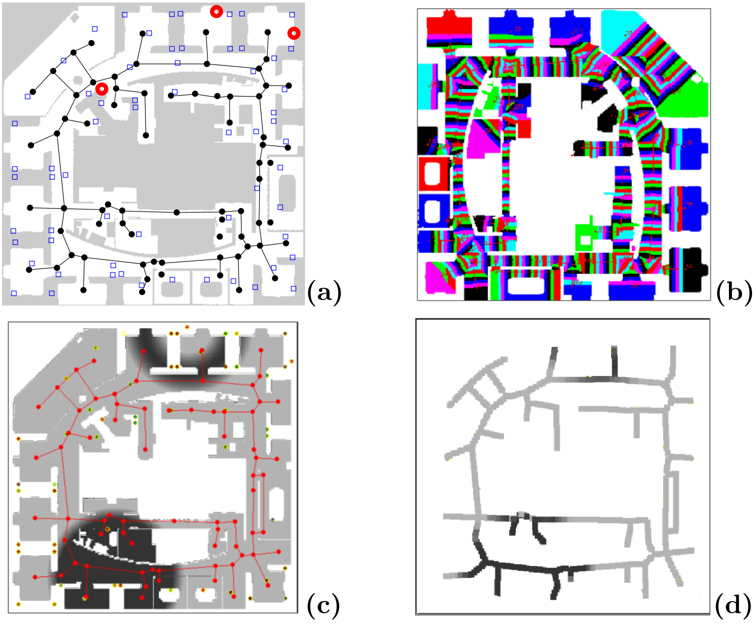

Figure 7.2: Voronoi graphs for location estimation: (a) Indoor environment along with manually pruned Voronoi graph. Shown are also the positions of ultrasound Crickets (circles) and infrared sensors (squares). (b) Patches used to compute likelihoods of sensor measurements. Each patch represents locations over which the likelihoods of sensor measurements are averaged. (c) Likelihood of an ultra-sound cricket reading (upper) and an infrared badge system measurement (lower). While the ultra-sound sensor provides rough distance information, the IR sensor only reports the presence of a person in a circular area. (d) Corresponding likelihood projected onto the Voronoi graph.

human movements. The current location of an object is represented by $x_k = \langle e_k, d_k \rangle$, where e_k denotes the current edge on the graph, d_k indicates the distance of the object from the start vertex of edge e_k. Given x_{k-1} and v_k, x_k is determined by the edge transition matrix $p(e_j|e_i)$, which describes the probability that the object transits to node e_j given that the previous node was e_i and an edge transition took place.

In general, the motion model of the indoor Voronoi tracking is similar to that of the flat model for GPS tracking. However, its sensor model $p(z_k \mid x_k)$ is quite different from that of GPS. At each time a single object can get measurements from more than one sensors. Denote the sequence of observations at time k as ${z_k}^1, \cdots, {z_k}^I$. By assuming the observations are generated independently, we have

$$p(z_k \mid x_k) \quad = \quad \prod_{i=1}^{I} p({z_k}^i \mid x_k) \tag{7.1}$$

A straightforward implementation of $p({z_k}^i \mid x_k)$ for Voronoi graphs would be to simply compute the likelihood of observations for positions on the graph, as done in the GPS tracking. However, in reality people can move anywhere in the free space, and thus computing the likelihoods only on the graph is not a valid and robust approach. Note that each discretized position on the graph actually represents a *patch* of the free space, as shown in Fig. 7.2(b). The patch $\mathcal{S}(x)$ consists of the set of all the 2d positions whose "projection" on the graph is x, or more strictly, $\mathcal{S}(x)$ is defined as

$$\mathcal{S}(x) \quad = \quad \{\nu \in \text{ free space } \mid x = \underset{x' \text{ on graph}}{\text{argmin}} \quad |x' - \nu|\} \tag{7.2}$$

Then, to compute the likelihood of an observation ${z_k}^i$ given a position x_k on the graph, we have to integrate over all 2d positions in the patch $\mathcal{S}(x_k)$:

$$p({z_k}^i | x_k) = \frac{1}{|\mathcal{S}(x_k)|} \sum_{\nu \in \mathcal{S}(x_k)} p({z_k}^i \mid \nu) \tag{7.3}$$

In our implementation of the sensor model, we discretize positions on the graph and precompute the patch for each position. Fig. 7.2(c) shows the original sensor models in the 2d space for infrared badge system and ultra-sound cricket system, and Fig. 7.2(d) shows the corresponding sensor model on the Voronoi graph by averaging the measurement likelihood within each patch.

7.2 Inference and Learning

In last chapter, we combined Kalman filters and particle filters for location estimation on a graph. A key assumption was the Gaussian distribution of the GPS sensor model. However, for many indoor location sensors, such as infrared sensors (see Section 7.3), the Gaussian assumption does not hold. Therefore, we only apply the particle filters for the inference without using the Kalman update. Because the limited space of indoor environment, the inference is still very efficient.

The application of particle filters to location estimation on a Voronoi graph is rather straightforward. We first sample the motion state m_k with probability proportional to $p(m_k \mid m_{k-1}, e_{k-1})$. If m_k = moving, then we randomly draw the velocity v_k from the Gaussian distribution and compute the traveled distance $v_k \Delta t$. Then we have to determine whether the motion along the edge results in a transition to another edge. If not, then $d_k = d_{k-1} + v_k \Delta t$ and $e_k = e_{k-1}$. Otherwise, $d_k = d_{k-1} + v_k \Delta t - |e_{k-1}|$ and the next edge e_k is drawn with probability $p(e_k \mid e_{k-1})$. If the motion state m_k = stopped, the position x_k is set to be x_{k-1}. The importance sampling step of the particle filter is implemented by weighting each sample proportional to the projected observation likelihood as given in (7.1), and the reweight step is identical to standard particle filters.

The task of learning in our model is to estimate the edge transition matrix $p(e_j|e_i)$ and the mode transition matrix $p(m_k|m_{k-1}, e_{k-1})$. Similar to the parameter estimation for transportation routines, we again apply the Expectation-Maximization (EM) algorithm. In a nutshell, each iteration of the EM begins with an expectation step, which estimates the trajectory of the person using particle filtering forward and backward through the data set. The trajectories are used to count the edge transitions of particles on the Voronoi graph and the switching between motion modes. These values are then converted into probabilities during the M-step, which generates a new model estimate. The updated model is then used in the next iteration to re-estimate the trajectory of the person. For the first E-step, we initialize the mode transition parameters with some reasonable values using background knowledge of typical human motion and a uniform distribution for the outgoing edges at each vertex of the Voronoi graph.

7.3 Experimental Results

We evaluate the performance of the Voronoi tracking (VT) approach based on data recorded at the Intel Research Lab Seattle. As shown in Fig. 7.2(a), the office environment is equipped with two different kinds of ID sensors, including 73 Versus infrared receivers which provide information about the presence of a person in the vicinity of a sensor and three Cricket

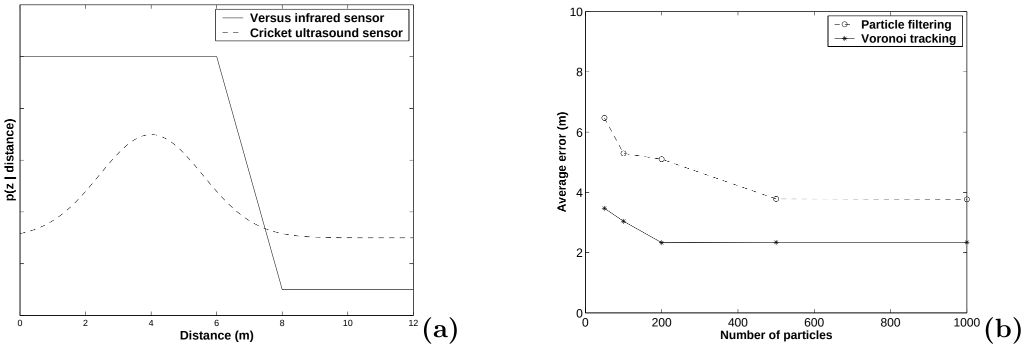

Figure 7.3: (a) Sensor model of ultrasound crickets and infrared badge system. The x-axis represents the distance from the detecting infrared sensor and ultrasound sensor (4m ultrasound sensor reading), respectively. The y-axis gives the likelihood for the different distances from the sensor. (b) Localization error for different numbers of samples.

ultrasound receivers which provide identity and distance estimates (see [46] for more details on the sensors). Fig. 7.3(a) shows a model of the uncertainty of the two sensor types, used to compute $p({z_k}^i \mid \nu)$ in (7.3). The sensor parameters are manually set based on experience. Note that especially the infrared badge sensor model is highly non-Gaussian. Additionally, both sensors suffer from a high probability of false-negative readings, *i.e.*, they frequently fail to detect a person.

To generate data for which ground truth is available, we equipped a mobile robot with two Versus badges, a Cricket beacon, and additionally with a Sick laser range-finder. Our experiment is based on a 35-minute-long log of sensor measurements received while driving the robot through the environment. The robot moved at an average velocity of 30 cm/s and was stopped at designated resting places. The laser range-finder allowed us to accurately estimate the path of the robot using the map shown in Fig. 7.2(a).

As an initial test, we determined the average localization error when using un-trained VT *vs.* a particle filter (PF) representing locations in the complete free space of the environment. The resulting error on the complete log was 2.34m for VT and 3.78m for PF. This result is extremely encouraging since it indicates that the projection onto the Voronoi graph does not only result in a good approximation of the PF, but yields *better* performance than the PF. Fig. 7.4 (b) and (c) show typical maximum likelihood trajectories using VT and PF,

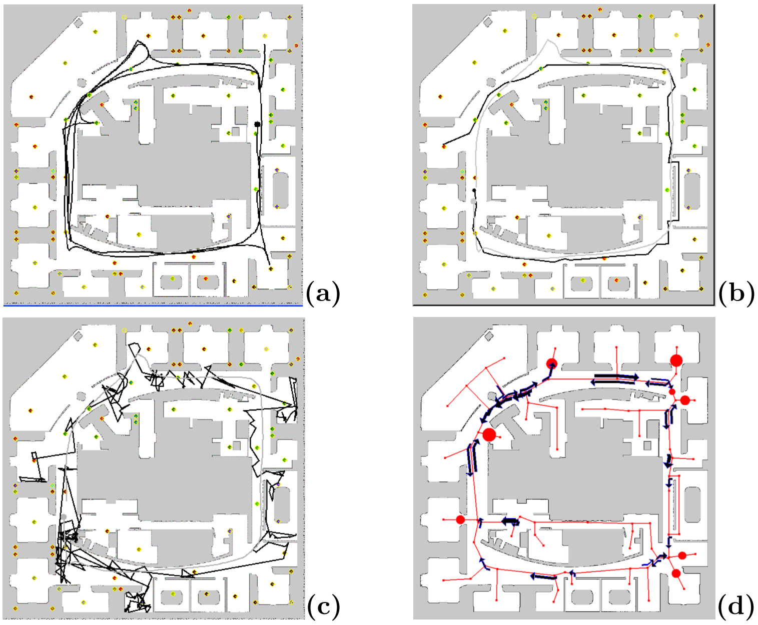

Figure 7.4: (a) Trajectory of the robot during a 25 minute period of training data collection. True path (in light color) and most likely path as estimated using (b) Voronoi tracking and (c) original particle filters. (d) Motion model learned using EM. The arrows indicate those transitions for which the probability is above 0.65. Places with high stopping probabilities are represented by disks. Thicker arcs and bigger disks indicate higher probabilities.

respectively. These paths were generated from the trajectory (history) of the most likely particle at the end of the run. The graphs clearly demonstrate the superior performance of the VT technique.

We also compared the tracking performance for different sample set sizes. The results are given in Fig. 7.3(b). It becomes clear that VT makes very efficient use of particles and it is able to track well using only 200 particles.

Next, we evaluated the learning performance of VT. We split the complete data log into a training set of 25 minutes and a test set of 10 minutes. We trained the VT model using the EM algorithm on the training set and determined the tracking error on the test data using the motion model learned at each iteration. The results are summarized in Table 7.1.

As can be seen, the algorithm converges after only 3 iterations of EM, and using the

Table 7.1: Evolution of test error during EM learning.

EM Iteration	Avg. Tracking Errors (m)	Error Reduction after Learning
before learning	2.63	-
1	2.27	13.7%
2	2.05	22.1%
3	1.84	30.0%
4	1.79	31.9%
5	1.76	33.1%

learned model increases the tracking accuracy significantly. This shows that the Voronoi graph is able to extract the correct motion patterns from the training data. This fact is supported by Fig. 7.4(d), which visualizes the motion model learned after 5 iterations. The model correctly reflects the path and resting locations of the robot.

7.4 Summary

We have presented an approach to tracking the location of people and learning their motion patterns in indoor environments. The technique is able to robustly estimate a person's location even when using only sparse, noisy information provided by id-sensors. The key idea of our approach is to use a particle filter that is projected onto a Voronoi graph of the environment. The resulting model is similar to the hierarchical DBN for modeling transportation routines. Using data collected by a mobile robot, we demonstrate that our approach has two key advantages. First, it is by far more efficient and robust than particle filters which estimate the location of people in the complete free space of an environment. Second, the Voronoi graph provides a natural discretization of human motion, which allows us to learn typical motion patterns using expectation maximization. More recent work has extended our approach by applying advanced sensor models and using mixed representation of Voronoi graph and free space [61, 26].

Chapter 8

CONCLUSION AND FUTURE WORK

8.1 Conclusion

The goal of our research is to develop fundamental techniques that enable machines to understand human activities. In this thesis, we have developed two techniques for recognizing people's activities and transportation routines from GPS data.

First, we have presented a framework of activity recognition that builds upon and extends existing research on statistical relational learning, such as conditional random fields and relational Markov networks. This framework is able to take into account complex relations between locations, activities, and significant places, as well as high level knowledges such as number of homes and workplaces. By extracting and labeling activities and significant places simultaneously, our approach achieves high accuracy on both extraction and labeling. The framework is very expressive. Using SQL-like templates, it can capture complicated relations and instance uncertainty. The framework also supports efficient inference and learning. We have presented efficient inference algorithms for aggregate features using FFT or local MCMC, and a novel approach for feature selection and parameter estimation using boosting with virtual evidences. Using GPS data collected by different people, we have demonstrated the feasibility of transferring knowledge from people who have labeled data to those who have no or very little labeled data.

Second, we have built a hierarchical dynamic Bayesian network model for transportation routines. It can predict a user's destination in real time, infer the user's mode of transportation, and determine when a user has deviated from his ordinary routines. The model encodes general knowledge such as street maps, bus routes, and bus stops, in order to discriminate different transportation modes. Moreover, our system could automatically learn navigation patterns at all levels from raw GPS data, without any manual labeling! Based on this work we have developed a personal guidance system called Opportunity Knocks, to help people with cognitive disabilities use public transit.

Although the two techniques are very different, they share a number of common characteristics. For example, both have hierarchical structures so as to bridge the gap between low level sensor data and high level activities; both encode a large amount of domain knowledges and complex relations; and both recognize activities in a collective manner so as to create a comprehensive and consistent interpretation of a user's data.

The focus of the thesis is location-based activity recognition from GPS data. In addition, we have shown preliminary results for indoor activity recognition and motion pattern learning. We believe many techniques we have developed, such as the efficient inference algorithms for aggregate features, the virtual evidence boosting algorithm, and the Rao-Blackwellized particle filtering in hierarchical models, can be applied into other probabilistic reasoning tasks as well.

8.2 Future Work

We have just begun to scratch the surface of what can be done with this general approach to modeling activity patterns of people. Many theoretical challenges remain unsolved, such as learning models with partially labeled data and clustering people based on different behavioral patterns. At the same time our technique can be applied in many domains, such as mobile user modeling and assistive technologies; building these practical systems is also interesting future work.

8.2.1 Semi-supervised Learning

One of the biggest problems in training discriminative activity models is that it requires a large amount of fully labeled data. In practice, it is very expensive and time-consuming to manually label all the training data. The idea of semi-supervised learning in our case is to train discriminative activity models using only *partially* labeled data. For example, we may only have labels for some time but not all the time, or in hierarchical activity models we may only have labels for high level activities but not low level activities. The goal is to learn CRF-like models that utilize all the data, including both labeled and unlabeled. There have been some progresses on applying CRFs in semi-supervised learning (see [93, 103, 48]). However, the learning algorithms in previous work mainly use ML criterion and are hard to scale to large data sets; at the same time it is unclear how pseudo-likelihood and virtual evidence boosting can be extended for semi-supervised cases. Therefore, it is still an open challenge to develop more efficient training algorithms for CRFs in a semi-supervised manner, and this work could have great impact for many practical applications.

8.2.2 Pattern Clustering

In this thesis, we have demonstrated the feasibility of transferring activity knowledge between different people: we train a model from some people and apply the learned model to others. This method works well in our experiments. However, we only used data from subjects whose activities are more or less similar, for example, they all have families and day-time jobs. In order to apply our approach to thousands of people, we must be able to handle very different behavior patterns. A promising approach is to cluster people based on their activity patterns and learn a generic model for each cluster. For a new person, we determine which cluster the person belongs to and then apply the model of that cluster to infer his activities. There are two main challenges. First, in this setting of clustering, each input includes all the data from a single person. What metrics shall we use to determine the similarities between the inputs? Shall we use all the RMN features directly, or shall we apply feature selection or dimension reduction? Second, how shall we determine the cluster that the person belongs to, since the labels of the new person are unknown? We may think this as a online *model selection* problem, and we could pick the model that maximize some criterion, such as the conditional likelihood of the MAP sequence.

8.2.3 Adaptive Mobile Devices

User modeling is important to adaptive user interfaces, personalized Web search, and proactive user assistance. For modeling desktop users, inputs from the keyboard and mouse are primary sources of information. In a mobile environment, however, it is essential to take people's physical activities into account. By integrating ubiquitous sensor data (*e.g.*, locations), mobiles devices can potentially better understand users' interaction patterns, and more accurately predict their needs. However, mobile devices have less memory and computational power, so the learning and inference must be very efficient even with limited resources. Future research on mobile user modeling will benefit from previous work on adaptive desktop systems and ubiquitous activity recognition, and will address the trade-off between reasoning performance and resource usage.

8.2.4 Long-term Health Care

The ability to automate activity tracking and anomaly detection will enable important applications in health care. However, we must connect our research more closely with findings from neuropsychology and other sources of domain knowledge. For example, if we have knowledge of how a specific neurological deficit (*e.g.*, mild Alzheimer's disease) impairs a variety of human activities, then we can develop patient-specific behavior models and provide targeted intervention. The challenge, however, is how to obtain such knowledge, since neither hand-coding nor completely supervised learning will be scalable. A feasible way could be to start with the general domain knowledge, and refine our knowledge in an unsupervised manner as real patients use the system. It may be also necessary to group patients based on their similarities and allow knowledge transfer between people. This research will not only help computers recognize user errors, but also help us understand the causes of these behavioral deficits in functional and computational terms.

8.2.5 From Sensors to Human Sense

People have invented a large variety of sensors that are capable of providing various information about the world, for example, RFID can tell which object has been touched, body sensors can continuously measure the body temperature and blood pressure, sensor networks can be used to detect anomalies in wild environments, *etc.* However, what people often need is high level information of contexts, such as activities, intentions, needs, healthy conditions, and so on. There exists a big gap between the low level sensor measurements and high level human sense. In this thesis, we focus on bridging the gap between location data and relevant activities using machine learning and probabilistic reasoning techniques.

We believe the framework can be applied in many other applications with similar goals. In order to provide efficient and well-founded solutions to practical applications, we must leverage synergies between artificial intelligence and ubiquitous computing, so that we can benefit from the advances in both domains.

BIBLIOGRAPHY

[1] C. Andrieu, N. de Freitas, A. Doucet, and M. I. Jordan. An introduction to MCMC for machine learning. *Machine Learning*, 2003.

[2] S. Arulampalam, S. Maskell, N. Gordon, and T. Clapp. A tutorial on particle filters for on-line non-linear / non-Gaussian Bayesian tracking. *IEEE Transactions on Signal Processing*, 2001.

[3] D. Ashbrook and T. Starner. Using GPS to learn significant locations and predict movement across multiple users. *Personal and Ubiquitous Computing*, 7(5), 2003.

[4] P. Bahl and V. Padmanabhan. RADAR: An in-building RF-based user location and tracking system. In *Proceedings of IEEE INFOCOM*, 2000.

[5] J. E. Baker. Reducing bias and inefficiency in the selection algorithm. In *Proc. of the Second International Conference on Genetic Algorithms*, 1987.

[6] Y. Bar-Shalom, X. R. Li, and T. Kirubarajan. *Estimation with Applications to Tracking and Navigation.* John Wiley, 2001.

[7] M. Bennewitz, W. Burgard, G. Cielniak, and S. Thrun. Learning motion patterns of people for compliant robot motion. *International Journal of Robotics Research (IJRR)*, 24(1), 2005.

[8] M. Bennewitz, W. Burgard, and S. Thrun. Using EM to learn motion behaviors of persons with mobile robots. In *Proc. of the IEEE/RSJ International Conference on Intelligent Robots and Systems (IROS)*, 2002.

[9] J. Besag. Statistical analysis of non-lattice data. *The Statistician*, 24, 1975.

[10] A. F. Bobick and Y. A. Ivanov. Action recognition using probabilistic parsing. Technical report, MIT Media Lab, 1998.

[11] E. O. Brigham. *Fast Fourier Transform and Its Applications.* Prentice Hall, 1988.

[12] H. H. Bui. A general model for online probabilistic plan recognition. In *Proc. of the International Joint Conference on Artificial Intelligence (IJCAI)*, 2003.

[13] H. H. Bui, S. Venkatesh, and G. West. On the recognition of abstract Markov policies. In *Proc. of the National Conference on Artificial Intelligence (AAAI)*, 2000.

[14] H. H. Bui, S. Venkatesh, and G. West. Policy recognition in the abstract hidden Markov model. *Journal of Artificial Intelligence Research*, 2002.

[15] E. Charniak and R. P. Goldman. A Bayesian model of plan recognition. In *Proc. of the National Conference on Artificial Intelligence (AAAI)*, 1993.

[16] H. Choset. *Sensor Based Motion Planning: The Hierarchical Generalized Voronoi Graph*. PhD thesis, Caltech, 1996.

[17] T. Choudhury, B. Clarkson, S. Basu, and A Pentland. Learning communities: Connectivity and dynamics of interacting agents. In *Proc. of the International Joint Conference on Neural Networks*, 2003.

[18] D. Colbry, B. Peintner, and M. E. Pollack. Execution monitoring with quantitative temporal Bayesian networks. In *6th International Conference on AI Planning and Scheduling*, 2002.

[19] R. Cowell, A. Dawid, S. Lauritzen, and D. Spiegelhalter. *Probabilistic Networks and Expert Systems*. Springer, 1999.

[20] N. de Freitas. Rao-Blackwellised particle filtering for fault diagnosis. *IEEE Aerospace*, 2002.

[21] T. Dean and K. Kanazawa. Probabilistic temporal reasoning. In *Proc. of the National Conference on Artificial Intelligence (AAAI)*, 1988.

[22] A. P. Dempster, N. M. Laird, and D. B. Rubin. Maximum-likelihood from incomplete data via the EM algorithm. *Journal of the Royal Statistical Society*, 1977.

[23] T. Dietterich, A. Ashenfelter, and Y. Bulatov. Training conditional random fields via gradient tree boosting. In *Proc. of the International Conference on Machine Learning (ICML)*, 2004.

[24] A. Doucet, N. de Freitas, and N. Gordon, editors. *Sequential Monte Carlo in Practice*. Springer-Verlag, New York, 2001.

[25] A. Doucet, N. de Freitas, K. Murphy, and S. Russell. Rao-Blackwellised particle filtering for dynamic Bayesian networks. In *Proc. of the National Conference on Artificial Intelligence (AAAI)*, 2000.

[26] B. Ferris, D. Hähnel, and D. Fox. Gaussian processes for signal strength-based location estimation. In *Proc. of Robotics: Science and Systems*, 2006.

[27] A. Fod, A. Howard, and M. J. Mataric. Laser-based people tracking. In *Proc. of the IEEE International Conference on Robotics & Automation (ICRA)*, 2002.

[28] W. Freeman, E. Pasztor, and O. Carmichael. Learning low-level vision. *International Journal of Computer Vision*, 2000.

[29] Y. Freund and R. E. Schapire. A decision-theoretic generalization of on-line learning and an application to boosting. *Journal of Computer and System Sciences*, 55(1):119–139, 1997.

[30] B. J. Frey and D. MacKay. A revolution: Belief propagation in graphs with cycles. In *Advances in Neural Information Processing Systems (NIPS)*, 1997.

[31] J. Friedman, T. Hastie, and R. Tibshirani. Additive logistic regression: a statistical view of boosting. *The Annals of Statistics*, 38(2):337–374, 2000.

[32] N. Friedman, L. Getoor, D. Koller, and A. Pfeffer. Learning probabilistic relational models. In *Proc. of the International Joint Conference on Artificial Intelligence (IJCAI)*, 1999.

[33] S. Geman and D. Geman. Stochastic relaxation, Gibbs distributions and the Bayesian restoration of images. *Transactions on Pattern Analysis and Machine Intelligence (PAMI)*, 1984.

[34] L. Getoor, N. Friedman, D. Koller, and A. Pfeffer. *Relational Data Mining*, chapter Learning Probabilistic Relational Models. Springer-Verlag, 2001.

[35] L. Getoor, N. Friedman, D. Koller, and B. Taskar. Learning probabilistic models of relational structure. In *Proc. of the International Conference on Machine Learning (ICML)*, 2001.

[36] L. Getoor and B. Taskar, editors. *Statistical Relational Learning.* forthcoming book, 2006.

[37] C. J. Geyer and E. A. Thompson. Constrained Monte Carlo Maximum Likelihood for dependent data. *Journal of Royal Statistical Society*, 1992.

[38] W. R. Gilks, S. Richardson, and D. J. Spiegelhalter. *Markov Chain Monte Carlo in Practice.* Chapman and Hall/CRC, 1995.

[39] V. Gogate, R. Dechter, C. Rindt, and J. Marca. Modeling transportation routines using hybrid dynamic mixed networks. In *Proc. of the Conference on Uncertainty in Artificial Intelligence (UAI)*, 2005.

[40] R. P. Goldman, C. W. Geib, and C. A. Miller. A new model of plan recognition. In *Proc. of the Conference on Uncertainty in Artificial Intelligence (UAI)*, 1999.

[41] K. Gopalratnam, H. Kautz, and D. Weld. Extending continuous time Bayesian networks. In *Proc. of the National Conference on Artificial Intelligence (AAAI)*, 2005.

[42] R. Hariharan and K. Toyama. Project Lachesis: parsing and modeling location histories. In *Geographic Information Science*, 2004.

[43] W. K. Hastings. Monte Carlo sampling methods using Markov chains and their applications. *Biometrika*, 1970.

[44] D. Heckerman. A tutorial on learning with Bayesian networks. Technical report, Microsoft Research, 1995.

[45] D. Heckerman, D. Meek, and D. Koller. Probabilistic models for relational data. Technical Report MSR-TR-2004-30, Microsoft Research and Stanford University, 2004.

[46] J. Hightower. *The Location Stacks.* PhD thesis, University of Washington, 2004.

[47] M. J. Huber, H. D Edmund, and M. P. Wellman. The automated mapping of plans for plan recognition. In *Proc. of the National Conference on Artificial Intelligence (AAAI)*, 1994.

[48] A. Kapoor. *Learning Discriminative Models with Incomplete Data.* PhD thesis, MIT, 2006.

[49] H. Kautz. *A Formal Theory of Plan Recognition.* PhD thesis, University of Rochester, 1987.

[50] K. Kersting and L. de Raedt. Towards combining inductive logic programming with Bayesian networks. In *Proceedings of the International Conference on Inductive Logic Programming*, 2001.

[51] G. Kitagawa. Monte Carlo filter and smoother for non-Gaussian nonlinear state space models. *Journal of Computational and Graphical Statistics*, 5(1), 1996.

[52] D. Koller and A. Pfeffer. Probabilistic frame-based systems. In *Proc. of the National Conference on Artificial Intelligence (AAAI)*, 1998.

[53] D. Koller and A. Prfeffer. Learning probabilities for noisy first-order rules. In *Proc. of the International Joint Conference on Artificial Intelligence (IJCAI)*, 1997.

[54] T. Kristjannson, A. Culotta, P. Viola, and A. McCallum. Interactive information extraction with constrained conditional random fields. In *Proc. of the National Conference on Artificial Intelligence (AAAI)*, 2004.

[55] E. Kruse and F. Wahl. Camera-based monitoring system for mobile robot guidance. In *Proc. of the IEEE/RSJ International Conference on Intelligent Robots and Systems (IROS)*, 1998.

[56] S. Kumar and M. Hebert. Discriminative random fields: A discriminative framework for contextual interaction in classification. In *Proc. of the International Conference on Computer Vision (ICCV)*, 2003.

[57] C. Kwok and D. Fox. Map-based multiple model tracking of a moving object. In *RoboCup 2004: Robot Soccer World Cup VIII*, 2004.

[58] J. Lafferty, A. McCallum, and F. Pereira. Conditional random fields: Probabilistic models for segmenting and labeling sequence data. In *Proc. of the International Conference on Machine Learning (ICML)*, 2001.

[59] A. LaMarca, Y. Chawathe, S. Consolvo, J. Hightower, I. Smith, J. Scott, T. Sohn, J. Howard, J. Hughes, F. Potter, J. Tabert, P. Powledge, G. Borriello, and B. Schilit. Place Lab: Device positioning using radio beacons in the wild. In *proceedings of Pervasive*, 2005.

[60] J. Lester, T. Choudhury, N. Kern, G. Borriello, and B. Hannaford. A hybrid discriminative-generative approach for modeling human activities. In *Proc. of the International Joint Conference on Artificial Intelligence (IJCAI)*, 2005.

[61] J. Letchner, D. Fox, and A LaMarca. Large-scale localization from wireless signal strength. In *Proc. of the National Conference on Artificial Intelligence (AAAI)*, 2005.

[62] R. Levine and G. Casella. Implementations of the Monte Carlo EM algorithm. *Journal of Computational and Graphical Statistics*, 10, 2001.

[63] L. Liao, T. Choudhury, D. Fox, H. Kautz, and B. Limketkai. Training conditional random fields using virtual evidence boosting. In *Proc. of the International Joint Conference on Artificial Intelligence (IJCAI)*, 2007.

[64] L. Liao, D. Fox, and H. Kautz. Learning and inferring transportation routines. In *Proc. of the National Conference on Artificial Intelligence (AAAI)*, 2004.

[65] L. Liao, D. Fox, and H. Kautz. Location-based activity recognition. In *Advances in Neural Information Processing Systems (NIPS)*, 2005.

[66] L. Liao, D. Fox, and H. Kautz. Location-based activity recognition using relational Markov networks. In *Proc. of the International Joint Conference on Artificial Intelligence (IJCAI)*, 2005.

[67] L. Liao, D. Fox, and H. Kautz. Extracting places and activities from GPS traces. *International Journal of Robotics Research (IJRR)*, 2006. accepted.

[68] L. Liao, D.J. Patterson, D. Fox, and H. Kautz. Learning and inferring transportation routines. *Artifitial Intelligence*, 2006. accepted.

[69] B. Limketkai, L. Liao, and D. Fox. Relational object maps for mobile robots. In *Proc. of the International Joint Conference on Artificial Intelligence (IJCAI)*, 2005.

[70] Y. Mao, F. R. Kschischang, and B. J. Frey. Convolutional factor graphs as probabilistic models. In *Proc. of the Conference on Uncertainty in Artificial Intelligence (UAI)*, 2004.

[71] A. McCallum. Efficiently inducing features or conditional random fields. In *Proc. of the Conference on Uncertainty in Artificial Intelligence (UAI)*, 2003.

[72] N. Metropolis, A. W. Rosenbluth, M. N. Rosenbluth, A. H. Teller, and E. Teller. Equations of state calculations by fast computing machines. *Journal of Chemical Physics*, 1953.

[73] M. Montemerlo, S. Thrun, D. Koller, and B. Wegbreit. FastSLAM: A factored solution to the simultaneous localization and mapping problem. In *Proc. of the National Conference on Artificial Intelligence (AAAI)*, 2002.

[74] R. Morales-Menéndez, N. de Freitas, and D. Poole. Real-time monitoring of complex industrial processes with particle filters. In *Advances in Neural Information Processing Systems (NIPS)*, 2002.

[75] S. Muggleton. Stochastic logic programming. In *Advances in inductive logic programming*, 1996.

[76] K. Murphy. Bayesian map learning in dynamic environments. In *Advances in Neural Information Processing Systems (NIPS)*, 1999.

[77] K. Murphy. *Dynamic Bayesian Networks: Representation, Inference and Learning.* PhD thesis, UC Berkeley, 2002.

[78] K. Murphy, Y. Weiss, and M. Jordan. Loopy belief propagation for approximate inference: An empirical study. In *Proc. of the Conference on Uncertainty in Artificial Intelligence (UAI)*, 1999.

[79] A. Ng and M. Jordan. On discriminative vs. generative classifiers: A comparison of logistic regression and Naive Bayes. In *Advances in Neural Information Processing Systems (NIPS)*, 2002.

[80] N. Oliver, E. Horvitz, and A. Garg. Layered representations for learning and inferring office activity from multiple sensory channels. In *Proceedings of Int. Conf. on Multimodal Interfaces*, 2002.

[81] H. Pasula, B. Marthi, B. Milch, S. Russell, and I. Shpitser. Identity uncertainty and citation matching. In *Advances in Neural Information Processing Systems (NIPS)*, 2002.

[82] H. Pasula and S. Russell. Approximate inference for first-order probabilistic languages. In *Proc. of the International Joint Conference on Artificial Intelligence (IJCAI)*, 2001.

[83] D. J. Patterson, D. Fox, H. Kautz, and M. Philipose. Fine-grained activity recognition by aggregating abstract object usage. In *Proceedings of the IEEE International Symposium on Wearable Computers*, 2005.

[84] D. J. Patterson, L. Liao, D. Fox, and H. Kautz. Inferring high-level behavior from low-level sensors. In *International Conference on Ubiquitous Computing (UbiComp)*, 2003.

[85] D. J. Patterson, L. Liao, K. Gajos, M. Collier, N. Livic, K. Olson, S. Wang, D. Fox, and H. Kautz. Opportunity Knocks: a system to provide cognitive assistance with transportation services. In *International Conference on Ubiquitous Computing (UbiComp)*, 2004. submitted.

[86] J. Pearl. *Probabilistic Reasoning in Intelligent Systems: Networks of Plausible Inference.* Morgan Kaufmann, 1988.

[87] F. Peng and A. McCallum. Accurate information extraction from research papers using conditional random fields. In *HLT-NAACL*, 2004.

[88] A. Pfeffer and T. Tai. Asynchronous dynamic Bayesian networks. In *Proc. of the Conference on Uncertainty in Artificial Intelligence (UAI)*, 2005.

[89] D. Poole. Logic programming, abduction and probability: a top-down anytime algorithm for estimating prior and posterior probabilities. *New Generation Computing*, 1993.

[90] D. Poole. Probabilistic Horn abduction and Bayesian networks. *Artificial Intelligence*, 1993.

[91] D. V. Pynadath. *Probabilistic Grammars for Plan Recognition*. PhD thesis, University of Michigan, 1999.

[92] D. V. Pynadath and M. P. Wellman. Probabilistic state-dependent grammars for plan recognition. In *Proc. of the Conference on Uncertainty in Artificial Intelligence (UAI)*, 2000.

[93] A. Quattoni, M. Collins, and T. Darrell. Conditional random fields for object recognition. In *Advances in Neural Information Processing Systems (NIPS)*, 2004.

[94] L. R. Rabiner. A tutorial on hidden Markov models and selected applications in speech recognition. In *Proceedings of the IEEE*. IEEE, 1989. IEEE Log Number 8825949.

[95] M. Richardson and P. Domingos. Markov logic networks. *Machine Learning*, 2006.

[96] S. Sanghai, P. Domingos, and D. Weld. Dynamic probabilistic relational models. In *Proc. of the International Joint Conference on Artificial Intelligence (IJCAI)*, 2003.

[97] D. Schulz, W. Burgard, and D. Fox. People tracking with a mobile robot using joint probabilistic data association filters. *International Journal of Robotics Research (IJRR)*, 2003.

[98] D. Schulz, D. Fox, and J. Hightower. People tracking with anonymous and ID-sensors using Rao-Blackwellised particle filters. In *Proc. of the International Joint Conference on Artificial Intelligence (IJCAI)*, 2003.

[99] F. Sha and F. Pereira. Shallow parsing with conditional random fields. In *Proceedings of Human Language Technology-NAACL*, 2003.

[100] Y. Shi, Y. Huang, D. Minnen, A. Bobick, and I. Essa. Propagation networks for recognition of partially ordered sequential action. In *Proc. of the IEEE Computer Society Conference on Computer Vision and Pattern Recognition (CVPR)*, 2004.

[101] A. Subramanya, A. Raj, J. Bilmes, and D. Fox. Recognizing activities and spatial context using wearable sensors. In *Proc. of the Conference on Uncertainty in Artificial Intelligence (UAI)*, 2006.

[102] E. Sudderth, A. Ihler, W. Freeman, and A. Willsky. Nonparametric belief propagation. In *Proc. of the IEEE Computer Society Conference on Computer Vision and Pattern Recognition (CVPR)*, 2003.

[103] M. Szummer. Learning diagram parts with hidden random fields. In *International Conference on Document Analysis and Recognition*, 2005.

[104] B. Taskar, P. Abbeel, and D. Koller. Discriminative probabilistic models for relational data. In *Proc. of the Conference on Uncertainty in Artificial Intelligence (UAI)*, 2002.

[105] B. Taskar, C. Guestrin, V. Chatalbashev, and D. Koller. Max-Margin Markov networks. In *Advances in Neural Information Processing Systems (NIPS)*, 2004.

[106] B. Taskar, M. Wong, P. Abbeel, and D. Koller. Link prediction in relational data. In *Advances in Neural Information Processing Systems (NIPS)*, 2003.

[107] S. Thrun, W. Burgard, and D. Fox. *Probabilistic Robotics.* MIT Press, 2005.

[108] S. Thrun, J. Langford, and D. Fox. Monte Carlo hidden Markov models: Learning non-parametric models of partially observable stochastic processes. In *Proc. of the International Conference on Machine Learning (ICML)*, 1999.

[109] L. Tierney. Markov chains for exploring posterior distributions. *The Annals of Statistics*, 1994.

[110] A. Torralba, K. P. Murphy, and W. T. Freeman. Contextual models for object detection using boosted random fields. In *Advances in Neural Information Processing Systems (NIPS)*, 2004.

[111] V. N. Vapnik. *Statistical Learning Theory.* John Wiley & Sons, 1998.

[112] A. Varshavsky, M. Chen, E. D. Lara, J. Froehlich, D. Haehnel, J. Hightower, A. LaMarca, F. Potter, T. Sohn, K. Tang, and I. Smith. Are GSM phones THE solution for localization? In *7th IEEE Workshop on Mobile Computing Systems and Applications (HotMobile)*, 2006.

[113] R. Want, A. Hopper, V. Falcao, and J. Gibbons. The active badge location system. *ACM Transactions on Information Systems*, 10(1), 2001.

[114] G. Wei and M.A. Tanner. A Monte Carlo implementation of the EM algorithm and the poor mans data augmentation algorithms. *Journal of the American Statistical Association*, 85, 2001.

[115] J. S. Yedidia, W. T. Freeman, and Y. Weiss. *Exploring Artificial Intelligence in the New Millennium*, chapter Understanding Belief Propagation and Its Generalizations. Morgan Kaufmann Pub, 2001.

[116] J. S. Yedidia, W. T. Freeman, and Y. Weiss. Constructing free-energy approximations and generalized belief propagation algorithms. *IEEE Transactions on Information Theory*, 51(7):2282–2312, 2005.

[117] J. S. Yedidia, W. T. Freeman, and Weiss Y. Constructing free energy approximations and generalized belief propagation algorithms. Technical report, MERL, 2002.

Appendix A

DERIVATIONS

A.1 Derivation of Likelihood Approximation using MCMC

Derivation of Eq. (4.8)

Suppose we already know the value $L(\tilde{\mathbf{w}})$ for a weight vector $\tilde{\mathbf{w}}$. Then we have (ignore the shrinkage prior for simplicity)

$$\begin{aligned} L(\mathbf{w}) - L(\tilde{\mathbf{w}}) &= -\log P(\mathbf{y} \mid \mathbf{x}, \mathbf{w}) + \log P(\mathbf{y} \mid \mathbf{x}, \tilde{\mathbf{w}}) \\ &= \log \frac{P(\mathbf{y} \mid \mathbf{x}, \tilde{\mathbf{w}})}{P(\mathbf{y} \mid \mathbf{x}, \mathbf{w})} \\ &= \log \frac{\exp\{\tilde{\mathbf{w}}^T \cdot \mathbf{f}(\mathbf{x}, \mathbf{y})\}/Z(\mathbf{x}, \tilde{\mathbf{w}})}{\exp\{\mathbf{w}^T \cdot \mathbf{f}(\mathbf{x}, \mathbf{y})\}/Z(\mathbf{x}, \mathbf{w})} \\ &= \log \frac{Z(\mathbf{x}, \mathbf{w})/Z(\mathbf{x}, \tilde{\mathbf{w}})}{\exp\{(\mathbf{w} - \tilde{\mathbf{w}})^T \cdot \mathbf{f}(\mathbf{x}, \mathbf{y})\}} \\ &= \log \frac{Z(\mathbf{x}, \mathbf{w})}{Z(\mathbf{x}, \tilde{\mathbf{w}})} - (\mathbf{w} - \tilde{\mathbf{w}})^T \cdot \mathbf{f}(\mathbf{x}, \mathbf{y}), \end{aligned} \tag{A.1}$$

where $Z(\mathbf{x}, \mathbf{w})/Z(\mathbf{x}, \tilde{\mathbf{w}})$ can be estimated using Monte-Carlo methods:

$$\begin{aligned} \frac{Z(\mathbf{x}, \mathbf{w})}{Z(\mathbf{x}, \tilde{\mathbf{w}})} &= \frac{\sum_{\mathbf{y}} \exp\{\mathbf{w}^T \cdot \mathbf{f}(\mathbf{x}, \mathbf{y})\}}{Z(\mathbf{x}, \tilde{\mathbf{w}})} \\ &= \sum_{\mathbf{y}} \exp\{(\mathbf{w} - \tilde{\mathbf{w}})^T \cdot \mathbf{f}(\mathbf{x}, \mathbf{y})\} \frac{\exp\{\tilde{\mathbf{w}}^T \cdot \mathbf{f}(\mathbf{x}, \mathbf{y})\}}{Z(\mathbf{x}, \tilde{\mathbf{w}})} \\ &= \sum_{\mathbf{y}} \exp\{(\mathbf{w} - \tilde{\mathbf{w}})^T \cdot \mathbf{f}(\mathbf{x}, \mathbf{y})\} P(\mathbf{y} \mid \mathbf{x}, \tilde{\mathbf{w}}) \\ &\approx \frac{1}{M} \sum_{i=1}^{M} \exp\{(\mathbf{w} - \tilde{\mathbf{w}})^T \cdot \mathbf{f}(\mathbf{x}, \tilde{\mathbf{y}}^{(i)})\}. \end{aligned} \tag{A.2}$$

At the last step of (A.2), we use MCMC to get M random samples, $\tilde{\mathbf{y}}^{(i)} (1 \leq i \leq M)$ from the distribution $P(\mathbf{y} \mid \mathbf{x}, \tilde{\mathbf{w}})$.

Substitute (A.2) into (A.1), we get

$$\begin{aligned} L(\mathbf{w}) &\approx L(\tilde{\mathbf{w}}) + \log\left(\frac{1}{M}\sum_{i=1}^{M}\exp\left\{(\mathbf{w}-\tilde{\mathbf{w}})^T \cdot (\mathbf{f}(\mathbf{x},\tilde{\mathbf{y}}^{(i)}) - \mathbf{f}(\mathbf{x},\mathbf{y}))\right\}\right) \\ &= L(\tilde{\mathbf{w}}) + \log\left(\frac{1}{M}\sum_{i=1}^{M}\exp\left\{(\mathbf{w}-\tilde{\mathbf{w}})^T \cdot \Delta\tilde{\mathbf{f}}^{(i)}\right\}\right), \qquad (A.3) \end{aligned}$$

where $\Delta\tilde{\mathbf{f}}^{(i)} = \mathbf{f}(\mathbf{x},\tilde{\mathbf{y}}^{(i)}) - \mathbf{f}(\mathbf{x},\mathbf{y})$ is the difference between sampled feature counts using $\tilde{\mathbf{w}}$ and the empirical feature counts.

Eq. (4.8) is just Eq. (A.3) plus a prior term.

A.2 Derivation of the LogitBoost Extension to Handle Virtual Evidence

Derivation of Eq. (4.21)

The goal of our optimization is to minimize the negative per-label-log-likelihood, defined as

$$L(F) \quad = \quad -\sum_{i=1}^{N}\log p(\mathbf{y}_i) \qquad (A.4)$$

where $p(\mathbf{y}_i)$ is is a short notation that represents the posterior probability of a true label *conditioned* on its evidences. In the cases with virtual evidence, $p(\mathbf{y}_i)$ can be computed using (4.20), or equivalently as the following:

$$\begin{aligned} p(\mathbf{y}_i) &= \frac{1}{1+\frac{\sum_{\mathbf{x}_i=1}^{X}\mathbf{ve}(\mathbf{x}_i)e^{(1-2\mathbf{y}_i)F(\mathbf{x}_i)}}{\sum_{\mathbf{x}_i=1}^{X}\mathbf{ve}(\mathbf{x}_i)e^{(2\mathbf{y}_i-1)F(\mathbf{x}_i)}}} \\ &= \frac{1}{1+G_i(F)} \qquad (A.5) \end{aligned}$$

where $G_i(F) \triangleq \frac{\sum_{\mathbf{x}_i=1}^{X}\mathbf{ve}(\mathbf{x}_i)e^{(1-2\mathbf{y}_i)F(\mathbf{x}_i)}}{\sum_{\mathbf{x}_i=1}^{X}\mathbf{ve}(\mathbf{x}_i)e^{(2\mathbf{y}_i-1)F(\mathbf{x}_i)}}$.

In (A.4), substitute the likelihood with (A.5), the objective function can be expressed as

$$L_F \quad = \quad \sum_{i=1}^{N} \log(1 + G_i(F)) \tag{A.6}$$

Similar to original LogitBoost, our extension performs Newton step to minimize (A.6), which can be reduced to a weighted least square error (WLSE) problem defined in Eq. (4.21). The derivation is shown below.

Suppose at one iteration the estimate is F. Then to take the Newton step, we first compute the derivative of L_{F+f} relative to $\mathbf{f}$ when $\mathbf{f} \rightarrow 0$. We have

$$\begin{aligned}
s \quad &\triangleq \quad \frac{\partial L_{F+f}}{\partial f}\Big|_{\mathbf{f}=0} \\
&= \quad \sum_{i=1}^{N} \frac{\frac{\partial G_i(F+f)}{\partial f}}{1 + G_i(F+f)}\Big|_{\mathbf{f}=0} \\
&= \quad \sum_{i=1}^{N} \frac{2(1-2\mathbf{y}_i)G_i(F)}{1+G_i(F)} && \text{(A.7)} \\
&= \quad \sum_{i=1}^{N} 2(1-2\mathbf{y}_i)(1-p(\mathbf{y}_i)) && \text{(A.8)}
\end{aligned}$$

where (A.7) follows from the following relation that can be easily verified

$$\frac{\partial G_i(F+f)}{\partial f}\Big|_{\mathbf{f}=0} \quad = \quad 2(1-2\mathbf{y}_i)G_i(F) \tag{A.9}$$

Second, we compute the Hessian as

$$\begin{aligned}
H \quad &\triangleq \quad \frac{\partial^2 L_{F+f}}{\partial f^2}\Big|_{\mathbf{f}=0} \\
&= \quad -\sum_{i=1}^{N} 2(1-2\mathbf{y}_i)\frac{\partial p(\mathbf{y}_i)}{\partial f}\Big|_{\mathbf{f}=0} && \text{(A.10)} \\
&= \quad -\sum_{i=1}^{N} 2(1-2\mathbf{y}_i)\frac{\partial \frac{1}{1+G_i(F+f)}}{\partial f}\Big|_{\mathbf{f}=0} && \text{(A.11)} \\
&= \quad \sum_{i=1}^{N} 4p(\mathbf{y}_i)(1-p(\mathbf{y}_i)) && \text{(A.12)}
\end{aligned}$$

where (A.10) follows by substituting the derivative with (A.8), Eq. (A.11) follows from (A.5), and we can get (A.12) by applying standard calculus and using (A.9).

The Newton update is then

$$\begin{aligned} F(\mathbf{x}) &\leftarrow F(\mathbf{x}) - \frac{s}{H} \\ &= F(\mathbf{x}) + \frac{\sum_{i=1}^{N}(\mathbf{y}_i - 0.5)(1 - p(\mathbf{y}_i))}{\sum_{i=1}^{N} p(\mathbf{y}_i)(1 - p(\mathbf{y}_i))} \\ &= F(\mathbf{x}) + \frac{\sum_{i=1}^{N} \alpha_i \frac{\mathbf{y}_i - 0.5}{p(\mathbf{y}_i)}}{\sum_{i=1}^{N} \alpha_i} \end{aligned} \tag{A.13}$$

where $\alpha_i = p(\mathbf{y}_i)(1 - p(\mathbf{y}_i))$. Therefore, we can get the "best" $\mathbf{f}$ by solving the following weighted least-square approximation

$$\begin{aligned} f^*(x) &= \underset{\mathbf{f}}{\operatorname{argmin}} \sum_{i=1}^{N} \alpha_i E \left(f(\mathbf{x}) - \frac{\mathbf{y}_i - 0.5}{p(\mathbf{y}_i)} \right)^2 \\ &= \underset{\mathbf{f}}{\operatorname{argmin}} \sum_{i=1}^{N} \sum_{\mathbf{x}=1}^{X} \alpha_i \mathbf{ve}(\mathbf{x}_i) \left(f(\mathbf{x}) - \frac{\mathbf{y}_i - 0.5}{p(\mathbf{y}_i)} \right)^2 \end{aligned} \tag{A.14}$$

which is just Eq. (4.21).

VITA

Lin Liao received his B.S. and M.S. in Automation from Tsinghua University, China, in 1998 and 2001. In 2001, he came to the U.S. and became a graduate student in the Department of Computer Science and Engineering at the University of Washington, where he received a second M.S. in 2003 and a Ph.D. in 2006. His research focuses on the combination of techniques from artificial intelligence, machine learning, and ubiquitous computing and their application to practical domains, such as human activity recognition and robotics.

Lin has published a dozen of referred papers, and the paper on ”Learning and Inferring Transportation Routines” won the Outstanding Paper Award at AAAI 2004. Lin received the Outstanding Graduate Award from Tsinghua University in 2001 and the CSE Educator's Fellowship from the University of Washington in 2005.

Lin has worked at Microsoft Research and Intel Research as interns and joined Google in 2006.